Spatial and temporal relationship between intrusive rocks and gold mineralisation in the Miller Dyke Complex, Abitibi greenstone belt, Ontario, Canada

by

Luis Alfonso Arteaga Melo

A thesis submitted in partial fulfilment

of the requirements for the degree of

Master of Science (MSc) in Geology

The Faculty of Graduate Studies

Laurentian University

Sudbury, Ontario, Canada

THESIS DEFENCE COMMITTEE/COMITÉ DE SOUTENANCE DE THÈSE
Laurentian Université/Université Laurentienne
Faculty of Graduate Studies/Faculté des études supérieures

Title of Thesis Titre de la thèse	Spatial and temporal relationship between intrusive rocks and gold mineralisation in the Miller Dyke Complex, Abitibi greenstone belt, Ontario, Canada
Name of Candidate Nom du candidat	Arteaga Melo, Luis
Degree Diplôme	Master of Science
Department/Program Département/Programme	Geology
Date of Defence Date de la soutenance	April 23, 2018

APPROVED/APPROUVÉ

Thesis Examiners/Examinateurs de thèse:

Dr. Dan Kontak
(Supervisor/Directeur de thèse)

Dr. Harold Gibson
(Co-supervisor/Co-directeur de thèse)

Dr. Pedro Jugo
(Committee member/Membre du comité)

Dr. Robert Linnen
(External Examiner/Examinateur externe)

Approved for the Faculty of Graduate Studies
Approuvé pour la Faculté des études supérieures
Dr. David Lesbarrères
Monsieur David Lesbarrères
Dean, Faculty of Graduate Studies
Doyen, Faculté des études supérieures

ACCESSIBILITY CLAUSE AND PERMISSION TO USE

ABSTRACT

The Miller Dyke Complex (MDC) is located 15 km south of the Kirkland Lake gold camp. It consists of a series of narrow, structurally controlled dykes, that range from felsic to mafic in composition, and are spatially associated with Au, ± Cu, ± Mo mineralisation. The MDC provides an excellent locality for a careful study of the igneous petrology and the different alteration assemblages associated with the mineralisation. The study is focused on the metasomatic processes related with alkali elements. It is shown that strong sodic alteration has a strong influence on the textural, mineralogical, and geochemical features of these rocks. Previously undescribed textures and mineralisation styles are documented, as well as the existence of a Paleoproterozoic hydrothermal reactivation event with metal deposition or remobilisation. The relationship between the alkali metasomatism and gold mineralisation is discussed within the regional context of the Abitibi greenstone belt.

Keywords: sodic alteration, alkali metasomatism, gold mineralisation, episyenite, quartz dissolution, hydrothermal alteration, Abitibi greenstone belt.

THESIS STRUCTURE AND CO-AUTHORSHIP STATEMENT

The thesis is written as a paper that, with modification of content and length, will be submitted to the journal Ore Geology Reviews, the candidate is the first author. This paper forms Chapter 1 of the thesis and it is co-authored with my supervisors H.L. Gibson and D.J. Kontak. The candidate performed the following tasks: geological mapping; core logging of 27 drill holes (5845.3 m); selection of samples for petrography, geochemistry, and geochronology; petrographic examination of thin-sections; SEM-EDS analysis and interpretation; geochemical data treatment and interpretation; construction of all the figures, diagrams, and tables in the thesis. The co-authors read drafts of this work, made edits, suggestions, and valuable intellectual contributions according to their experience. Although the co-authors provided advice and guidance, the candidate is responsible for all the conclusions and interpretations presented in this thesis.

ACKNOWLEDGEMENTS

I would like to express my gratitude to my supervisors Dr. Harold Gibson, and Dr. Daniel Kontak; their vast experience and input to this project made me a better researcher and definitely a much better writer. They also helped me to understand many things about the Archean environment, previously unknown to me. Many thanks to Dr. Pedro Jugo, part of my thesis committee, for his valuable contributions, opinions, and edits to the final manuscript.

My infinite appreciation to Talisker Exploration Services Inc. and its directors Ruben Padilla, Terry Harbort, and Chris Lodder for many years of lessons, trust, friendship, and the opportunity to explore in amazing places of the world.

Significant recognition to George Pollock, president of NorthStar Goldcorp, for allowing me to conduct this research at the Miller Property. Osisko Mining Inc., especially its Exploration VicePresident, Mr Gernot Wober, is thanked for providing the initial funding to support this project.

All my gratitude to my family, friends, and fellow graduate students at Laurentian University.

Finally, but especially, thanks to Marie for her continuous support and motivation; for her beautiful soul and smile; for being the extraordinary woman she is; and for giving me the fortune to share with her this adventure.

TABLE OF CONTENTS

LIST OF FIGURES

LIST OF TABLES

LIST OF APPENDICES

CHAPTER 1. Textural, mineralogical, and geochemical changes associated with strong alkali metasomatism in Archean granitoids – an example from the Abitibi Greenstone Belt, Canada

Abstract

Sodium and potassium are some of the most abundant and mobile elements in the Earth´s crust, consequently, they are very active participants in the formation of alteration minerals in many hydrothermal systems. However, few studies are fully devoted to examining their behaviour, characteristics, and relationship with mineralisation within systems in the Abitibi. The Miller dyke complex (MDC) located south of the Kirkland Lake camp in the Archean Abitibi greenstone belt (AGB) is a suite of felsic dykes hosted by mafic - to intermediate metavolcanic rocks, with Au ± Cu ± Mo associated mineralisation. Given the unusual character and textures of some of the altered rocks and their rarity in the AGB, the MDC is used to investigate via an integrated petrological – geochemical – geochronological study, the nature of the intense alkali metasomatic processes associated with this mineralisation. The felsic intrusive rocks show strong textural modifications that include: 1) pervasive red staining due to extensive albite-hematite alteration; 2) dissolution of magmatic quartz, biotite, and hornblende; 3) development of episyenitic textures; 4) dissolution of quartz veins; and 5) different episodes of brecciation. These textural and mineralogical changes are accompanied by significant geochemical variations, such as enrichment or depletion of major and trace elements due to alteration of primary minerals and precipitation of secondary phases such as albite, chlorite, zircon, titanite, and apatite among others. In situ U-Pb zircon geochronology yielded a 2662 ± 18 Ma age, which combined with the results of Re-Os geochronology (2680 ± 8 Ma) suggests that the MDC dykes are part of the Timiskaming magmatic event. These ages define a very intimate link among alkaline magmatism, alkali metasomatism, and gold mineralisation, which has been previously recognised in the AGB but which is still not fully understood. The presence of 2069 ± 6 Ma titanite crystals, within dissolution cavities indicates that the earlier Archean hydrothermal system was reactivated in the Paleoproterozoic with associated mineralisation and/or remobilisation of Au, Cu, and Mo, which occurs in close association with the titanite.

1. Introduction

Sodic and potassic alteration are an integral part of many magmatic-hydrothermal systems including Cu-Au porphyry deposits (Carten 1986; Dilles et al. 2000; Sillitoe 2010); IOCG deposits (Oliver et al. 2004; Groves et al. 2010; Richards & Mumin 2013; Kontonikas-Charos et al. 2014); rare metal pegmatites (Kontak 2006; Gysi et al. 2016); carbonatites (Wooley 1982; Garson et al. 1984; Le Bas 2008), among others. The Na, Na-K, or Na-Ca alteration assemblages developed in these hydrothermal systems can be directly associated with mineralisation or just part of accessory, and generally barren alteration zones of these systems. Albitisation is the process of replacement of a primary mineral, generally K-feldspar or plagioclase by hydrothermal albite. The process has been experimentally reproduced and the details of the replacement mechanism are carefully described by several workers (Engvik et al. 2008; Putnis 2009; Hövelmann et al. 2010; Putnis & Austrheim 2010; and Norberg et al. 2014).

The Abitibi Greenstone Belt (AGB) is one of the best-studied and most metal-endowed greenstone belts in the world. Its mineral inventory includes ore deposits such as: Au-rich and base metal volcanogenic massive sulfides (VMS), Au only deposits including orogenic lode Au, banded iron formation (BIF) hosted Au, and intrusion-related Au, as well as magmatic Ni-Cu-PGE deposits. AGB gold deposits have produced more than 120 Moz Au, which was valued at approximately $120 billion in 2005 (Thurston et al., 2008), in addition to significant reserves and resources. The upside exploration potential for this area is reflected in continued exploration and the opening of new mines in recent years across the entire belt (e.g., West Timmins, Canadian Malartic, Goldex, Detour Lake). Although the presence of sodic metasomatic rocks is widely recognised in the gold-rich Archean Abitibi Greenstone Belt (AGB), Canada, there are no studies devoted to fully investigate their textural, mineralogical, and geochemical characteristics or their relationship with Au mineralisation.

Episyenites (Lacroix, 1920) are rocks characterised by hydrothermal leaching of quartz, generally accompanied by precipitation of alkali feldspars. The latter process produces rocks that may be albitites. Episyenites are rare and have only been reported from two locations in the AGB: the Côté Gold deposit (Katz, 2016) in the Swayze greenstone belt, where they are part

of the sodic alteration assemblage, but do not have any direct relationship with the Au mineralisation; and the Taschereau-Launay plutonic complex (Jebrak & Doucet, 2002), located north of Val d´Or where they host disseminated Au-Mo mineralisation. Albitites on the other hand, are relatively common and have been reported in several deposits in the AGB (Burrows, 1993; Morasse et al. 1995). It is our contention that episyenites in the AGB have been misinterpreted or overlooked and that they are more common than currently assumed.

The present study started with the discovery of extensive zones of episyenite within a felsic dyke complex associated with gold mineralisation near Kirkland Lake, Ontario, Canada during an exploration program in 2015. Here we present a detailed description of the textural, mineralogical, and geochemical characteristics of the episyenites, and discuss their formation in context of the regional setting, their potential as host rock for mineralisation, and their ability to record multiple generations of hydrothermal events. The study is based on field mapping, and core logging with supporting lithogeochemistry, extensive petrographic work with complementary imaging and analysis using scanning electron microscopy. In addition, in situ U–Pb dating of magmatic zircon, in situ U-Pb dating of hydrothermal titanite, and Re-Os dating of molybdenite are used to constrain the timing of relevant geological events.

2. Regional and Local Geological Setting

The Archean AGB (Fig 1) is an 800 by 300 km east-west trending package of volcanic and sedimentary rocks that extends from Wawa, Ontario in its southwest extreme to the Val d´Or and Chibougamau areas of Quebec in its southeast and northeast terminations, respectively (Jackson & Fyon, 1991). The volcanic and sedimentary units of the AGB range from 2798 Ma to approximately 2670 Ma, which Ayer et al. (2005) divided into eleven assemblages based on lithological, geochemical, and geochronological features. These assemblages are separated by depositional gaps or disconformities, as defined and discussed by Thurston et al. (2008). A broad spectrum of intrusions of variable compositions, from dioritic to syenitic, crosscut the aforementioned volcano-sedimentary assemblages. Beakhouse (2011) classified these intrusions into four groups, according to their relative time of emplacement and relationship with the regional deformation events. The oldest intrusions (i.e., ca. ≈2747 Ma to ≈2680 Ma),

referred to as pre-tectonic or syn-volcanic, are characterised by their large-batholitic size and predominantly high-Al TTG geochemical signatures; examples of this group are the Round Lake, Kenogamissi, and Lake Abitibi batholiths, among others. The second group of plutons (i.e., ca. ≈2693 Ma to ≈2685 Ma), referred to early-syntectonic, is dominated by feldspar and quartz-feldspar porphyries. These are especially abundant along the major structural breaks, such as the Porcupine-Destor fault zone (PDFZ) near Timmins. The next group at (i.e., ca. ≈2686 Ma to ≈2676 Ma) include syntectonic granodioritic and lesser quartz-monzodioritic intrusions that were emplaced synchronously with the first regional deformation event, preferentially within the central part of the AGB. Finally, the late-tectonic plutons emplaced between ≈2680 and ≈2668 Ma are characterised by their alkaline affinity (i.e., syenitic), and their common spatial association with major regional faults, Timiskaming type sedimentary rocks, and Au mineralisation (e.g., syenite associated deposits; Robert, 2001).

Some of the most important gold mining camps in the AGB are located along major structural breaks, especially the PDFZ and the Cadillac-Larder Lake fault zone (CLLFZ). The area of this study is located 15 km south of the Kirkland-Lake camp (Fig 2), on the common border of the Boston, McElroy, Pacaud, and Catharine townships. The most comprehensive geological study of this area was presented by Jackson (1994), who described the stratigraphy in this area as comprising three different metavolcanic units; the nomenclature of these units was subsequently redefined by Ayer et al. (2005) for the Ontario side versus the Quebec side of the AGB. Table 1 shows the equivalence between the units proposed by Jackson (1994) and those from Ayer et al. (2005) for the study area.

Table 1. Comparison of stratigraphic nomenclature for the study area from Jackson (1994) and Ayer et al. (2005)

Stratigraphic unit Jackson (1994)	**Assemblage Ayer et al. (2005)**	**Age – Ma Ayer et al.(2005)**	**Dominant rock type**
Skead assemblage	Upper Blake River	2701 – 2696	Felsic- to intermediate metavolcanic rocks
Catharine assemblage	Stoughton – Roquemaure	2723 – 2720	Ultramafic, mafic and felsic metavolcanic rocks

Pacaud structural complex	Pacaud	2750 – 2735	Ultramafic, mafic and felsic metavolcanic rocks

The larger study area is underlain by mafic to intermediate metavolcanic rocks that range in age from 2742 ± 2 Ma in the southwest part to 2711 ± 4 Ma to the north. The volcanic sequence strikes NW and dips sub-vertically to the NE with progressive younger ages in that direction. Several large granitoid bodies intrude the volcanic sequence.

The Round Lake batholith (RLB) outcrops 3 km south-west of the study area (Fig 2). The RLB is a large multiphase pluton, containing tonalitic to granodioritic phases, which is foliated along its margins. The RLB is described by LaFleur (1986) and Beakhouse (2011) and ages as old as 2743 ± 1 Ma are reported (Ketchum et al. 2008). However, the north-east margin of the RLB, which falls within the study area, has an age of 2697 ± 4 Ma (Ketchum et al. 2008). Late-tectonic, alkaline plutons outcrop 4 to 6 km north-east of the study area; they are primarily syenitic, although they may include mafic and ultramafic alkaline phases. This alkaline plutons include the Otto, Lebel, and McElroy stocks (Fig 2), and ages for these plutons range from 2680 ± 1 Ma for the Otto stock to 2673 ± 2 Ma for the Lebel stock (Ayer et al. 2000), which agree with the age of regional alkaline magmatism and the Timiskaming sediments in the AGB (Beakhouse, 2011).

Within the detailed study area of Fig , a series of north-west striking dykes intrude the mafic and intermediate metavolcanic rocks of the Stoughton – Roquemaure and Upper Blake River assemblages. For simplicity, this group of dykes is referred to herein as the Miller Dyke Complex (MDC). The MDC is characterised by four intrusive phases, with textures and modal compositions that include equigranular quartz-monzodiorites to tonalites; porphyritic tonalites to granodiorites; fine-grained aplitic dykes, and mafic dykes. The MDC comprises three intrusive centres located approximately 500 m apart, as well as smaller isolated dykes. From south to north, the intrusive centres are referred to as the Allied zone, Planet zone, and Meilleur zone (Fig 3). Although different intrusive phases are present in each one of these zones, the contacts between them are not clear or mappable due to their small size and scarcity of outcrops.

3. Methods

3.1 Fieldwork and Sampling

Mapping conducted in 2015 by Oban Mining Corporation was reviewed by the author and modified where necessary (Fig 3). In this study, field work focused on detailed lithological and alteration re-logging of 15 drill holes drilled in 2014 by Northstar Gold Corp, and 12 drill holes drilled in 2015 by Oban Mining Corp (now Osisko Mining Inc.), for a total of 5845.3 m of core.

3.2 Petrography

Seventy-two samples, mainly from drill core were collected for petrographic examination. Samples were selected to be representative of the spectrum of textural and compositional variations of the dykes, the different alteration assemblages, and the different mineralisation styles. Polished thin-sections were prepared and examined using an optical microscope in both reflected and transmission modes.

3.3 Scanning electron microscope (SEM) energy dispersive spectroscopy (EDS)

The SEM analyses focused on the identification of alteration mineralogy and assessment of textural features. Of the seventy-two polished thin sections, a subset of twenty-three representative samples was examined using a JEOL6400 scanning electron microscope-energy dispersive spectrometry (SEM-EDS) in the Central Analytical Facility (CAF) at Laurentian University. The data were collected using an accelerating voltage of 20 kV, beam current of 1 nA and collection time of 5 seconds for spot analysis, although longer times were used for X-ray mapping. The data were processed using the INCA software package from Oxford Instruments.

3.4 Geochemistry

Twenty-one samples were collected from drill core and outcrops for whole-rock geochemistry and were included as part of the petrographic study referred to above. The samples were prepared at ALS Laboratories in Sudbury, Ontario by crushing until 70% < 2 mm; splitting off 250 g; and pulverizing the split until 85% < 75 microns. Then the samples were analysed at ALS Burnaby, BC according to the procedures described in Table 2 (ALS, 2016).

Table 2. Summary of analytical methods used for lithogeochemical analysis of rock samples.

Method	Element – Detection Limit	Description
ME-ICP06	Al_2O3, BaO, CaO, Cr_2O_3, Fe_2O_3, K_2O, MgO, MnO, Na_2O, P_2O_5, SiO_2, SrO, TiO_2, LOI (0.01 – 100%)	Lithium borate fusion, acid digestion and ICP-AES
ME-MS81	Ba 0.5-10,000, Hf 0.2-10,000, Sn 1-10,000, Y 0.5-10,000, Ce 0.5-10,000, Ho 0.01-1,000, Sr 0.1-10,000, Yb 0.03-1,000, Cr 10-10,000, La 0.5-10,000, Ta 0.1-2,500, Zr 2-10,000, Cs 0.01-10,000 Lu 0.01-1,000 Tb 0.01-1,000, Dy 0.05-1,000 Nb 0.2-2,500 Th 0.05-1,000, Er 0.03-1,000 Nd 0.1-10,000 Tm 0.01-1,000, Eu 0.03-1,000 Pr 0.03-1,000 U 0.05-1,000, Ga 0.1-1,000 Rb 0.2-10,000 V 5-10,000, Gd 0.05-1,000 Sm 0.03-1,000 W 1-10,000 (PPM except when % is indicated)	Lithium borate fusion, acid digestion and ICP-MS
ME-MS61L	Ag 0.002-100, Cu 0.02-10,000, Na 0.001%-10%, Sr 0.02-10,000, Al 0.01%-25%, Fe 0.002%-50%, Nb 0.005-500, Ta 0.01-500, As 0.05-10,000, Ga 0.05-10,000, Ni 0.08-10,000, Te 0.04-500, Ba 1-10,000, Ge 0.05-500, P 0.001%-1%, Th 0.004-10,000, Be 0.02-1,000, Hf 0.004-500, Pb 0.01-10,000, Ti 0.001%-10%, Bi 0.005-10,000, In 0.005-500, Rb 0.02-10,000, Tl 0.004-10,000, Ca 0.01%-25%, K 0.01%-10%, Re 0.002-50, U 0.01-2,500, Cd 0.005-1,000, La 0.005-10,000, S 0.01%-10%, V 0.1-10,000, Ce 0.01-500, Li 0.2-10,000, Sb 0.02-10,000, W 0.008-10,000, Co 0.005-10,000, Mg 0.01%-25%, Sc 0.01-10,000, Y 0.01-500, Cr 0.3-10,000, Mn 0.2-50,000, Se 0.2-1000, Zn 0.2-10,000, Cs 0.01-500, Mo 0.02-10,000, Sn 0.02-500, Zr 0.1-500 (PPM except when % is indicated)	Four acid digestion and ICP-MS
Au-ICP22	Au (0.001 – 10 ppm)	Gold by fire assay and ICP-AES in 50g nominal sample weight
C-IR07	C (0.01 – 50%)	Total Carbon by Leco furnace

The lithogeochemical samples were selected to characterise the different intrusive phases, alteration types, and to evaluate element mobility during alkali metasomatic processes. Assay results from the 2014 and 2015 drilling campaigns were provided by Northstar Gold Corp and Oban Mining Corp (now Osisko Mining Inc). The assay data were used to characteristize the

different styles of mineralisation, but are not included within the thesis as the data is confidential. All the data were reviewed, processed, and analysed using ioGAS® software version 6.2.1.

3.5 Geochronology

Samples were collected to determine the age of emplacement of the dykes, to constrain the age of the main sodic alteration episodes, and to constrain the timing of Au mineralisation. A sample of a weakly altered equigranular intrusive (MI-PL-DAT-01), collected from an outcrop at the Planet zone, was submitted to the GeoAnalytical Lab at Washington State University for in situ U-Pb zircon geochronology; the complete analytical details are provided in Chang et al (2006). Additionally, a polished thin section was sent to the LA-ICP-MS facility at the University of New Brunswick for in situ U-Pb age determination of hydrothermal titanite grains with the complete analytical details described in McFarlane & Luo (2012). Lastly, three samples of molybdenite from veins and breccias, collected from the three different zones of the project (Allied, Planet, and Meilleur) were sent to the crustal geochronology laboratory at the University of Alberta for Re-Os geochronology with the detailed analytical procedures provided in Selby & Creaser (2004). Detailed results are provided in Appendix 3 and a summary for each method is presented below within the results section.

4. Results

4.1 Geology of the Miller Dyke Complex

The MDC shown in Figure 3 (Allied, Meilleur, and Planet intrusions), as well as smaller isolated dykes, occur along fault zones associated with the Catharine Fault system (Fig 2), which extends for at least 10 km. The Allied and Planet intrusions are hosted by a mafic metavolcanic unit, consisting of y massive, aphanitic basalt with lesser pillow and variolitic flows; whereas the Meilleur intrusion is hosted by intermediate volcanic rocks that are typically porphyritic and have an andesitic composition. The alteration in both volcanic units is mainly chlorite,

carbonate, epidote, actinolite, with minor sericite zones in the andesitic unit (the latter only observed in drill core). Multiple gold occurrences occur within and around the intrusions, where they are associated with small shear or fracture zones hosting centimetre-scale quartz veins with tourmaline and pyrite. Some of these occurrences were extensively trenched or pitted and they constitute most of the surface gold anomalies shown in Figure 3. Fracturing and quartz veining associated with mineralisation typically has a NW strike, similar to the dykes and the regional orientation of the Catharine Fault zone. Despite the number of gold anomalies, no wide or well-defined veins were observed during mapping or in drill core; most of the quartz veins hosted by the MDC dykes are centimetre-scale, strike NW and dip shallowly to the NE or SW.

The dyke complex is multiphase, and displays both textural and compositional variations. Mineralisation is hosted within the dykes and their adjacent wall rocks; the different styles are described below.

4.2 Petrology of the Dyke Rocks

Four intrusive phases have been recognised at the MDC (Fig 4). There are three felsic intrusive phases. The first and volumetrically most significant is equigranular, medium-grained, and mainly composed by euhedral to subhedral crystals of plagioclase (≈70 – 85 %), K-feldspar (15 – 20 %), quartz (5—15 %), hornblende and/or biotite (0 – 10 % combined) (Fig 4A); the feldspars are generally red in hand sample and cloudy in thin section, affected by sericite alteration and exhibiting polysynthetic, tartan and minor chessboard twinning. Biotite and hornblende are the only mafic minerals present, both always chloritised. Accessory phases include magnetite, zircon, apatite, and titanite. The second phase is medium to coarse-grained porphyritic (Fig 4B), showing euhedral to subhedral phenocrysts (60 – 70 %) of plagioclase and K-feldspar; the groundmass (30 – 40 %), contains feldspar, quartz, and accessory zircon, titanite, and apatite. Mafic minerals are uncommon but fine-grained phenocrysts of chloritised hornblende are recognised. The third felsic intrusive phase is represented by fine-grained aplitic dykes, with granular or saccharoidal texture, comprised of feldspar and quartz in similar proportions; with no mafic minerals present. A common characteristic of the three felsic phases is a red-brick to

pink colour (Fig 4A, B, C), which is variable in the equigranular and porphyritic phases and generally more intense in the aplitic phase.

The only mafic phase present is sparse, and it is fine-grained porphyritic; characterised by euhedral plagioclase and amphibole phenocrysts in a very fine-grained groundmass where only feldspars are identified. In terms of temporal relationships among the three felsic phases, the porphyritic phase crosscuts the equigranular phase and it is cut by the aplitic phase. No direct crosscutting relationship was observed between the mafic dykes and any of the felsic phases; it was only observed within the metavolcanic host rocks.

Modal compositions for the felsic dykes include quartz monzodiorite, monzodiorite, quartz diorite, and tonalite, (Fig 4). These modal classifications are based on weakly to moderately altered samples, whose texture and composition have not been completely modified by hydrothermal alteration and are assumed to reflect the original mineralogy. Textural, chemical, and mineralogical variations from this baseline are considered in further sections below.

Based on twinning, plagioclase feldspar with polysynthetic twinning is more abundant than K-Feldspar with tartan twinning; hydrothermal albite characterised by chessboard twinning is also observed. SEM – EDS analyses of feldspars indicate that most of the plagioclase is end member albite Ab_{100}. Compositions of feldspars from five least altered equigranular and porphyritic felsic dyke samples were estimated to determine the magmatic composition of the feldspar before alteration; these compositions are summarised in Figure 5. Least altered samples were selected based on the degree of textural preservation, as well as the presence of magmatic mafic minerals (hornblende, biotite), and primary K-feldspar and quartz. Point analyses for the feldspar grains indicate that remnants of calcium are present in only a few of the least altered plagioclase grains where compositions indicate oligoclase (An_{30-10}). The most calcic composition is An_{66} (sample MI-PL-PET-02). A summary of the characteristics of the described intrusive phases is presented in Table 3.

Table 3. Summary of characteristics of the different intrusive phases observed at the MDC

Intrusive phase	Texture	Grain size	Phenocrysts	Modal composition
Felsic I	Equigranular	Medium – coarse	N/A	Quartz monzodiorite Monzodiorite Quartzdiorite Tonalite
Felsic II	Porphyritic	Medium – coarse	Plagioclase, K-Feldspar, Quartz	Granodiorite Quartzdiorite Tonalite
Felsic III	Aplitic	Fine	N/A	Tonalite
Mafic	Porphyritic	Fine	Plagioclase, Amphibole	

4.3 Mineralisation

Three mineralisation styles were observed, and features which typify them are summarised in Table 4, including geochemical characteristics from multi-element assays. These styles are described in sequence and then their timing relationships are described.

4.3.1 Quartz vein mineralisation

The most important Au mineralisation style is represented by quartz veins, mainly hosted within the felsic dykes, although locally present in the volcanic wall-rocks. The veins are generally poor in sulfides, with <2% total pyrite, trace tellurides and bismuth minerals. Visible gold (VG) presence is sporadic and fine-grained (<500µm). Carbonate and tourmaline are locally present as accessory minerals within the veins. The veins are commonly 1-5 cm wide, flat, planar, and oriented subparallel (i.e., sheeted) rather than as stockwork zones (Fig 6A to F). Vein density ranges from 1-2 veins/m up to >20 veins/m. Zones of Au-bearing veins are intersected over 100 m wide intervals in drilling, and they represent the main exploration target for bulk mineralisation. Au assays range from a few hundred parts per billion (ppb) to several parts per million (ppm) (≈100 ppb Au to 1-2 ppm Au) for 1m average core samples.

4.3.2 Contact hosted mineralisation

The second style of mineralisation occurs at the contact between felsic dykes and mafic metavolcanic rocks. The contact zones are commonly intensely fractured for several meters perpendicular to the contact, and altered to a fine-grained assemblage of carbonate, albite, chlorite, pyrite and trace chalcopyrite (Fig 7A, B, C, D). Pyrite, up to 10% by volume, occurs as subhedral crystals with fine inclusions of rutile, apatite, xenotime, and chalcopyrite. Anhedral chalcopyrite was observed filling fractures and interstitial to silicate minerals. Although gold grades associated with this style are generally > 1ppm and occasionally > 10ppm Au, gold was not observed during SEM imaging. This style of mineralisation records the highest-grade intersections and represents an important exploration target.

4.3.3 Disseminated and patchy mineralisation

The third and least economically significant mineralisation style is represented by disseminated and patchy sulfides, principally pyrite, chalcopyrite, and molybdenite, that are randomly distributed within cavities in the sodic altered rocks (Fig 8D, E, F), or along the margins of some irregular, discontinuous and truncated quartz - chlorite veins (Fig 8A, B, C). Erratic gold values (e.g., from <0.1 ppm to 2.4 ppm) are associated with this style, but anomalous Cu (500 ppm – 3.5 %) and Mo (50 ppm – 5900 ppm) values are characteristic. Chalcopyrite was also observed in microfractures within titanite crystals in cavities.

The timing relationships among these three mineralisation styles are not clearly defined. The quartz vein mineralisation crosscuts all the intrusive phases, except the mafic dyke rocks. The disseminated and patchy Cu-Mo ± Au mineralisation is interpreted to postdate the quartz vein mineralisation because it occurs within the margins of, and in fractures that cut irregular quartz veins, as well as lining cavities in episyenites. The timing relationship between the contact hosted mineralisation and other styles of mineralisation styles is unknown.

Table 4. Summary of mineralisation styles present at the Miller Dyke Complex.

Mineralisation style	Ore mineralogy	Extension in drill	Au grades

		hole	
Quartz vein hosted	Py, ± Tellurides, ± VG	From ~10m to 100 m	From 0.1 ppm to ~2 ppm
Contact zone hosted	Py, ± Ccp	From <1m to 5 m	From 1 ppm to 20 ppm
Disseminated – sodic alteration associated	Py, Ccp, Mo	From ~1m to ~40 m	Erratic and from barren to ~2 ppm; locally elevated Cu-Mo

4.4 Alteration

Albite is the most abundant and important alteration mineral present at the MDC. It is the focus of this project; its characteristics and relationship with mineralisation are described and discussed in the following sections.

4.4.1 Albite Alteration

Albite alteration has been classified into three groups based on their distribution and relative timing. These three groups are explained below.

4.4.1.1 Albite Alteration 1

Albite alteration 1 is manifest as albite-pyrite envelopes mantling Au-bearing quartz veins that cross-cut felsic dyke rocks. The albite-pyrite alteration grades outward to chlorite-calcite-pyrite and then to distal calcite-chlorite (Fig 9A, B, C). However, not all Au-bearing quartz veins have this sequence of alteration uniformly developed, and in some cases, one or more of the envelope zones can be absent. The albite-pyrite envelopes range from mm to cm in width and increase with increasing vein width. Albite-pyrite alteration zones range in colour from very intense red to white, with pink being the most common colour (Fig 9D, E); pyrite is generally <1%. Two textural varieties of albite are observed: 1) large albite crystals or crystals aggregates that range between 400 µm and 1mm, often with chessboard twinning and irregular, "corroded" borders (Fig 9F); and 2) aggregates or masses of very fine-grained, anhedral albite

where singular grains are smaller than 50 µm; this type occurs in open spaces or embayments on vein margins (Fig 9F).

4.4.1.2 Albite Alteration 2

Albite alteration 2 is pervasive and affects most of the dykes at the MDC. Characteristic of this alteration is the replacement of primary plagioclase and K-Feldspar by albite (Ab_{100}). The albitisation preserves the original euhedral to subhedral shapes of the feldspar crystals. Fine-grained inclusions of sericite are abundant in albite grains, and their abundance correlates with a reddish to pink colour of the rocks (Fig 10A, B), and creates a dark-brown, rusty appearance on the crystals when observed in thin section (Fig 10E, F). Another characteristic of this alteration is the development of microporosity (Fig 10D) that ranges from <1 µm to ~50 µm within the Ab_{100} grains. Some dykes, generally those located towards the edge of the Allied zone in the mineralised area, have a dark-grey colour rather than red (Fig 10C); however, SEM-EDS analyses indicate that in these rocks the feldspars are still predominantly albite in composition.

Albite 2 alteration is occasionally manifest by the presence of macroscopic pores or cavities in the new hydrothermal albite. The size of the pores ranges from hundreds of microns to several millimetres and their shapes can be sub-rounded to angular. The percentage of these cavities is variable, ranging from 1% up to 30%, and they impart a strong vuggy texture to the rock. (Fig 11A, B). The presence of these cavities coincides with a depletion of quartz and mafic minerals; however, the primary porphyritic or equigranular textures of these rocks are still recognised. In hand sample, the zones of Albite 2 with this texture vary in colour from very light pink to dark reddish, and the cavities are partially coated by fine pink to translucent albite (Ab_{100}) and locally K-feldspar (Fig 11C). These pores are either completely or partially filled by different minerals including chlorite, epidote, titanite, apatite, zircon, pyrite, chalcopyrite, and molybdenite (Fig 11D, E and Fig 12A to F). After fine albite, chlorite is by far the most abundant alteration mineral within the cavities. It is fine-grained, ranging from massive to vermicular. Titanite is also very common; it is intensely fractured and generally euhedral to subhedral and up to 3 mm in size. Epidote and apatite, both as subhedral to euhedral crystals, are less common. Pyrite is the

most ubiquitous sulfide and displays variations in size (<50µm to 1 mm) and shape (subhedral to euhedral). Chalcopyrite and molybdenite are common and typically occupy the central part of the cavities (Fig 8E, F). Chalcopyrite is also present along fractures in pyrite or titanite crystals.

4.4.1.3 Albite Alteration 3

Albite alteration 3 occurs in metavolcanic rocks adjacent to the felsic dykes. In hand sample (Fig 13A), this alteration has a brown-beige colour. Its consists on a fine-grained mineralogical assemblage only identifiable using the SEM-EDS (Fig 13B), which includes an assemblage of albite-calcite-chlorite-pyrite ± chalcopyrite. This alteration only occurs in highly fractured metavolcanic rocks, where the intrusions exhibit a high density of veins, or where there are numerous dykes close to the contact. This albite alteration is associated with Au grades > 1ppm, and often >10 ppm, forming drill hole intersections up to 4m with 12 ppm. Despite the high grade of these contact zones, native gold was not observed in any of the samples examined either petrographically or with the SEM. Apatite and xenotime are common accessory minerals.

4.4.2 Skarn Alteration

The presence of "skarn-like" alteration is restricted to metavolcanic rocks near the contact with the felsic intrusive phases. It is very common, although not volumetrically significant. It consists of cm-size patches and thin (1-3cm) veins of garnet – chlorite – calcite – epidote – pyrite ± chalcopyrite ± magnetite (Fig 14A, B). The skarn patches may be zoned or irregular. The alteration contains up to 15% pyrite with trace chalcopyrite but is typically barren of gold.

4.4.3 Chlorite – clay and quartz-hematite alterations

Chlorite-clay (Fig 14C, D) or quartz-hematite (Fig 14E, F), present in small veins or breccia zones, crosscut all the previously described alteration types. The chlorite-clay association is more abundant, and it forms the matrix to cm to m-size breccia zones containing fragments of felsic intrusive or metavolcanic rocks, as well as vein fragments. Chalcopyrite is often present as a

cement around some of the broken vein fragments. As this alteration is not associated with gold mineralisation it is not described or discussed further.

The silica – hematite assemblage occurs as very thin stringers, and patches of fine grained reddish quartz, which resembles jasperoid, lining fractures in altered and broken core. These veins crosscut the chlorite-clay breccias, as well as the Au-bearing quartz veins. Sulfides are not associated with this assemblage. White to locally pink carbonate is present as calcite veins, dissemination and as a breccia matrix.

4.5 Geochemistry

The major, trace, and rare earth (REE) data for 21 analysed samples of dykes are presented in Appendix 2 and a summary of the most relevant elements used in the presented diagrams is shown in Table 5. The data are discussed in the context of rock classification, major and trace element data, and mass balance in the following sections.

4.5.1 Rock classification

The classification of the MDC dykes is challenging due to the mobility of major elements associated with feldspars but also trace elements contained in secondary phases developed within the cavities of some of the altered dykes.

Despite the expected mobility of Na and K, SiO_2 seems to be relatively stable (Fig 17), and the dykes can be grouped based on their silica content. The samples fall into three main groups, which correspond to their textural and petrographic characteristics; these are mafic dykes, felsic dykes (equigranular and porphyritic) and aplitic dykes. The rocks are classified according to their position in Zr/TiO_2 versus Nb/Y diagram. The two mafic dyke rocks analysed have SiO_2 values around 50 wt. % and plot in the andesite/basalt field of the Zr/TiO_2 versus Nb/Y diagram (Fig 15).

Table 5. Geochemical data used in figures beow. Major and trace element data analyized using ALS methods ME-ICP06 and ME-MS81, respectively, as described in Table 2.

	MI-PL-LGC-01	MI-PL-LGC-02	MI-AL-LGC-03	MI-AL-LGC-04	MI-AL-LGC-05	MI-AL-LGC-06	MI-AL-LGC-08	MI-AL-LGC-09	MI-AL-LGC-11	MI-AL-LGC-12	MI-AL-LGC-13	MI-AL-LGC-15	MI-AL-LGC-16	MI-AL-LGC-17	MI-AL-LGC-21	MI-AL-LGC-23	MI-ME-LGC-24	MI-ME-LGC-25	MI-ME-LGC-26	MI-AL-LGC-27	MI-AL-LGC-28
Ba	1570	344	1180	994	562	627	1070	783	960	124	65.3	326	149	193.5	104.5	1815	96.7	1260	1250	908	93.8
Ce	41.1	8.6	50.6	47.8	43.8	68.1	57.2	51	51.9	38.5	6.6	39.7	15.8	5.7	13.2	51.4	18.7	48	48.7	58.1	2.8
Cr	30	10	20	20	20	30	30	40	20	20	20	40	10	20	10	20	140	20	20	40	10
Cs	2.04	3.66	1.96	1.23	0.92	1.33	1.16	1.11	1.44	0.44	0.17	1.07	1.54	1.09	0.85	3.75	6.33	1.86	0.9	1.01	0.09
Dy	1.27	0.23	1.25	1.37	1.09	1.31	1.64	1.62	1.42	1.27	1.11	1.07	0.18	0.67	6.18	1.48	4.36	1.27	1.22	1.69	0.44
Er	0.52	0.14	0.67	0.72	0.59	0.73	0.84	0.76	0.8	0.7	0.59	0.49	0.15	0.35	3.98	0.67	2.68	0.58	0.72	0.8	0.34
Eu	0.89	0.17	0.74	0.73	0.66	0.92	0.96	0.99	0.77	0.77	0.63	0.6	0.11	0.33	1.39	1.02	1.14	0.83	0.75	0.95	0.35
Ga	19	18.2	19.2	19.3	20	21.2	20.1	20.6	18.6	20.6	23.9	17.1	19.1	16.5	22.6	21.1	19.2	19.6	19.3	19.7	19.7
Gd	2.25	0.3	2.06	2.09	1.68	2.24	2.66	2.69	2.33	2.11	1.95	1.39	0.23	1.01	5.23	2.53	3.94	1.9	2.01	2.74	0.93
Hf	3.3	2.2	3.6	3.8	3.5	3.7	3.7	3.8	3.8	3.9	4.1	2.6	2.5	3.1	3	3.8	2.5	3.6	3.4	4	3.2
Ho	0.24	0.04	0.25	0.25	0.22	0.24	0.3	0.33	0.28	0.22	0.23	0.19	0.05	0.14	1.33	0.26	0.98	0.25	0.23	0.27	0.1
La	21	4.1	28.2	24.7	23.1	39.9	31.1	27.7	26.2	17.5	2.1	21.5	11.3	2.5	4.8	26.9	8.6	26	26.2	30.7	0.7
Lu	0.08	0.03	0.1	0.1	0.1	0.09	0.11	0.12	0.11	0.12	0.08	0.09	0.06	0.08	0.5	0.1	0.42	0.09	0.11	0.09	0.11
Nb	6.9	3.5	7.4	7.3	6.9	7.7	6.8	6.7	7.7	6.5	7.9	2.8	3.8	3.8	3.6	5.6	4.2	6.5	6.2	6.6	4.1
Nd	18.5	3.3	19.2	19	17.3	25.3	24.7	21.8	20.6	16.7	7.7	15	3.4	3.8	11.3	23.4	12.2	18.8	19.9	24.2	3.4
Pr	5.08	0.92	5.57	5.48	5.16	7.77	6.78	6.15	6.1	4.71	1.34	4.57	1.25	0.84	2.2	6.38	2.64	5.55	5.62	6.86	0.54
Rb	83.4	167	103	87.6	68.6	68.7	73.7	74.3	83.9	13.6	4.9	50.3	81.2	92.5	9.2	111.5	5.7	105	85.9	58.6	4.3
Sm	3.35	0.64	3.27	3.22	3.02	3.7	4.06	3.72	3.56	3.15	2.57	2.18	0.44	1.03	3.99	3.97	3.57	3.07	3.12	3.95	1.25
Sn	1	0.5	1	1	1	1	1	1	1	1	1	0.5	0.5	0.5	1	1	1	1	1	1	0.5
Sr	925	146.5	446	302	232	263	618	340	262	181	145	204	53.8	43.7	200	1090	350	673	723	527	37.1
Ta	0.4	0.3	0.4	0.5	0.4	0.5	0.4	0.4	0.5	0.4	0.5	0.2	0.2	0.3	0.3	0.4	0.3	0.4	0.5	0.4	0.3
Tb	0.27	0.04	0.23	0.27	0.21	0.25	0.35	0.32	0.26	0.26	0.22	0.17	0.04	0.11	0.94	0.32	0.68	0.23	0.25	0.33	0.08
Th	3.44	4.13	4.96	5.35	5.43	5.62	5.21	4.95	5.03	5.23	6.48	3.54	7.87	9.43	0.34	3.91	0.72	5.08	5.43	5.31	8.23
Tm	0.08	0.03	0.09	0.08	0.09	0.1	0.12	0.12	0.12	0.11	0.07	0.07	0.02	0.06	0.55	0.08	0.42	0.1	0.15	0.11	0.06
U	1.42	2.12	1.95	2.44	2.54	2.57	2.05	2.08	3.08	2.04	2.47	0.85	3.35	3.62	0.14	1.86	0.2	1.9	2.14	1.97	2.64
V	30	2.5	33	35	40	39	45	61	31	38	51	31	2.5	2.5	408	41	348	28	29	41	2.5
W	1	1	1	2	4	3	3	9	1	1	1	2	1	1	1	0.5	0.5	0.5	0.5	1	0.5
Y	6.1	1.7	6.9	7	5.9	7.7	8.6	9.2	7.7	7.1	6.6	5.6	1.8	4.7	34.3	7.7	25	6.8	7	8.1	4
Yb	0.46	0.17	0.68	0.71	0.56	0.7	0.69	0.88	0.76	0.74	0.52	0.59	0.21	0.46	3.57	0.64	2.74	0.61	0.64	0.67	0.45
Zr	126	45	136	141	131	146	144	146	156	148	157	112	58	72	106	144	92	130	134	151	72
SiO2 %	69.8	78	71.5	68.5	71.4	67.9	66.7	66.4	68.4	72.4	65.2	68.1	77.5	75.7	50.7	68.5	49.2	70.1	70.8	69.2	70.7
Al2O3 %	15.05	12.55	14.3	14.5	14.4	15.05	15.05	15.4	15.6	15.4	18.5	15.45	12.6	11.85	12.25	16.1	13.9	14.75	14.9	14.8	18.2
Fe2O3 %	2.54	0.86	2.38	2.29	1.97	2.98	3.18	3.06	2.25	2.3	3.41	3.12	0.81	0.82	18.6	3.25	12.8	2.17	2.14	3.01	0.7
CaO %	2.03	0.51	1.43	1.7	1.33	1.89	2.55	2.81	1.55	0.78	0.47	2.83	0.36	2.02	8.09	2.47	11.35	1.57	1.61	2.16	0.13
MgO %	0.94	0.13	0.8	0.78	0.74	1.19	1.28	1.06	0.94	1.1	1.74	1.53	0.06	0.06	4.39	1.2	7.33	0.77	0.75	1.32	0.14
Na2O %	4.97	4.1	5.12	5.54	6.05	6.17	5.4	5.79	6.06	7.93	9.51	5.71	5.24	4.38	2.03	5.17	1.97	5.47	5.49	5.51	10.2
K2O %	3.22	4.25	3.64	3.34	2.59	2.56	2.74	2.98	3.53	0.49	0.65	1.64	3.19	4.03	0.31	3.41	0.13	3.45	3.46	2.63	0.81
Cr2O3 %	0.005	0.005	0.005	0.005	0.005	0.005	0.01	0.01	0.005	0.005	0.005	0.01	0.005	0.005	0.005	0.005	0.02	0.005	0.005	0.01	0.005
TiO2 %	0.29	0.05	0.25	0.26	0.23	0.36	0.37	0.4	0.27	0.24	0.27	0.23	0.05	0.04	1.71	0.36	1.18	0.23	0.24	0.37	0.06
MnO %	0.04	0.01	0.03	0.02	0.02	0.03	0.05	0.03	0.03	0.02	0.02	0.05	0.01	0.01	0.25	0.05	0.22	0.04	0.04	0.05	0.005
P2O5 %	0.13	0.005	0.1	0.09	0.09	0.17	0.17	0.17	0.11	0.1	0.11	0.13	0.005	0.005	0.13	0.17	0.13	0.09	0.09	0.17	0.01
SrO %	0.11	0.02	0.05	0.04	0.03	0.03	0.07	0.04	0.03	0.02	0.02	0.02	0.005	0.005	0.02	0.12	0.04	0.08	0.08	0.06	0.005
BaO %	0.17	0.04	0.13	0.11	0.06	0.07	0.12	0.09	0.11	0.01	0.01	0.04	0.02	0.02	0.01	0.2	0.01	0.14	0.14	0.1	0.01
LOI %	0.85	0.28	1.3	1.79	1.76	2.23	1.9	3.03	1.68	1.07	1.56	2.66	0.46	1.74	1.76	0.85	2.58	1	0.71	1.63	0.34

The felsic dyke samples (n=16), which include porphyritic and equigranular dykes that are commonly associated with Au-Cu mineralisation have SiO_2 values between 65.2 and 72.4 wt. % and save for two samples plot in the trachyandesite field (Fig 15). The two remaining samples (MI-AL-LGC-15 and MI-AL-LGC-28) plot near the limit of comendite/pantellerite with trachyandesite (Fig 15). The latter sample has extremely low TiO_2 compared with the rest of the felsic dykes. The remaining three samples with the highest SiO_2 contents (75.7 to 78 wt. %) are representative of the aplite dykes. Two of these samples fall in the trachyte field, and one

sample (MI-AL-LGC-17) falls in the comendite/pantellerite field (Fig 15) due to its lower TiO_2 content.

4.5.2 Major element chemistry

In terms of alkali (Na_2O + K_2O) contents, the mafic dykes have an average value of 2.2 wt. %, whereas aplites and felsic dykes have values ranging from 7.35 and 11.01 wt. %, including samples with values of up to 10.2 wt. % Na_2O (sample MI-AL-LGC-28). The samples retain their three separate groupings and in the subalkaline field of Figure 16, except for three samples (MI-AL-LGC-11, 13, and 28) which have elevated alkali contents (>9 wt. %).

On Harker-type plots (Fig 17), the three lithological and geochemical groups clearly plot as different populations with defined elemental trends with respect to silica. The noted exceptions relate a few samples of felsic dyke rocks which show anomalous enrichment in Na_2O (7.9 to 10.2 wt. %) with complementary depletion in K_2O. Not shown in the Harker diagrams are the LOI data (see Table 5), which ranges from 0.28 to 3.03 wt. %, but does not show any particular trend.

4.5.3 Trace element chemistry

The three lithological and geochemical groups have distinct trace elements patterns, as illustrated in a primitive mantle (PM)- normalised spidergram (Fig 18) and chondrite-normalised REE diagram (Fig 19). The mafic dyke rocks are not shown in the trace element diagrams because they have a general flat pattern and are not associated with the sodic alteration process. In contrast, the felsic dyke rocks define a distinct field with enrichment in LILE and depletion in High Field Strength Elements (HFSE), (Fig 18). The felsic dykes display positive Ba and negative Th, Ta, Nb, P, and Ti anomalies. However, three felsic dyke samples (MI-AL-LGC-12, 13, 28) depart from the general pattern as they display relative depletion of the LILE Rb, Cs and Ba, and lesser so for U and K, and variable depletion for some of the HFSE (e.g., LREE), Sr and P.

Aplitic dyke samples are characterised by negative PM-normalised anomalies of Ba, Sr, P, Ti, Ta and Nb (Fig 18); sample 17 departs from the general behaviour of the aplites for some elements such as Sr, La, Tb, Y. The REE data normalised to CI chondrite (Fig 19) reflects the patterns noted in the PM spider diagram. The felsic intrusive dyke rocks show strongly fractionated patterns. The felsic dykes are characterised by: 1) High LREE (>100 times chondrite) and steep slopes with $(La/Lu)_N$ values up to and 47; 2) Insignificant Eu anomalies (Eu* = 0.81 to 1.18). However, two of the samples (13 and 28) depart from the pattern and show depletion of LREE and in one case also the HREE. The aplitic dykes have U-shaped REE patterns and lack Eu anomaly.

4.6 Geochronology

4.6.1 U-Pb dating of felsic dyke rocks

A sample of least altered, medium-grained, equigranular, reddish felsic dyke rock (MI-PL-DAT-01; Fig 20) with an apparently unmodified chemical signature (Fig 18) was selected for U-Pb dating. Zircons were separated and mounted for U-Pb analysis by LA ICP-MS. The results are summarised in Table 6 and presented in detail in Appendix 3. A total of 36 spots coming from 75 separated zircons were analysed and of these 34 were used to define a concordia age of 2662 ± 18Ma (Figure 20).

4.6.2 Re-Os dating of molybdenite samples

Three samples of molybdenite (MI-PL-DAT-12, MI-AL-DAT-18, MI-ME-DAT-17) collected from drillholes from the three intrusion centres, Planet, Allied, and Mellieur, and shown in Figure 21A to C, were sent for Re-Os geochronology. The details of the method are summarised in Appendix 3 and results presented in Table 4. The pooled results provide an age of 2680 ± 8 Ma, the error being reduced based on the fact that these four samples all represent the same mineralising event (R. Creaser, pers. commun., 2018). The significance of these results is

discussed in Section 5.4. In the three cases, molybdenite is accompanied by anomalous values of gold ranging between 2.1 and 6.4 ppm.

4.6.3 U-Pb dating of hydrothermal titanite

A polished thin section sample of altered felsic dyke rock (MI-AL-PET-70) containing hydrothermal titanite lining the walls of cavities in a breccia zone with quartz, calcite, chlorite, albite, and pyrite (Fig 22A, B) was selected for in situ U-Pb using LA ICP-MS methodology. Two subhedral grains (Fig 22C, D) were selected for dating and were examined using the SEM-EDS to select areas for spots analysis. The titanites are fresh, euhedral to subhedral with weak zoning due to variable Fe content, are variably fractured and contain pyrite and chalcopyrite inclusions. The points for analysis were selected in areas with few fractures so as to reduce the chance of compromising the U-Pb analysis. The low U content of the titanites, in places at or below the detection limit, compromised many of the analyses including all those from grain 2, which are therefore not reported. Of the 20 points with sufficient U to provide useful results, several were discordant (Fig 23A) and were omitted from the age calculation. The 11 remaining analyses define a concordia age of 2069 ± 6 Ma (Fig 23B).

Table 6. Summary of results for U-Pb and Re-Os geochronology samples from the MDC

Sample	Method	Mineral	Rock description	Concordia age
MI-PL-DAT-01	U-Pb	Zircon	Equigranular felsic dyke. Least altered sample	2662 ± 18 Ma
MI-PL-DAT-12	Re-Os	Molybdenite	Molybdenite – calcite veinlets in albite altered intrusive	2676 ± 12 Ma
MI-ME-DAT-17	Re-Os	Molybdenite	Molybdenite-albite bands in quartz veins with apparent crack and seal texture	2676 ± 12 Ma
MI-AL-DAT-18	Re-Os	Molybdenite	Molybdenite cementing hydrothermal breccia with fragments of	2690 ± 12 Ma 2685 ± 12 Ma (Duplicated)

			intrusive and quartz veins	
MI-AL-PET-70	U-Pb	Titanite	Cavity - Breccia zone in episyenite. Strong sodic alteration	2069.3 ± 6 Ma

5. Discussion

5.1 Origin of secondary textures

5.1.1 Dissolution of primary quartz

Several sodic-altered MDC intrusive rocks are characterised by low contents coinciding with the presence of cavities which are attributed to the removal of quartz. Quartz dissolution and alkali metasomatism are not necessarily related processes, but frequently occur together. This association is observed in granitic rocks globally, in localities including Africa, Australia, Brazil, and those from several Hercynian granitic massifs in western Europe. These latter settings are among the best-studied cases and documented by Cathelineau (1986), Recio et al.(1997), Rossi et al.(2005), Boulvais & Rouffet (2007), and López-Moro et al, (2013), among others.

As quartz is one of the most abundant minerals in the Earth´s crust, its behaviour in aqueous systems has been thoroughly investigated. Quartz solubility in pure water systems was first experimentally determined by Kennedy (1950), for temperatures up to 900°C and a pressure range between 200 and 1000 bars. Khitarov (1956), and Kitahara (1960) refined the model, whereas the more recent works of Manning (1994) and Akinfiev & Diamond (2009) have extended the fluid composition to include variables such of NaCl or CO_2 and also expanded the P-T range up to 1000°C and 2000 bars. These authors have demonstrated that quartz solubility increases with temperature and/or pressure, except for a very small window in P-T space where the solubility curves have a negative slope and is referred to as the quartz retrograde solubility region. The arrows in Figure 24 illustrate different paths to increase quartz solubility in an aqueous fluid.

Quartz dissolution at the MDC as well as that described by the aforementioned authors is a post-magmatic or sub-solidus process and therefore associated with the retrograde solubility field. Cathelineau (1986) and López-Moro (2013) estimated the temperature of this process, based on fluid inclusion studies, to have been between 250° and 400°C. The implicated fluids generally have low salinities (0-10 wt. % eq. NaCl) and were necessarily quartz undersaturated at some point. From Figure 24 it is apparent that a heating fluid or alternatively a cooling fluid within the retrograde solubility field can dissolve more silica and trigger quartz dissolution.

5.1.2 Nature of episyenites and relationship to mineralisation

The term episyenite, as originally proposed by Lacroix (1920), refers to hydrothermally altered rocks that are depleted in quartz and whose feldspars have been modified from their original compositions. Although is found in many different geological settings, episyenitisation is one of the least studied and understood post-magmatic alteration processes. The term is rarely used outside of Europe, where it has been studied in several Hercynian granitic massifs in Italy, France, and Spain.

Episyenitisation involves the leaching of magmatic quartz from an originally granitic rock, the precipitation of new alkali (K-Na) feldspar, and the displacement of the bulk composition of the original rock towards the alkali feldspar apex of a QAP diagram (around the syenitic field) (Streckeisen, 1976). Episyenites are characterised by the presence of pores or dissolution cavities, once occupied by quartz and other minerals. Despite the presence of these cavities, the primary texture of the rock is relatively well preserved or at least still identifiable in the remaining rock. The cavities are partly or wholly filled with a wide range of secondary minerals (Fig 12A to F) that can be deposited at any time after the dissolution episode. The episyenites then have enhanced porosity and permeability. As expected, this spatial overlapping of multi-generation minerals complicates the geochronological studies and the fluid pressure-temperature (P/T) assessment of these rocks.

Another important textural feature of episyenites is their common red-brick colour. This colouring has been explained by the presence of very fine-grained hematite inclusions within

albite crystals or by the presence of Fe^{+3} within the feldspar structure. A complete discussion about the red colouring in feldspars is presented by Putnis et al. (2007).

Although there is no formal classification scheme for episyenites, they have been divided on the basis of the composition of the secondary alkali feldspar, into sodic or potassic episyenites. Classification could also reflect the secondary mineralogy present in the cavities, thus albite-rich, chlorite-rich, epidote-rich, and so forth (López-Moro et al. 2013). The MDC episyenites are dominantly sodic, although some samples show a narrow rim of K-Feldspar lining the dissolution cavities (Fig 11).

Episyenites are known from many different locations and of variable ages through the geological record. Episyenites are generally barren of mineralisation, but they can contain a broad range of commodities, including U (Polito et al. 2009; Alexandre 2010; Ashton 2010; Wilde 2013; Dolníček et al. 2014), Sn-W (Borges et al. 2009; Charoy & Pollard 1989), and Au (Theodore et al. 1987; Jébrak & Harnois 1990; Jébrak 1992; Jébrak & Doucet 2002; Béziat et al. 2008; López-Moro et al. 2013). Many episyenites are located in shear zones or other structural features, and their enhanced porosity forms an excellent fluid pathway for metalliferous fluids.

Of the many settings described for episyenites, those associated with U deposits, are the best known and studied. Episyenites associated with Au have only been described in a few localities (see summary in Fig 25) and of these, only two locations have been reported in Archean rocks from the AGB, being the examples the Mesegay gold occurrence, located north from the PDFZ on the Quebec side of the AGB, hosted by the Archean Taschereau-Launay plutonic complex (Jébrak & Harnois, 1990; Jébrak, 1992; Jébrak & Doucet, 2002); and the Côté Gold deposit, hosted by the Chester intrusive complex (Katz et al. 2016) in the Swayze greenstone belt of Ontario. Episyenites are part of the mineralisation rocks in the former place, and post-date the gold mineralisation in the latter. In both locations, magmatic intrusion-related origins are proposed by the respective authors. The MDC represents the second report of episyenites in the Ontario side of the AGB, and the first directly associated with Au, Cu, Mo mineralisation.

5.1.3 Quartz vein dissolution

A particular set of irregular quartz veins (Fig 26A to F), clearly differ from the rectilinear Au-bearing veins described in previous sections, are characterised by abnormal geometry, lateral discontinuity, restriction to episyenites and strong correlation with chalcopyrite and molybdenite. These veins are interpreted here as affected by dissolution of quartz during the same event that produced the episyenites.

In other intrusion-related systems, such as porphyry systems, partial dissolution of veins is a key process in the formation of economic Cu, Mo, ± Au mineralisation. Landtwing et al. (2005), using fluid inclusions and cathodoluminescence imaging, demonstrated that the precipitation of bornite and chalcopyrite at the Bingham Canyon deposit, Utah, USA, occurred between 425° and 350°C, coinciding exactly with the quartz retrograde solubility field. The same relationship has been observed for many other porphyry deposits based on the texture of mineralised B-type veinlets in these systems (Gustafson & Hunt 1975; Sillitoe 2010). Of note is that B-type veins are characterised by granular quartz with a central or marginal suture of sulfide mineralisation (molybdenite, chalcopyrite, or pyrite) whereby the suture represents the filling of aligned dissolution cavities within the vein.

In the porphyry case, the formation and partial dissolution of B-type veins, as well as Cu-sulfide precipitation, is inferred to occur in a still hot, semi-plastic magma, near the ductile-brittle transition. In comparison, at the MDC the time lapse between vein formation and vein dissolution remains unknown. Remobilisation might explain erratic gold values around dissolved veins, but at present no textural or chemical evidence supports this scenario. Furthermore, some gold might also be genetically associated with the post-dissolution Cu-Mo mineralisation event.

5.1.4 Dissolution of mafic minerals

Hornblende and biotite are common minerals in least altered dykes of the MDC; however, their content decrease with progressive sodic alteration and they are absent in episyenites. Previous studies on episyenites do not indicate that leaching of mafic minerals occurs with quartz dissolution, but is our interpretation that this process occurred at the MDC. As will be

illustrated, mass balance calculations indicate liberation of Fe and Mg; these elements can either be removed by fluids or incorporated into secondary phases such as pyrite, hematite, or chlorite.

5.1.5 Brecciation and other textures

The association of episyenites with fracture or fault zones as well as their enhanced permeability concentrate the flow of hydrothermal fluids and facilitates the formation of multiple breccia zones (Fig 27 A, B, F) and overprinting of alteration textures. Although in most cases the primary igneous textures are preserved, extensive dissolution accompanied by the precipitation of alkali feldspars, resulted in some unusual textures as illustrated in Figure 27C, D, E.

5.2. Mineralogical changes associated with alkali metasomatism

Alkali metasomatism at MDC is mainly represented by different styles and episodes of albitisation, which are accompanied by a number of additional alteration minerals. Two basic mechanisms are considered for the formation of these minerals: 1) replacement of a pre-existing mineral phase through coupled dissolution-precipitation (CDP), and 2) precipitation of minerals in open spaces. Both are explained below, and textural examples at the macro and micro scales are provided.

5.2.1 Coupled dissolution-precipitation (CDP)

The CDP concept was originally proposed by Goldsmith & Laves (1954), as discussed in Ruiz-Agudo et al. (2014), to account for the transformation of feldspars under hydrothermal conditions. CDP is an important geological process that explains how a mineral is transformed into another in the presence of a fluid, in contrast to replacement by solid state diffusion. The CDP process can be applied to many types of hydrothermal alteration or metasomatism present and associated with multiple ore deposit types (Putnis & Austhreim, 2010). Despite this, the CDP process is rarely referred to in the ore deposit literature, reflecting the need for detailed

work at the microscopic scale and integration of the SEM or similar equipment. CDP is triggered by disequilibrium between a solid phase and a surrounding fluid, resulting in the dissolution of the solid at the mineral-fluid interface. Simultaneously, the fluid becomes saturated in one or more new minerals and starts precipitating them in the newly generated space around the partially dissolved parental crystal (Fig 28). Porosity and permeability are both necessary for maintaining fluid flow towards the centre of the original crystal and replacing it with the new mineral. This porosity may be generated by different mechanisms, such as differences in the molar volume between primary and secondary minerals, differences in the dissolution and precipitation rates, or fracturing. If the permeability is maintained, the process advances until eventually the parental crystal is entirely replaced by the new mineral with preservation of the external shape (i.e., pseudomorphic replacement). If ideal conditions are not maintained, the replacement can take place without preservation of crystal shape, creating abnormal crystals, crystals aggregates, or mineral zoning with the parental mineral preserved in the core surrounded by the newly formed mineral. Experimental reproductions of the CDP process, especially for different feldspar minerals, have been conducted extensively in recent years (Putnis 2002; Engvik et al. 2008; Putnis 2009; Hövelmann et al. 2010; Putnis & John 2010; Putnis & Austrheim 2010; Norberg et al. 2011; Ruiz-Agudo 2014; Norberg et al. 2014; and Putnis 2015). Such work has shown that the replacement of any feldspar by albite is an extremely fast process, with crystal growth rates of 50 to 100 μm attained in only a few weeks, at temperatures of 600°C. Such reaction rates are instantaneous with respect to geological time (e.g., 1 cm crystal only requiring a few years). Depending how much fluid can circulate through a magmatic-hydrothermal system and how long it can remain active, which is an average of 2.5 to 4 Ma in the case of porphyry deposits (e.g., Sillitoe & Mortensen 2010), the albitisation process could occur continuously and repeatedly over long periods of time. The process can also occur in different directions, for example: an original orthoclase crystal might be dissolved by a sodium-rich fluid and then albitised, but the character of the fluid can change, and the newly formed albite might be in disequilibrium with the surrounding fluid; resulting in potassic alteration, and formation of secondary orthoclase. The result of such a scenario is that two secondary feldspars spatially overlap in the same crystal leaving no evidence of the primary

magmatic mineralogy. Sodic alteration at the MDC is an example of this process, where the final observed product of extensive alteration is mostly albite, but in a few cases, remnants of K-feldspar are observed as either cores or rims in the aforementioned albite crystals (Fig 29).

It is suggested here that the CDP process is responsible for the formation of most of the secondary albite present in the MDC, except for albite hosted within dissolution cavities or around dissolved veins. The process also accounts for other observed alteration reactions, such as sericite replacing feldspars through dissolution along twinning planes, and chlorite replacing biotite and hornblende with pseudomorphic textures.

5.2.2 Precipitation in open spaces

In addition to the CDP process, which is responsible for mineral modifications at the crystal scale, occluding an open space is another way of forming a new alteration mineral in a host rock. For example, this is the mechanism by which veins are generated. A dilating fracture facilitates the circulation of hydrothermal fluids which can subsequently precipitate different minerals. Although several types of veins are common in the MDC, this section will focus on open spaces generated by dissolution of minerals, especially quartz, associated with the alkali metasomatism processes. Three specific types of open spaces were generated and subsequently used by fluids for mineral precipitation: 1) dissolution cavities associated with episyenitic textures, 2) dissolved margins of pre-existent quartz veins, and 3) micro-porosity generated in newly formed crystals due to negative molar volumes changes during the CDP process.

As previously discussed, dissolution cavities are generated by the dissolution of quartz, biotite and hornblende. These cavities were partially or totally filled with a variety of alteration minerals (Fig 12A to F), including albite, K-feldspar, chlorite, epidote, titanite, apatite, zircon, pyrite, chalcopyrite, and molybdenite. Dissolved veins margins are filled essentially by fine-grained chlorite and sulfides and provide an excellent time marker for the dissolution process. Micro-porosity in secondary albite crystals can be abundant, and it provides a host for

precipitation of minerals at a very small scale ranging from ~50 µm to nanometre size. Common minerals found in these pores include zircon and apatite.

5.3. Geochemical changes associated with alkali metasomatism

5.3.1. Major element chemistry

Alteration of the felsic dyke rocks resulted in modification of some major elements, such as Na, K, Al, Ca, and Fe, which reflects mineralogical changes in the altered rocks, such as the loss of quartz and mafic minerals. Despite the leaching of quartz, SiO_2 remained relatively stable due to the extensive crystallisation of albite, which contains 67% SiO_2. As an example, the least altered felsic dykes contain between 60 and 75 % total modal feldspar, whereas episyenites contain 90 – 95 % albite; the formation of this new albite requires a significant amount of SiO_2, that we interpret as coming from the leached quartz. The primary igneous composition of the dykes can not be accurately determined but only be approximated from the composition of the least altered sample, which petrographically equates to a quartz-monzodiorite and compositionally, based on the Zr/TiO_2 versus Nb/Y plots, falls in the trachy-andesite field (Fig 15). In that sense, we believe that the MDC comprises a group of dykes with different compositions, some of them towards the tonalitic side of the QAP diagram and others towards the granite or monzogranite side that have been homogeneized via albitisation.

Although Al is traditionally considered an immobile element, alkali metasomatic environments are one of the few situations where it can behave strongly mobile (Hövelmann et al, 2010; Norberg et al, 2014). Al_2O_3 was mobile during the destruction of original Ca-bearing plagioclase which for our least altered dyke may contain up to ≈25% Al_2O_3 (An_{30}) and precipitation of albite which only contains 20% Al_2O_3; biotite was also removed and contains up to 12% Al_2O_3. The dissolution of calcic plagioclase indicates the mobility of Ca, although the Ca content might be reflecting the presence of calcite as an alteration product. The femic elements, Fe_2O_3 and MgO, were mobile during the dissolution of biotite and hornblende, but a certain amount of Fe is retained in pyrite and chlorite. As illustrated in Figure 30, all the felsic dyke samples have

sodium values higher than those typical of comparable igneous compositions. As most of the feldspars are sodic end-member (Ab_{100}), the addition of Na to the system is strictly necessary. For example, some of the most altered samples with well developed episyenitic texture, especially sample MI-AL-LGC-28 show (≈10.2% Na_2O – 70.7% SiO_2 – 18.2% Al_2O_3), values that almost perfectly match the composition of ideal albite (≈11% Na_2O – 67% SiO_2 – 20% Al_2O_3), suggesting the total replacement of all the primary feldspars by albite, the destruction of all other magmatic minerals and the precipitation of a significant amount of albite within the dissolution cavities. Potassium values (Fig 30) for some samples, lie along a typical trend; however, some of the samples have low K, consistent with destruction of biotite and albitisation of orthoclase.

5.3.2. Trace and REE chemistry

Aplitic dykes display U-shaped HREE pattern, which is commonly observed in several aplites (Glazner et al. 2008). According to this author, the U-shape is caused by fractionation of hornblende and titanite in the parental magma and indicates a genetic relationship between the aplite and the pluton that is hosting it. Variations in the REE patterns for felsic dykes can be explained in terms of two processes: 1) alteration or dissolution primary REE-bearing minerals such as zircon, apatite, and titanite, which needs to be addressed with additional SEM work and 2) precipitation of similar REE-bearing phases within dissolution cavities; titanite, apatite and zircon were observed. Additionally, xenotime was observed in contact alteration zones.

Although minerals such as zircon, titanite and apatite are generally resistant to weathering and other physical processes, it has been shown that they can be also be affected by CDP processes, especially in strongly alkaline environments (Rubatto, 2008, Seydoux-Guillaume, 2012; Putnis 2002; Harlov et al. 2005). These workers have shown textural variations between pristine cores and generally porous reprecipitated rims, with significant differences in REE contents between the two zones. Also noted in these studies is the occurrence of new REE and HFSE-rich mineral phases (e.g., zircon, apatite, titanite) which precipitate in micro-pores and fractures of other alteration minerals. The CDP process affecting these phases may be triggered by either one or all of the following: 1) intense fluid mediated alteration; 2) deformation; or 3) radiation damage

where enrichment in U or Th is a factor. In the case of the latter, detailed geochronological studies of dissolved – reprecipitated zircons reveal substantial age differences between the time of formation of the original magmatic phase and the alteration event (Tomaschek et al, 2003).

The lack of Eu anomalies for the felsic dyke rocks is noted. This feature is known to characterize other felsic suites in the AGB (Beakhouse, 2011) and has been interpreted to reflect an oxidised melt which stabilizes Eu^{3+} over Eu^{2+}, a feature also known in some oxidised Phanerozoic porphyry deposit settings (Trail et al, 2012). In fact, Eu and Ce anomalies are often used as a proxy to determine the oxygen fugacity of the magmatic system. Europium speciation as Eu^{3+} inhibits partitioning of Eu into plagioclase and precludes, therefore, the formation of Eu anomalies.

In terms of the other trace elements, three strongly altered samples (MI-AL-LGC 12, MI-AL-LGC 13 and MI-AL-LGC-28) are depleted in some of the LILE, specifically Cs, Rb, Ba. These three elements are commonly associated with K in minerals such as feldspars and biotite, and their depletion coincides with the dissolution of these minerals in the felsic dyke rocks at MDC. Uranium and Th depletion coincides with negative anomalies in P, and Zr, suggesting again the alteration of phases such as apatite, zircon or titanite. Strontium displays both positive and negative anomalies in a chondrite-normalised plot (Fig 18). Strontium is preferentially accommodated in calcium-bearing plagioclase which was extensively replaced by albite.

5.3.3. Mass Balance

Mass balance is used to quantitatively assess the mobility of elements during hydrothermal alteration, metamorphism, and other geological processes. The isocon method (Grant, 1986) is a simple technique which provides a graphical estimate of mass or volume variations and mobility of chemical elements without significant data manipulation. The method is based on the graphical comparison of an altered sample with a least altered sample interpreted to be representative of its probable original composition. The immobile elements define the isocon

line, whereas elements showing relative gains and losses depart from this line and plot above or below the isocon, respectively.

Mass balance assessment of alteration for the MDC dykes is a challenge because superimposed alteration events has preculded recognition of precursors to monitor the successive stages (yypes) of altetraion. Thus, a least altered samples was used as a precursor from which to measure element mobility associated with multiple alteration events that reflect the entire alteration history of each sample. Additionally, geochemistry and petrography clearly indicate the mobility of major and trace elements that are traditionally considered immobile (Al, Zr, Ti, REE), complicating the construction of the isocon line.

Four samples with various degrees of alkali metasomatism were selected and individually compared with a representative least altered sample, basically to illustrate the issues with the mass balance at the MDC. The least altered sample was chosen based on preservation of magmatic K-feldspar and quartz, biotite and hornblende, preservation of the original magmatic texture,. The alteration intensity of the altered samples was assessed using compositional parameters, such as Na_2O, K_2O and Sr contents, the presence of Au mineralisation, and modification of primary textures. Of the aforementioned criteria, the Na_2O content seems to be the most appropriate parameter and samples are ranked in Table 7 in terms of their relative degree of alteration.

Table 7. Summary of samples used for the mass balance calculation

Sample	Na_2O content (%)	Au content (ppm)	Comments
MI-AL-LGC-01	4.97	<0.001	Least altered
MI-AL-LGC-15	5.71	0.011	
MI-AL-LGC-12	7.93	<0.001	
MI-AL-LGC-13	9.51	0.117	
MI-AL-LGC-28	10.2	0.009	Most altered

Figure 31 is a summary of the mass balance analysis for the samples listed in Table 4. Despite the problems described before, some patterns can be observed and are worth to mention here. Na_2O is enriched in all samples, up to 105% in the most altered sample. When mineralisation is present, as in samples LGC-15 and LGC-13, Au is strongly enriched along with elements

contained in sulfides such as Ag, Te, Bi, and S. Cu and Mo are generally lost indicating an initial enrichment in the least altered sample, but also indicating a poor correlation of these two elements with Au. K_2O is lost in all samples from 50% to 85%, as well as the large ion lithophile elements (LILE) associated with feldspars. CaO is generally lost up to nearly 100% as a consequence of the albitisation, except in the sample LGC-15 which seems to have an overprinting of carbonate alteration, indicated by a 500% gain in C. Mass changes are difficult to determine graphically because the isocon is not reliable; development of cavities suggests a loss of mass, but the general preservation of the texture indicates the volume could be preserved suggesting changes in the density of the rock.

5.4. Implications of the geochronological data

A goal of this study was to constrain the ages of: (a) the magmatism generating the MDC, (b) the alkali metasomatic processes affecting it, and (c) the mineralising events. The MDC is located between two clearly different magmatic domains: 1) the 2697 ± 4 Ma Round Lake batholith (Ketchum et al., 2008) which outcrops ~3 km SE from the study area (Fig 2) and is a pre-tectonic intrusion (Beakhouse, 2011); and 2) a group of late-tectonic plutons located near Kirkland Lake and which includes the Lebel and Otto stocks (Fig 2) with ages of 2673 ± 2 Ma and 2680 ± 1 Ma, respectively (Ayer & Trowell, 2000). Despite the significant error, the U-Pb zircon age of 2662 ± 18 Ma obtained for a least altered sample of the MDC overlaps with the Timiskaming magmatic event (2680 – 2668 Ma) (Beakhouse, 2011). The Timiskaming magmatic event represents widespread clastic sedimentation, alkaline magmatism and spatially related Au mineralisation.

Two mineralisation events are well defined at MDC: 1) the gold-bearing quartz veins that pre-date the episyenitisation process, and 2) the Cu - Mo ± Au mineralisation hosted by dissolution cavities, which post-dates episyenitisation and quartz veining. The pooled results from Re-Os geochronology (2680 ± 8 Ma), combined with the magmatic age suggests that the emplacement of the dykes, early albitisation, quartz veining, first Au mineralisation event, episyenitisation, and second Au – Cu - Mo mineralisation event occurred in a relatively short

period of time (2680 – 2674 Ma). This window of time implies that both mineralisation events are associated with the Timiskaming event.

The titanite hosted by dissolution cavities in the episyenites yielded an age of 2069 ± 6 Ma, which is significantly younger than the dykes and the Au mineralisation. The MDC titanite is hosted by a dissolution-brecciated zone very rich in Na, but also in metals with Au values as high as 3 ppm, Ag up to 4 ppm, Cu 1%, and Mo up to 6 ppm. In particular, the titanite analysed is cut by fractures with chalcopyrite (Fig 22C inset) which most likely indicates Paleoproterozoic remobilisation of metals at the local scale. This age is anomalous for the AGB, as noted by the fact that it is only the second Paleoproterozoic age reported from a gold deposit in the southern AGB. It follows on the recently reported 1730 ± 5 Ma U-Pb monazite age from carbonate-quartz-epidote-hematite veins at the Young-Davidson deposit ~50 km SW of Kirkland Lake (Zhang et al., 2014). These veins crosscut the Au-bearing syenite and post-mineral diabase dykes but are not directly associated with any mineralisation. In that case, the growth of monazite and vein formation is attributed to the far field 1750 – 1700 Ma Killarnean or Yavapai magmatic/metamorphic event, which may have reactivated Archean structures.

A number of dyke swarms have been dated through the Superior Province with ages between 2.2 and 2.0 Ga, from which the closest ones are the Marathon, Fort Frances, Senneterre, and Biscotasing (Hall & Davis, 2004), and they may be associated with the Paleoproterozoic hydrothermal activity at the MDC. Regardless of the source of the Paleoproterozoic fluids, reactivation of the Catharine fault system with related fluid circulation is considered a probable mechanism for the metal mobilisation through the already emplaced dykes. Thus the geochronological data and all the crosscutting relationships are used as the evidence for the paragenesis proposed for the MDC (Fig 33).

5.5. Considerations about the alkaline fluids

Results of the research provide the foundation for interpreting a hierarchy of fluid flow pathways and related alteration in the hydrothermal system at the MDC. Assuming that the source of the fluids resulting in the intense metasomatism of the MDC is the group of plutons

that comprise the Otto and Lebel stocks, and that the MDC is temporally related to this magmatic event around ~2680 Ma, it is suggested that the Catharine fault system acted as a first-order structure that permitted the emplacement of the dykes and later was a long-lived and reactivated conduit for fluid flow during the various stages of alteration. The Catharine fault system (Fig 2) is an NW striking structural zone running close to the contact between the mafic rocks of the Stoughton-Roquemare assemblage and the intermediate to felsic rocks of the Upper Blake River assemblage. The fault is not considered to be a single structure but a composite one (Fig 32A), because some of the dykes of the MDC are located on its north side (Meilleur zone) whereas the rest is on its southern side (Allied and Planet zones). The Catharine fault has been interpreted as formed synchronously or slightly after the emplacement of the Round Lake batholith (2697 ± 4 Ma), and to dip at a high angle to the NE (Jackson, 1994). The fault zone is characterised by abundant carbonate alteration and associated sulfides, fracturing, and quartz veining which comprise a number of small mineral occurrences.

Second order pathways are represented by small fracture or fault zones crosscutting the dyke rocks, which host intense alteration zones such as breccia and episyenite bodies. The size of these metasomatic alteration zones ranges from ~5 m up to ~60 m (Fig 32B) in apparent thickness in drill core. Within these alteration zones, the fluids moved through micro-fractures but also through the dissolution cavities generated by the episyenitisation process (Fig 32C), which seem to be interconnected. For an individual crystal, the CDP process can proceed in two different ways (Fig 32D, E): 1) inwards from the external fluid-grain interface towards the center of the crystal using micro-porosity, or 2) if the crystal is previously fractured, the fluid can go directly to the center of the crystal and then replace it outwards from the core to the margins of the grain. Figure 32 shows a summary of these different scales of fluid movement.

We have demonstrated that sodic alteration is spatially associated with the various styles Au mineralisation at the MDC. However, clear evidence of a genetic relationship between alteration and mineralisation is lacking. The same situation is observed in many different Au settings through the AGB where sodic metasomatism, such as in albitite dykes, has been recognised regionally and shown to be spatially and temporally associated with gold in several

orogenic and intrusion-related deposits, (Burrows et al, 1993; Ayer et al., 2005), but its role or relationship with the mineralisation is not clear.

In addition, the presence of primary alkaline intrusive rocks as small plutons proximal to the two most important structural breaks, the PDFZ and CLLFZ, is well established (e.g., Ayer et al., 2005; Beakhouse, 2011). These intrusions have a strong temporal and spatial relationship with Au mineralisation and have been recognised as forming a distinctive type of gold deposit which is informally referred to as syenite-associated (Robert, 2001; Robert et al., 2007; Kontak et al., 2008). The type of dykes, mineralisation styles, geochronological data, and alteration characteristics allow to classify the Au mineralisation present at the MDC as belonging to that group.

Nevertheless, the nature of the mineralising fluid is not understood and furthermore, the fluid and alteration are not necessarily related to alkaline magmatism. In contrast, the spatial proximity of the MDC to alkaline plutons, the strong alkaline metasomatism caused by fluids which probably originated from these intrusions, and their emplacement as part of the same magmatic event at ca. 2680 Ma, indicate that there is an intimate association of magmatism, alteration, and mineralisation. Although further study is warranted, the observations presented are considered to be sufficient to argue for a causative association between magmatism and fluids.

Sodic alteration can be present in many magmatic-hydrothermal systems, such as IOCG, porphyry, VMS, and albitite-hosted uranium deposits. The causative fluids in each case can have different origins, including magmatic, basinal brines, metamorphic, seawater or mixed (Lang et al. 1995). In some of these deposits, the sodic alteration can be directly associated with the ore, whereas in others it is simply an accessory alteration. Sodic alteration in some Archean provinces, such as the AGB, appear to be more common and widespread than in some Phanerozoic magmatic provinces. The same empirical observation has been noted for the western United States, where Battles & Barton (1996) pointed out that Na and Na-Ca alteration assemblages are very common in Permian and Jurassic rocks, but uncommon in Cretaceous and younger rocks. These authors suggested this difference was attributable to the transition from a marine environment to a fully emergent continental arc wherein the latter setting seawater

was not available. We suggest that a similar argument might be applied when comparing the AGB to modern arc environments where Na alteration is generally restricted to specific parts of magmatic hydrothermal settings.

Episyenitic textures have previously been reported in only two localities in the AGB: 1) the Taschereau – Launay plutonic complex in Quebec, where Jebrak and Doucet (2001) proposed a porphyry model for the Au-Mo mineralisation present; and 2) the Côte Gold deposit in the Swayze greenstone belt, where Katz (2016) reported the existence of the texture after tonalite, but its formation post-dated the Au mineralising event. Recognition of the episyenitisation process at the MDC and its association with Au-Cu-Mo mineralisation is one of the main contributions of this work. Furthermore, the results of the study demonstrate that episyenites may represent a previously unrecognised target for mineralisation in the AGB. That episyenites had not previously been recognised or overlooked may reflect a lack of awareness of their nature, origin, and potential to host mineralisation, although they are recognised globally (Fig 25) to be important as an ore host. Additional studies and further understanding of these rocks and the alteration/mineralisation process might open exploration opportunities for disseminated Au-Cu-Mo deposits in the AGB.

6. Conclusions

A combined petrographical, geochemical, and geochronological study of the MDC felsic dykes illustrates how strong alkali metasomatism can modify the mineralogy, texture, and chemistry of a rock. Major and trace elements are gained or lost by the transformation of feldspars, the liberation of LILE and dissolution-reprecipitation of REE-bearing minerals. Textural modifications go from pseudomorphic replacement which generally preserves magmatic textures, to development of episyenitic textures and different styles of brecciation associated with dissolution processes. Future work should include isotopic studies to understand how Sr and other LILEs behave as they are released from a dissolved feldspar crystal.

It is empirically suggested that the dykes from the MDC were emplaced at a shallow level in the crust and based on the conditions necessary to develop episyenites, the main sodic alteration

and dissolution stages occurred at temperatures from ~370°C to ~520°C with pressures between 150 and 600 bars. However, a detailed fluid inclusion study of the veins combined with oxygen isotopes in different generations of feldspars would help to determine those conditions more accurately.

The textural characteristics of episyenites make them good recorders of hydrothermal events, as evidenced by the age obtained for hydrothermal titanite hosted within dissolution cavities (2069 ± 6 Ma). This Paleoproterozoic hydrothermal event was accompanied by precipitation or remobilisation of Cu, Mo, Au, Ag, and has not been previously reported in the AGB.

Generation of open spaces via dissolution is an excellent mechanism to provide the permeability required to host mineralisation, as proven by global examples of deposits such as U, Sn, REE in episyenites, and/or Au-Ag in advanced argillic vuggy silica textured rocks.

Alkali metasomatism is widely present in Archean magmatic-hydrothermal systems and its close relationship with alkalic magmatism and gold mineralisation is undeniable, although poorly understood. Archean intrusion-related systems appear to have better developed and more extensive sodic alteration zones than some Phanerozoic counterparts such as porphyry deposits.

References

Akinfiev, Nikolay N., and Larryn W. Diamond. "A simple predictive model of quartz solubility in water–salt–CO 2 systems at temperatures up to 1000 C and pressures up to 1000MPa." *Geochimica et Cosmochimica Acta* 73.6 (2009): 1597-1608.

Alexandre, Paul. "Mineralogy and geochemistry of the sodium metasomatism-related uranium occurrence of Aricheng South, Guyana." *Mineralium Deposita* 45.4 (2010): 351-367.

ALS Geochemistry. Schedule of services and fees. 2016. www. alsglobal.com

Andrews, A. J., et al. "The silver deposits at Cobalt and Gowganda, Ontario. II: An experiment in age determinations employing radiometric and paleomagnetic measurements." *Canadian Journal of Earth Sciences* 23.10 (1986): 1507-1518.

Ashton, K. E. "The Gunnar mine: An episyenite-hosted, granite-related uranium deposit in the Beaverlodge uranium district." *Summary of Investigations* 2 (2010): 2010-4.

Ayer, J.A., Thurston, P.C., Bateman, R., Dubé, B., Gibson, H.L., Hamilton, M.A., Hathway,B., Hocker, S.M., Houlé, M.G., Hudak, G., Ispolatov, V.O., Lafrance, B., Lesher, C.M.,MacDonald, P.J., Péloquin, A.S., Piercey, S.J., Reed, L.E. and Thompson, P.H. “Overview of results from the Greenstone Architecture Project: Discover Abitibi Initiative”Ontario Geological Survey, Open File Report 6154, (2005): 146p.

Ayer, J. A., et al. "Geological compilation of the Kirkland Lake area." *Abitibi greenstone belt* (2000): 3425.

Bacon, Charles R., and Timothy H. Druitt. "Compositional evolution of the zoned calcalkaline magma chamber of Mount Mazama, Crater Lake, Oregon." *Contributions to Mineralogy and Petrology* 98.2 (1988): 224-256.

Beakhouse, G.P. The Abitibi Subprovince plutonic record: Tectonic and metallogenic implications; Ontario Geological Survey, Open File Report 6268, (2011): 161p.

Boulvais, Philippe, et al. "Cretaceous albitisation and dequartzification of Hercynian peraluminous granite in the Salvezines Massif (French Pyrénées)." *Lithos* 93.1 (2007): 89-106.

Bigot, Ludovic. Gold mineralisation at the syenite-hosted Beattie gold deposit at Duparquet, NeoArchean Abitibi Belt, Quebec, Canada. Université du Quebec à Montreal. MSc thesis, (2012).

Borges, RégisMunhozKrás, et al. "Phase separation, fluid mixing, and origin of the greisens and potassic episyenite associated with the Água Boa pluton, Pitinga tin province, Amazonian Craton, Brazil." *Journal of South American Earth Sciences* 27.2 (2009): 161-183.

Burrows, D. R., et al. "Structural controls on formation of the Hollinger-McIntyre Au quartz vein system in the Hollinger shear zone, Timmins, southern Abitibi greenstone belt, Ontario." Economic Geology 88.6 (1993): 1643-1663.

Carten, Richard B. "Sodium-calcium metasomatism; chemical, temporal, and spatial relationships at the Yerington, Nevada, porphyry copper deposit." *Economic Geology* 81.6 (1986): 1495-1519.

Cathelineau, Michel. "The hydrothermal alkali metasomatism effects on granitic rocks: quartz dissolution and related subsolidus changes." *Journal of Petrology* 27.4 (1986): 945-965.

Chang, Zhaoshan, et al. "U-Pb dating of zircon by LA-ICP-MS." *Geochemistry, Geophysics, Geosystems* 7.5 (2006).

Charoy, B., and P. J. Pollard. "Albite-rich, silica-depleted metasomatic rocks at Emuford, Northeast Queensland; mineralogical, geochemical, and fluid inclusion constraints on hydrothermal evolution and tin mineralisation." *Economic Geology* 84.7 (1989): 1850-1874.

Cox, K. G. "BELL, JD: PANKHURST, RJ (1979) The interpretation of igneous rocks." *William Clowes, London, Britain*.

Dilles, John H., G. Lang Farmer, and Cyrus W. Field. "Sodium-calcium alteration by non-magmatic saline fluids in porphyry copper deposits: Results from Yerington, Nevada." *Mineralogical Association of Canada Short Course* 23 (1995): 309-338.

Engvik, Ane K., et al. "Albitisation of granitic rocks: the mechanism of replacement of oligoclase by albite." *The Canadian Mineralogist* 46.6 (2008): 1401-1415.

Ewart, A., and W. L. Griffin. "Application of proton-microprobe data to trace-element partitioning in volcanic rocks." *Chemical Geology* 117.1 (1994): 251-284.

Fournier, Robert O. "Hydrothermal processes related to movement of fluid from plastic into brittle rock in the magmatic-epithermal environment." Economic Geology 94.8 (1999): 1193-1211.

Fowler, A. D., and Ronald Doig. "The significance of europium anomalies in the REE spectra of granites and pegmatites, Mont Laurier, Quebec." *Geochimica et Cosmochimica Acta* 47.6 (1983): 1131-1137.

Garson, M. S., et al. "Fenites, breccia dykes, albitites, and carbonatitic veins near the Great Glen Fault, Inverness, Scotland." *Journal of the Geological Society* 141.4 (1984): 711-732.

Gaschnig, Richard M., et al. "Migrating magmatism in the northern US Cordillera: in situ U–Pb geochronology of the Idaho batholith." *Contributions to Mineralogy and Petrology* 159.6 (2010): 863-883.

Geisler, Thorsten, UrsSchaltegger, and Frank Tomaschek. "Re-equilibration of zircon in aqueous fluids and melts." *Elements* 3.1 (2007): 43-50.

Goldsmith, Julian R., and Fritz Laves. "The microcline-sanidine stability relations." *Geochimica et Cosmochimica Acta* 5.1 (1954): 1IN15IN39-48IN419.

Grant, James A. "The isocon diagram; a simple solution to Gresens' equation for metasomatic alteration." *Economic Geology* 81.8 (1986): 1976-1982.

Groves, David I., et al. "Iron oxide copper-gold (IOCG) deposits through Earth history: Implications for origin, lithospheric setting, and distinction from other epigenetic iron oxide deposits." *Economic Geology* 105.3 (2010): 641-654.

Gustafson, Lewis B., and John P. Hunt. "The porphyry copper deposit at El Salvador, Chile." *Economic Geology* 70.5 (1975): 857-912.

Gysi, Alexander. "The role of pegmatites and acidic fluids for hydrothermal Zr and REE transport in the Strange Lake peralkaline granitic pluton." *Second Eugene E. Foord Pegmatite Symposium*. 2016.

Halls, Henry C., and Donald W. Davis. "Paleomagnetism and U Pb geochronology of the 2.17 Ga Biscotasing dyke swarm, Ontario, Canada: evidence for vertical-axis crustal rotation across the Kapuskasing Zone." Canadian Journal of Earth Sciences 41.3 (2004): 255-269.

Halter, Werner E., Anthony E. Williams-Jones, and Daniel J. Kontak. "The role of greisenisation in cassiterite precipitation at the East Kemptville tin deposit, Nova Scotia." *Economic Geology*91.2 (1996): 368-385.

Harlov, Daniel E., Richard Wirth, and Hans-Jürgen Förster. "An experimental study of dissolution–reprecipitation in fluorapatite: fluid infiltration and the formation of monazite." *Contributions to Mineralogy and Petrology* 150.3 (2005): 268-286.

Hövelmann, Jörn, et al. "The replacement of plagioclase feldspars by albite: observations from hydrothermal experiments." *Contributions to Mineralogy and Petrology* 159.1 (2010): 43-59.

Jackson, S. L., and J. A. Fyon. "The western Abitibi subprovince in Ontario." *Geology of Ontario. Edited by PC Thurston, HR Williams, RH Sutcliffe, and GM Stott. Ontario Geological Survey, Special* 4. Part 1 (1991): 405-484.

Jackson, S., "The Precambrian Geology of Pacaud and Catharine Townships and Portions of Adjacent Townships, District of Timiskaming, Ontario". Ontario Geological Survey, Open File Report 5884. (1994): 184 p.

Jébrak, Michel, and Luc Harnois. "Two-stage evolution in an Archean tonalite suite: the Taschereau stock, Abitibi (Quebec, Canada)." *Canadian Journal of Earth Sciences* 28.2 (1991): 172-183.

Jébrak, Michel, and Pierre Doucet. "Geology and gold–molybdenum porphyry mineralisation of the Archean Taschereau–Launay plutons, Abitibi, Quebec." *Precambrian Research* 115.1 (2002): 329-348.

Katz, Laura. “Geology of the Archean Côté Gold Au(-Cu) Intrusion-Related Deposit, Swayze Greenstone Belt, Ontario” PhD Thesis. Laurentian University. Sudbury, Ontario (2016): 347 p.

Kennedy, George Clayton. "A portion of the system silica-water." *Economic Geology* 45.7 (1950): 629-653.

Ketchum, John WF, et al. "Pericontinental crustal growth of the southwestern Abitibi subprovince, Canada—U-Pb, Hf, and Nd isotope evidence." *Economic Geology* 103.6 (2008): 1151-1184.

Khitarov, N. I. "The 400 C isotherm for the system H 2 O-SiO 2 at pressures up to 2,000 kg/cm 2." *Geochemistry* 1956 (1956): 55-61.

Kitahara, Shigeto. "The solubility of quartz in water at high temperatures and high pressures." *Rev. Phys. Chem. Japan* 30 (1960): 109-114.

Kontak, Daniel J. "Nature and origin of an LCT-suite pegmatite with late-stage sodium enrichment, Brazil Lake, Yarmouth County, Nova Scotia. I. Geological setting and petrology." *The Canadian Mineralogist* 44.3 (2006): 563-598.

Kontak, D.J., Dubé, B. and Benham, W.R. 2008. The Upper Beaver project, Kirkland Lake area: investigation of a syenite-associated copper-gold deposit with magnetite-epidote-feldspar alteration; *in* Summary of Field Work and Other Activities 2008, Ontario Geological Survey, Open File Report 6226, p.12-1 to 12-12.

Kontonikas-Charos, Alkis, Cristiana L. Ciobanu, and Nigel J. Cook. "Albitisation and redistribution of REE and Y in IOCG systems: insights from Moonta-Wallaroo, Yorke Peninsula, South Australia." *Lithos* 208 (2014): 178-201.

Lacroix, M. A. "Les rocheséruptives du Crétacepyrénéen et la nomenclature des rocheséruptivesmodifiées." *ComptesRenduesAcadSci France* 170 (1920): 685-690.

Lafleur, Pierre Jean. *The Archean Round Lake Batholith, Abitibi Greenstone Belt a synthesis*. University of Ottawa (Canada), 1986.

Landtwing, Marianne R., et al. "Copper deposition during quartz dissolution by cooling magmatic–hydrothermal fluids: the Bingham porphyry." *Earth and Planetary Science Letters* 235.1 (2005): 229-243.

Le Bas, Michael J. "Fenites associated with carbonatites." *The Canadian Mineralogist* 46.4 (2008): 915-932.

López-Moro, Francisco Javier, et al. "Constraints regarding gold deposition in episyenites: the Permian episyenites associated with the Villalcampo Shear Zone, central western Spain." *International Journal of Earth Sciences* 102.3 (2013): 721-744.

McFarlane, Chris RM, and Yan Luo. "U-Pb geochronology using 193 nm excimer LA-ICP-MS optimised for in-situ accessory mineral dating in thin sections." *Geoscience Canada* 39.3 (2012).

Manning, Craig E. "The solubility of quartz in H2O in the lower crust and upper mantle." *Geochimica et Cosmochimica Acta* 58.22 (1994): 4831-4839.

Morasse, Suzanne, et al. "A pre-2686 Ma intrusion-related gold deposit at the Kiena Mine, Val d'Or, Quebec, southern Abitibi Subprovince." Economic Geology 90.5 (1995): 1310-1321.

Nash, W. P., and H. R. Crecraft. "Partition coefficients for trace elements in silicic magmas." *Geochimica et Cosmochimica Acta* 49.11 (1985): 2309-2322.

Norberg, Nicholas, et al. "Element mobilisation during feldspar metasomatism: an experimental study." *European Journal of Mineralogy* 26.1 (2014): 71-82.

Oliver, Nicholas HS, et al. "Modeling the role of sodic alteration in the genesis of iron oxide-copper-gold deposits, Eastern Mount Isa block, Australia." *Economic Geology* 99.6 (2004): 1145-1176.

Paces, James B., and James D. Miller. "Precise U-Pb ages of Duluth complex and related mafic intrusions, northeastern Minnesota: Geochronological insights to physical, petrogenetic, paleomagnetic, and tectonomagmatic processes associated with the 1.1 Ga midcontinent rift system." *Journal of Geophysical Research: Solid Earth* 98.B8 (1993): 13997-14013.

Philpotts, John A., and C. C. Schnetzler. "Phenocryst-matrix partition coefficients for K, Rb, Sr and Ba, with applications to anorthosite and basalt genesis." *Geochimica et Cosmochimica Acta* 34.3 (1970): 307-322.

Putnis, A. "Mineral replacement reactions: from macroscopic observations to microscopic mechanisms." *Mineralogical Magazine* 66.5 (2002): 689-708.

Putnis, Andrew, et al. "Hematite in porous red-clouded feldspars: evidence of large-scale crustal fluid–rock interaction." *Lithos* 95.1 (2007): 10-18.

Putnis, Andrew. "Mineral replacement reactions." *Reviews in mineralogy and geochemistry* 70.1 (009): 87-124.

Putnis, Andrew. "Transient porosity resulting from fluid–mineral interaction and its consequences." *Rev Mineral Geochem* 80 (2015): 1-23.

Putnis, Andrew, and H. Austrheim. "Fluid-induced processes: metasomatism and metamorphism." *Geofluids* 10.1-2 (2010): 254-269.

Putnis, Andrew, and Timm John. "Replacement processes in the Earth's crust." *Elements* 6.3 (2010): 159-164.

Recio, C., et al. "Characterisation of multiple fluid-granite interaction processes in the episyenites of Avila-Béjar, Central Iberian Massif, Spain." *Chemical Geology* 143.3-4 (1997): 127-144.

Richards, Jeremy P., and A. Hamid Mumin. "Magmatic-hydrothermal processes within an evolving Earth: Iron oxide-copper-gold and porphyry Cu±Mo±Au deposits." *Geology* 41.7 (2013): 767-770.

Robert, François. "Syenite-associated disseminated gold deposits in the Abitibi greenstone belt, Canada." *Mineralium Deposita* 36.6 (2001): 503-516.

Robert, François., Brommecker, R., Bourne, B. T. , Dobak, P. J. , McEwan, C. J. , Rowe, R. R. , Zhou, X. “Models and Exploration Methods for Major Gold Deposit Types.” Ore Deposits and Exploration Technology, Paper 48

Rollinson, Hugh Richard, and Hugh R. Rollinson. “Using geochemical data: evaluation, presentation, interpretation”. No. 550.84 ROL. 1993.

Rossi, M., et al. "Geochemical variations and element transfer during shear-zone development and related episyenites at middle crust depths: insights from the Mont Blanc granite

(French—Italian Alps)." *Geological Society, London, Special Publications* 245.1 (2005): 373-396.

Rubatto, Daniela, et al. "Dissolution-reprecipitation of zircon at low-temperature, high-pressure conditions (Lanzo Massif, Italy)." *American Mineralogist* 93.10 (2008): 1519-1529.

Ruiz-Agudo, Enacarnación., C. V. Putnis, and Andrew Putnis. "Coupled dissolution and precipitation at mineral–fluid interfaces." *Chemical Geology* 383 (2014): 132-146.

Selby, David, and Robert A. Creaser. "Macroscale NTIMS and microscale LA-MC-ICP-MS Re-Os isotopic analysis of molybdenite: Testing spatial restrictions for reliable Re-Os age determinations, and implications for the decoupling of Re and Os within molybdenite." Geochimica et Cosmochimica Acta 68.19 (2004): 3897-3908.

Seydoux-Guillaume, Anne-Magali, et al. "Low-temperature alteration of monazite: Fluid mediated coupled dissolution–precipitation, irradiation damage, and disturbance of the U–Pb and Th–Pb chronometers." *Chemical Geology* 330 (2012): 140-158.

Sillitoe, Richard H. "Porphyry copper systems." *Economic geology* 105.1 (2010): 3-41.

Sillitoe, Richard H., and James K. Mortensen. "Longevity of porphyry copper formation at Quellaveco, Peru." *Economic Geology* 105.6 (2010): 1157-1162.

Sláma, Jiří, et al. "Plešovice zircon—a new natural reference material for U–Pb and Hf isotopic microanalysis." *Chemical Geology* 249.1 (2008): 1-35.

Thurston, P. C., et al. "Depositional gaps in Abitibi greenstone belt stratigraphy: A key to exploration for syngeneticmineralisation." *Economic Geology* 103.6 (2008): 1097-1134.

Theodore, Ted G., Will N. Blair, and John Thomas Nash. *Geology and gold mineralisation of the Gold Basin-Lost Basin mining districts, Mohave County, Arizona*. No. 1361-1362. USGPO, 1987.

Tomaschek, Frank, et al. "Zircons from Syros, Cyclades, Greece—recrystallisation and mobilisation of zircon during high-pressure metamorphism." *Journal of Petrology* 44.11 (2003): 1977-2002.

Wilde, Andy. "Towards a model for albitite-type uranium." *Minerals* 3.1 (2013): 36-48.

Trail, Dustin, E. Bruce Watson, and Nicholas D. Tailby. "Ce and Eu anomalies in zircon as proxies for the oxidation state of magmas." *Geochimica et Cosmochimica Acta* 97 (2012): 70-87.

Woolley, Alan Robert. "A discussion of carbonatite evolution and nomenclature, and the generation of sodic and potassic fenites." *Mineralogical Magazine* 46.338 (1982): 13-17.

Zhang, Jian, et al. "Paleoproterozoic hydrothermal reactivation in a neoarchean orogenic lode-gold deposit of the southern Abitibi subprovince: U-Pb monazite geochronological evidence from the Young-Davidson mine, Ontario." *Precambrian Research* 249 (2014): 263-272.

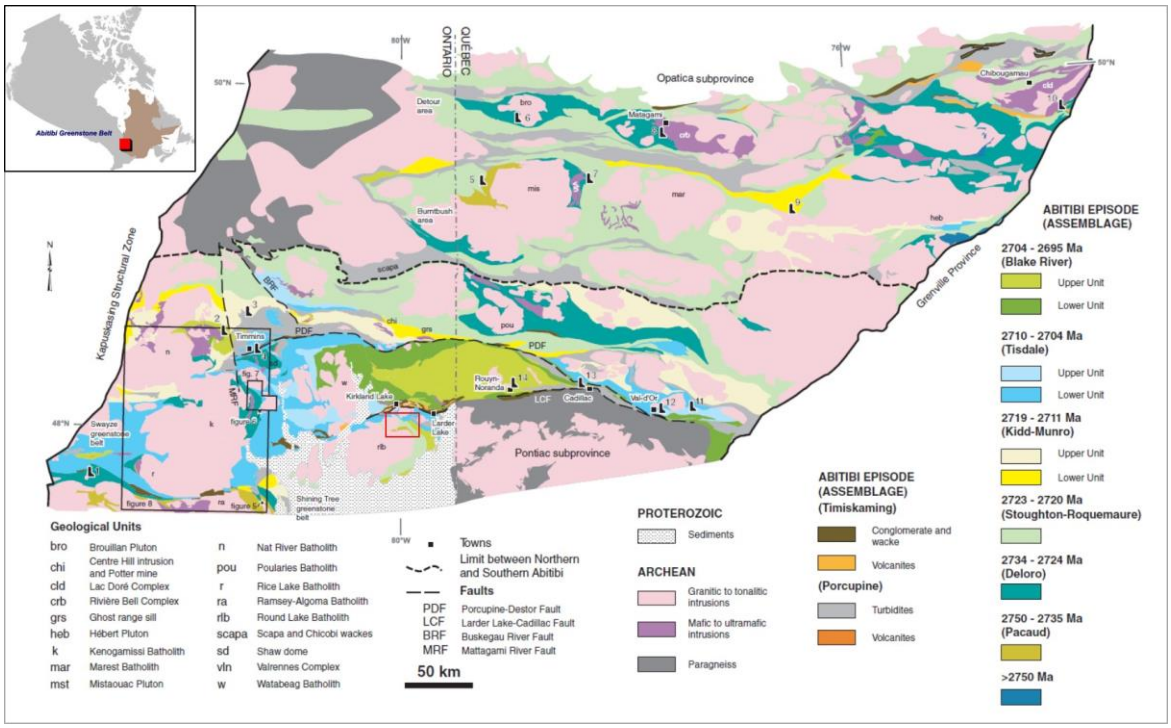

Figure 1. Regional geological map of the Abitibi Greenstone Belt showing main lithological assemblages, structures, and some of the main deposits. Modified from Thurston et al. (2008).

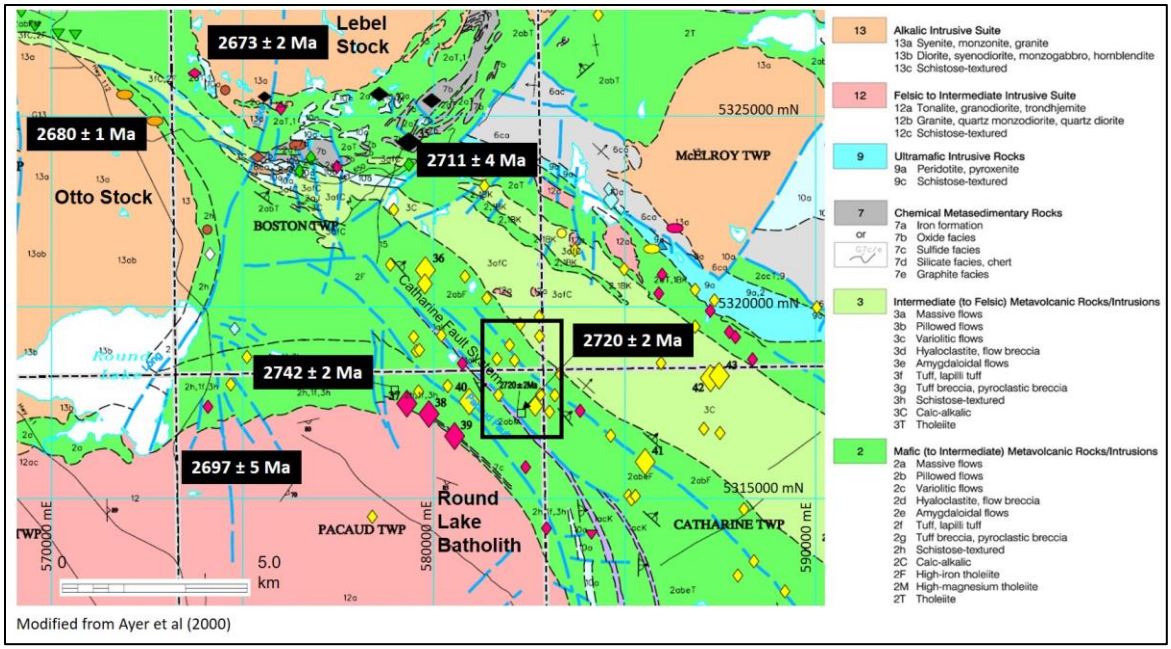

Figure 2. Sub-regional geological map of the south part of the Kirkland Lake camp. The black box shows the area of this study at the NE margin of the Round Lake Batholith. Relevant U-Pb ages of the metavolcanic units and near granitoid bodies have been highlighted. Purple and yellow diamonds in the work area represent Cu and Au prospects or occurrences, respectively. Modified from Ayer et al. (2000)

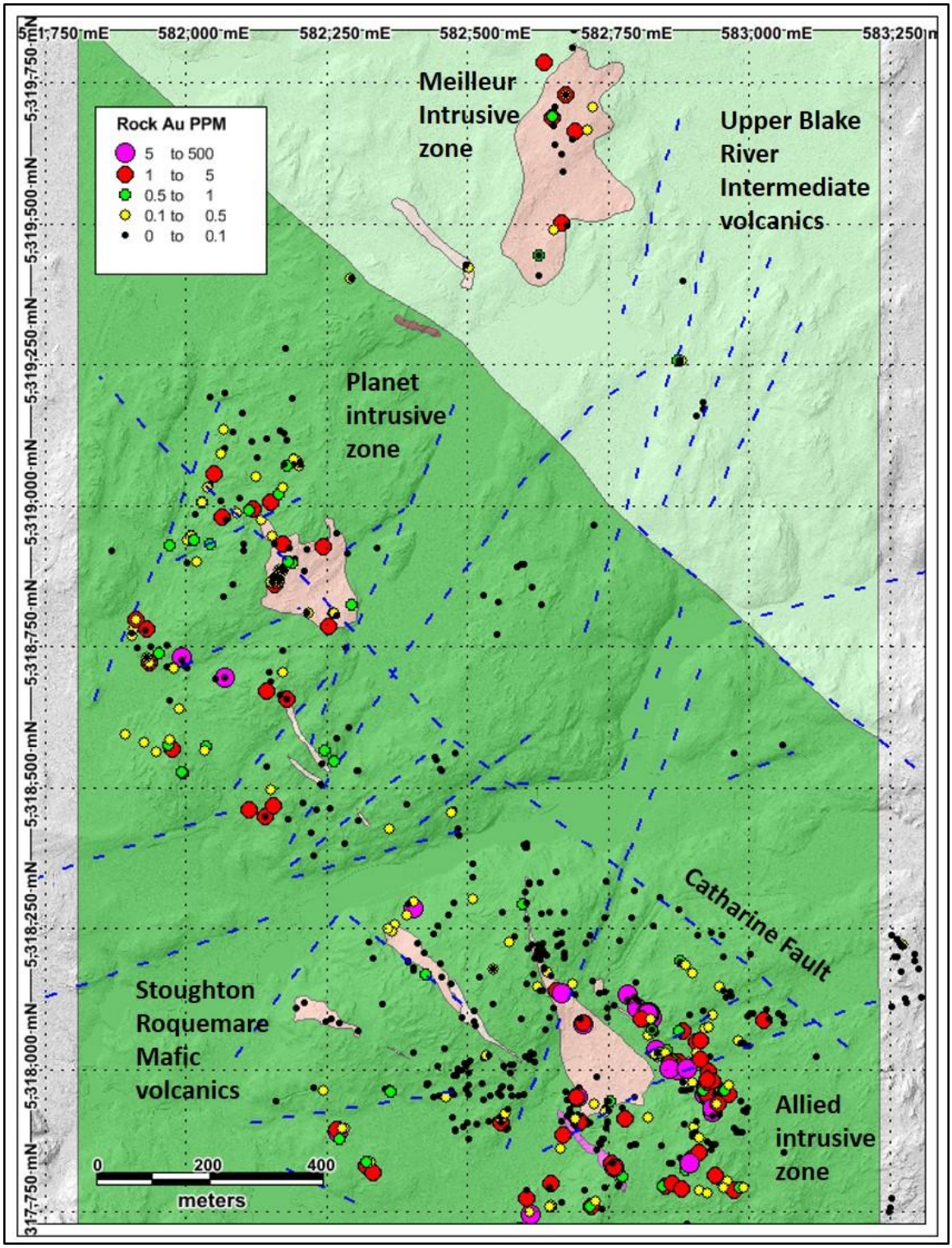

Figure 3. Geological map of the study area showing the stratigraphic units according to Jackson (1994) as well as the three intrusive centers recognized at the MDC and surface rock sampling with Au whole rock content from Oban Mining.

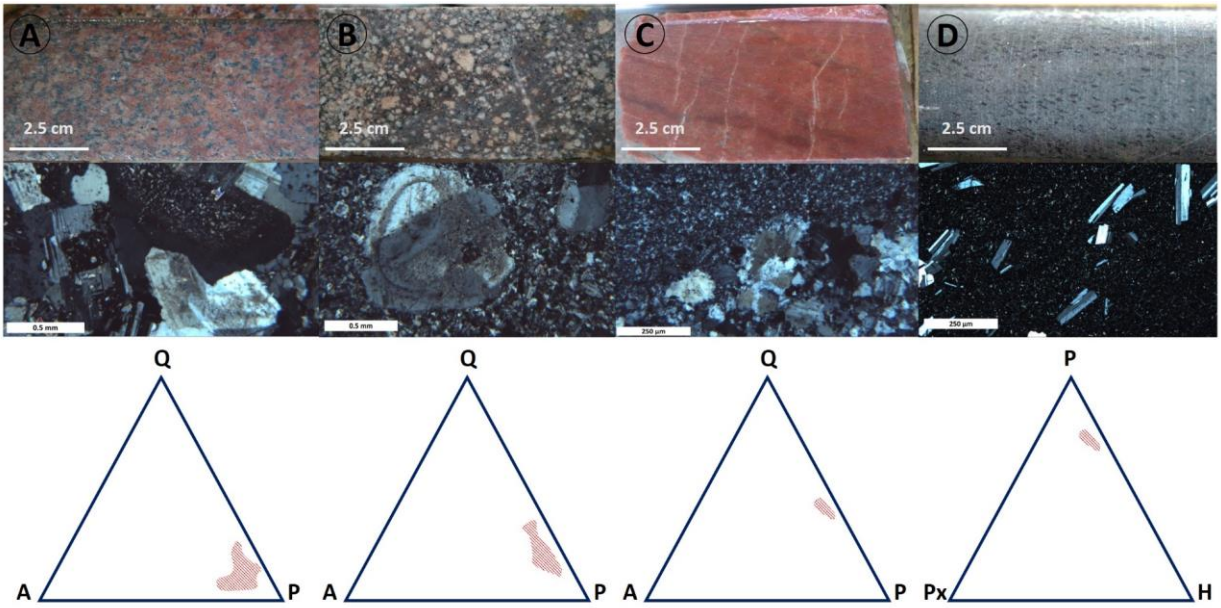

Figure 4. Textural characteristics at macro and microscopic scale of the four different types of dykes observed at the MDC. The IUGS classification diagrams used for each rock are shown in the lower part indicating the modal compositional range of different samples examined. A) Equigranular intrusion mainly composed by plagioclase feldspar with minor K-Feldspar, quartz, biotite, and hornblende; the modal classification from petrographic examination include quartz monzodiorite, monzodiorite, quartz diorite, and tonalite (n=16). B) Porphyritic to crowded porphyritic intrusion with plagioclase and locally K-Feldspar phenocrysts in a fine-grained groundmass with the same minerals plus quartz; modal classification include granodiorite, tonalite and quartzdiorite (n = 11). C) Fine grained aplitic intrusion with granular-saccharoidal texture where only plagioclase feldspar and quartz can be identified; this rock is tonalitic based on petrographic examination (n=6). D) Fine grained porphyritic mafic dykes with plagioclase and amphibole phenocrysts in a fine-grained groundmass where only plagioclase can be identified in thin section; (n=2). The red dashed area in the classification diagrams represent the zone where examined samples plotted after counting an average of 100 points for each thin section (Q = quartz, A = alkali feldspar, P = plagioclase). For the mafic dykes, an approximate composition is plotted based on composition of phenocrysts since the groundmass is too fine to count points (P = plagioclase, H = hornblende, Px = Pyroxene).

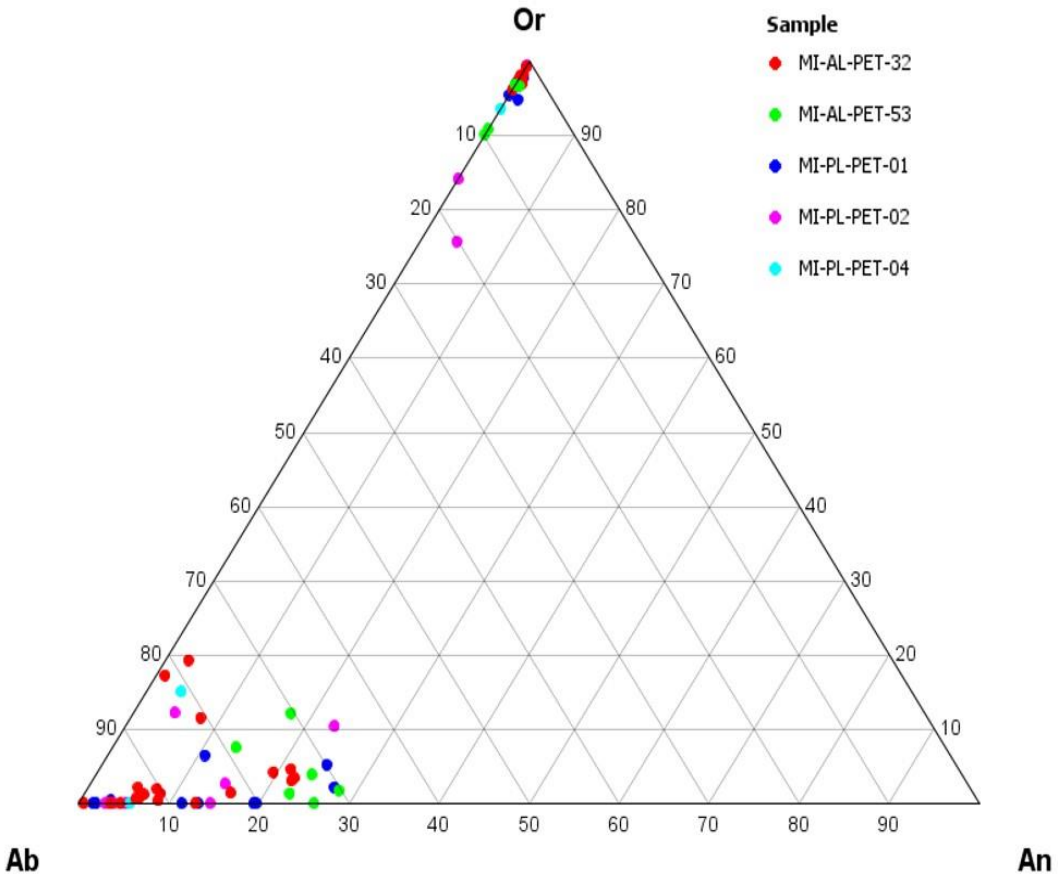

Figure 5. Summary of the compositions of feldspars (n=66) as determined from SEM-EDS analysis from five "weakly" altered samples of felsic dykes. The feldspars analyzed are euhedral to subhedral crystals from equigranular and porphyritic dykes from the Allied and Planet zones.

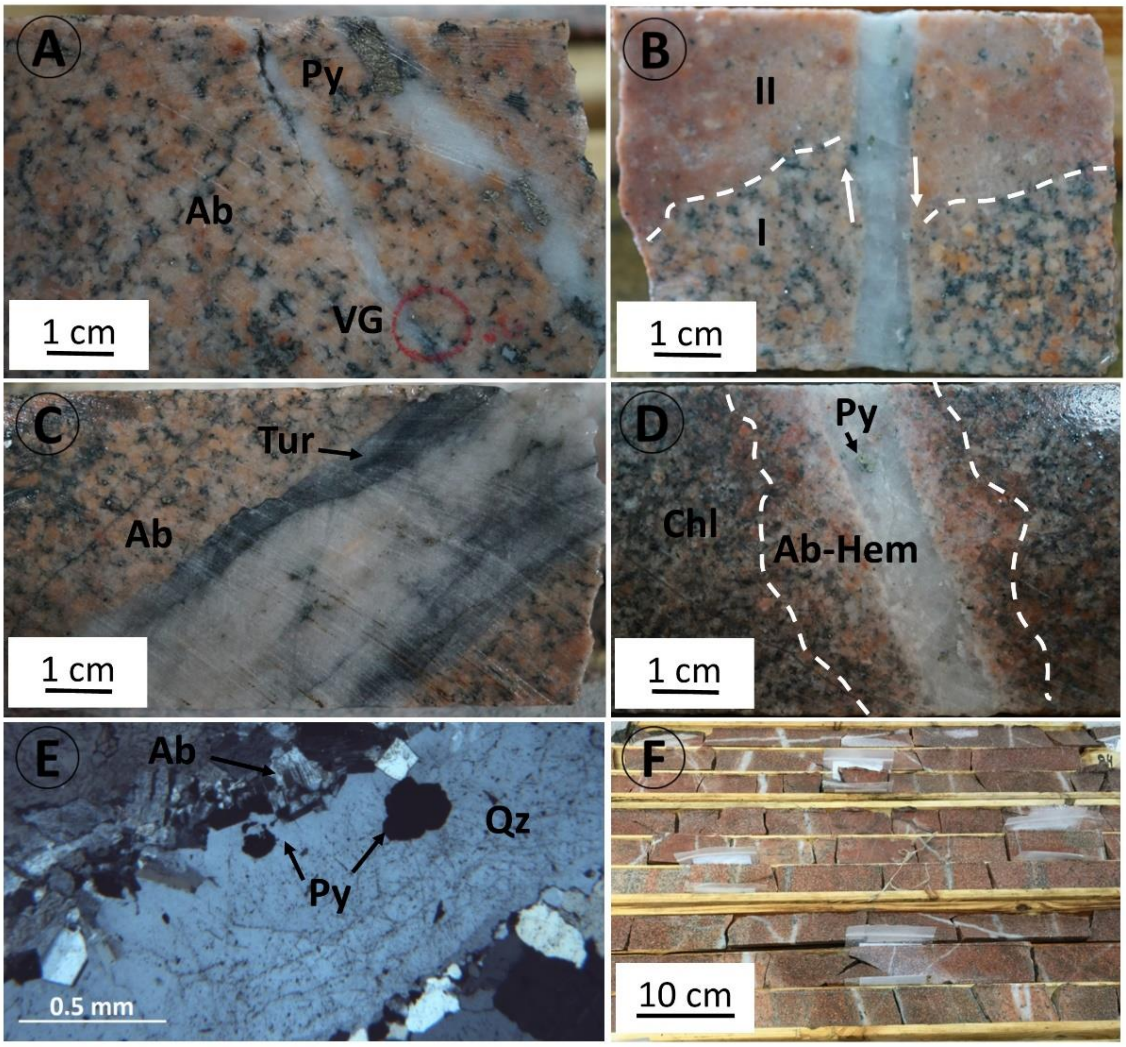

Figure 6. Examples of vein associated mineralisation. A) Two parallel quartz veins with pyrite and visible gold hosted by a light pink coloured albitized equigranular dyke. B) Quartz vein with small pyrite crystals crosscutting a contact between an equigranular (I) and a porphyritic (II) dyke showing a slight dextral movement along the vein plane. C) Quartz vein with fine grain tourmaline bands parallel to its margin, the proximal halo of the vein is strongly albitized. D) Quartz vein with pyrite showing a proximal halo of albite and hematite and a more distal chlorite alteration zone. E) Photomicrograph of a millimetric quartz vein with associated pyrite and a narrow albite alteration halo. F) Normal density of quartz veins in the mineralized zones showing alteration haloes around some of them and preferential parallel “sheeted” geometry. Ab=Albite, Py=Pyrite, Hem=Hematite, VG=Visible Gold, Tur=Tourmaline, Chl=Chlorite, Qz=Quartz.

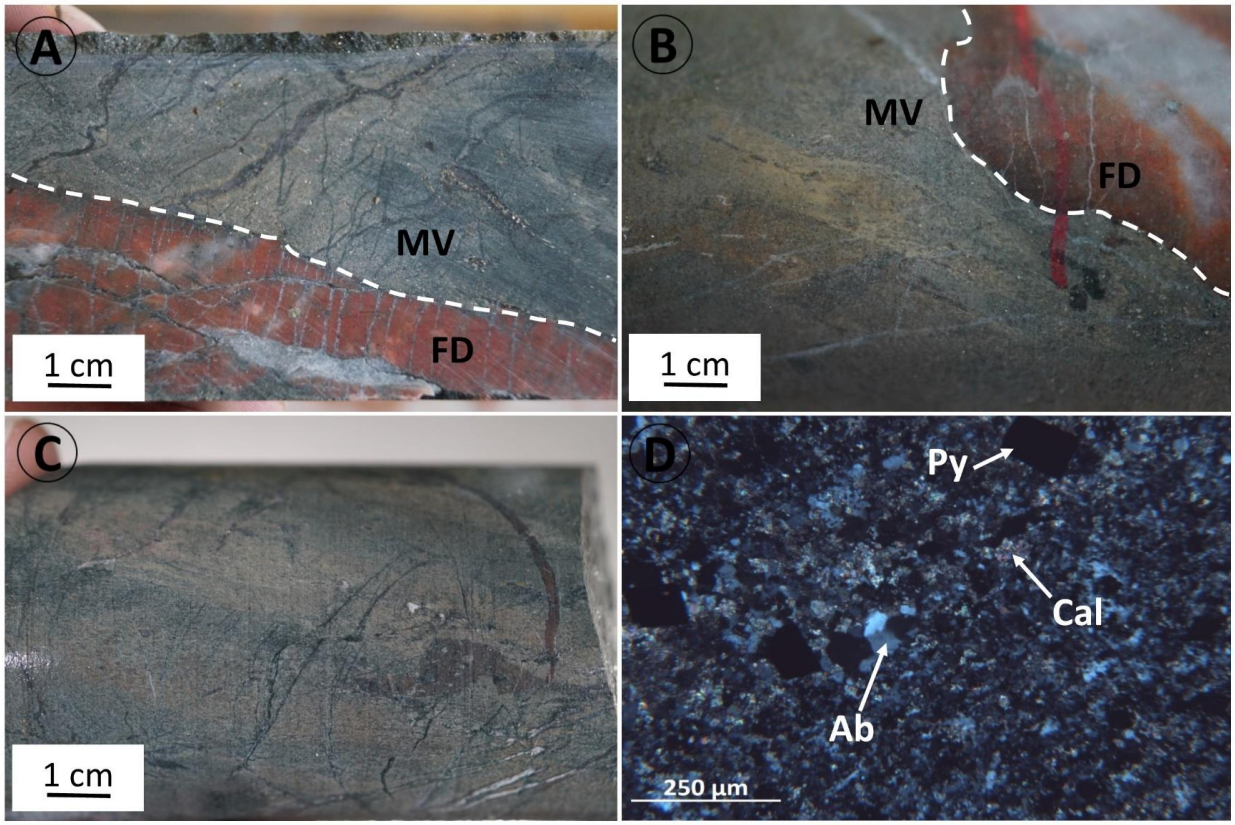

Figure 7. Examples of contact hosted mineralisation. A) Contact zone between felsic dyke (FD) and mafic volcanic rock (MV) showing intense alteration in the volcanic rock characterised by beige-greenish colour with abundant fine sulfide, mostly pyrite. Some quartz veinlets in the felsic dyke seem to continue along the contact and then become sinuous in the volcanic rock. B) Contact between felsic dyke (FD) and mafic volcanic rock (MV) with strong alteration in the latter accompanied by abundant pyrite dissemination; dark pink, beige, and green colours suggest the presence of albite, sericite, and chlorite, respectively. C) Beige and green bands in pervasively altered volcanic rock in a mineralized contact zone. Late calcite stringers are also observed crosscutting the described alteration. D) Photomicrograph of the fine-grained alteration in the volcanic rock where very fine anhedral crystals and aggregates of albite, carbonate, and coarser disseminated pyrite. MV= Mafic Volcanics, FD= Felsic dyke, Py= Pyrite, Ab=Albite, Cal=Calcite.

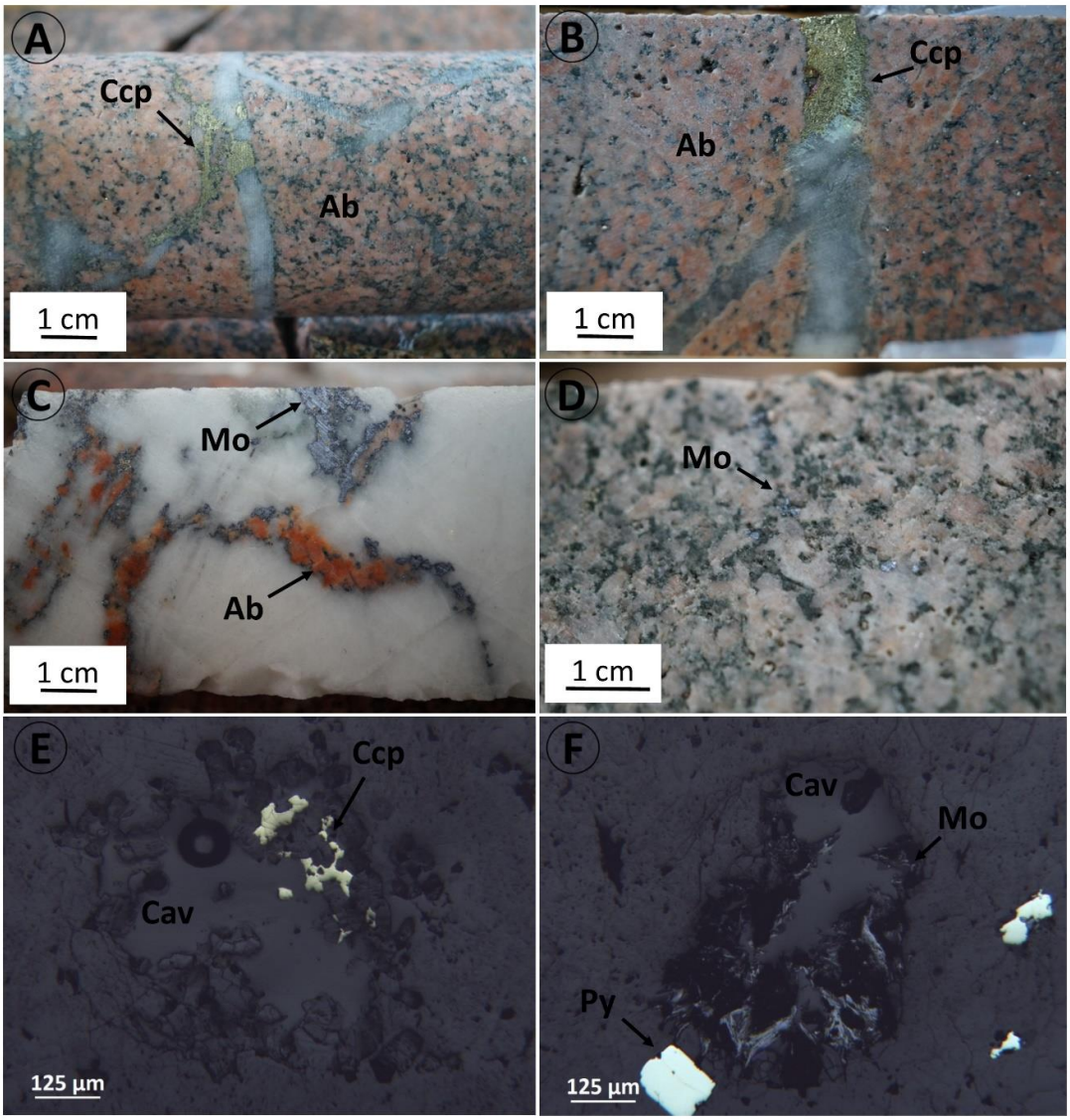

Figure 8. Examples of Cu-Mo ± Au mineralization hosted in cavities and vein margins. A) Chalcopyrite patches along the margins of irregular and discontinuous quartz veins where the host rock shows a strong pink color suggesting strong albite alteration. B) Chalcopyrite mass filling a space in a quartz vein with strong albite alteration. C) Molybdenite and intense red albite forming irregular ribbons in a milky quartz vein. D) Disseminated fine-grained molybdenite lining cavities in a pink albite altered rock with abundant chlorite disseminated. E) and F) show respectively chalcopyrite and molybdenite crystals lining the walls of sub-millimetric cavities in felsic dykes (Both reflected light – 5x). Ccp= Chalcopyrite, Ab=Albite, Mo=Molybdenite, Cav=Cavity, Py=Pyrite.

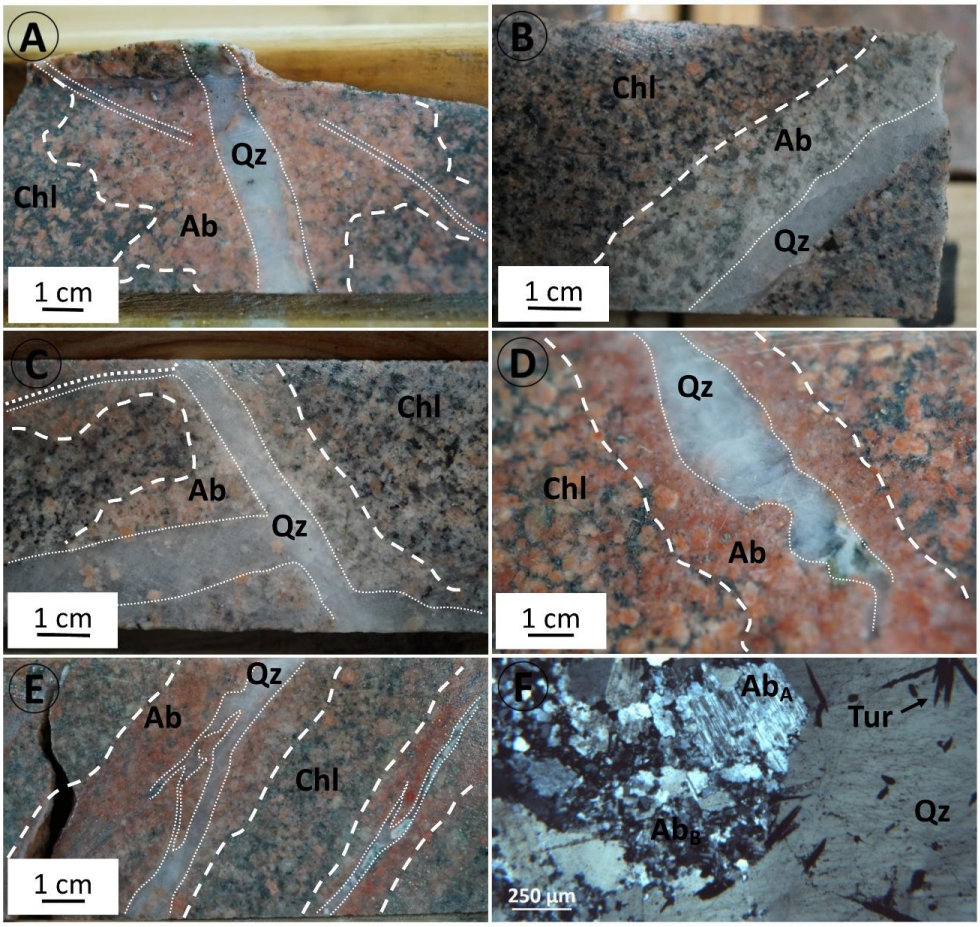

Figure 9. Examples of albite alteration type 1. Thin dashed lines represent margin of quartz veins whereas thicker lines indicate extension of albite 1 alteration. A) Irregular reddish albite halo mantling quartz veinlet and a narrower (mm) quartz stringer. Note the decreased abundance of mafic minerals within the proximal albite halo; in every case the distal halo is richer in chlorite. B) Quartz vein with a light pink albitization halo only on its top margin. These albite haloes are in many cases absent. C) Light pink albite halo mantling a quartz vein stockwork zone. D) Intense red albite halo around an irregular quartz vein. E) Narrow parallel quartz-carbonate stringers with pink-red albite envelopes. F) Photomicrograph of a quartz vein with associated tourmaline crystals and two different textural varieties of albite: Ab_A represents large irregular crystals with "chessboard twinning" and Ab_B consists on aggregates of very fine crystals formed in a small embayment at the margin of the vein (Sample MI-AL-PET-11 (2.5X – crossed nicols). Qz=Quartz, Ab=Albite, Chl=Chl, Tur=Tourmaline.

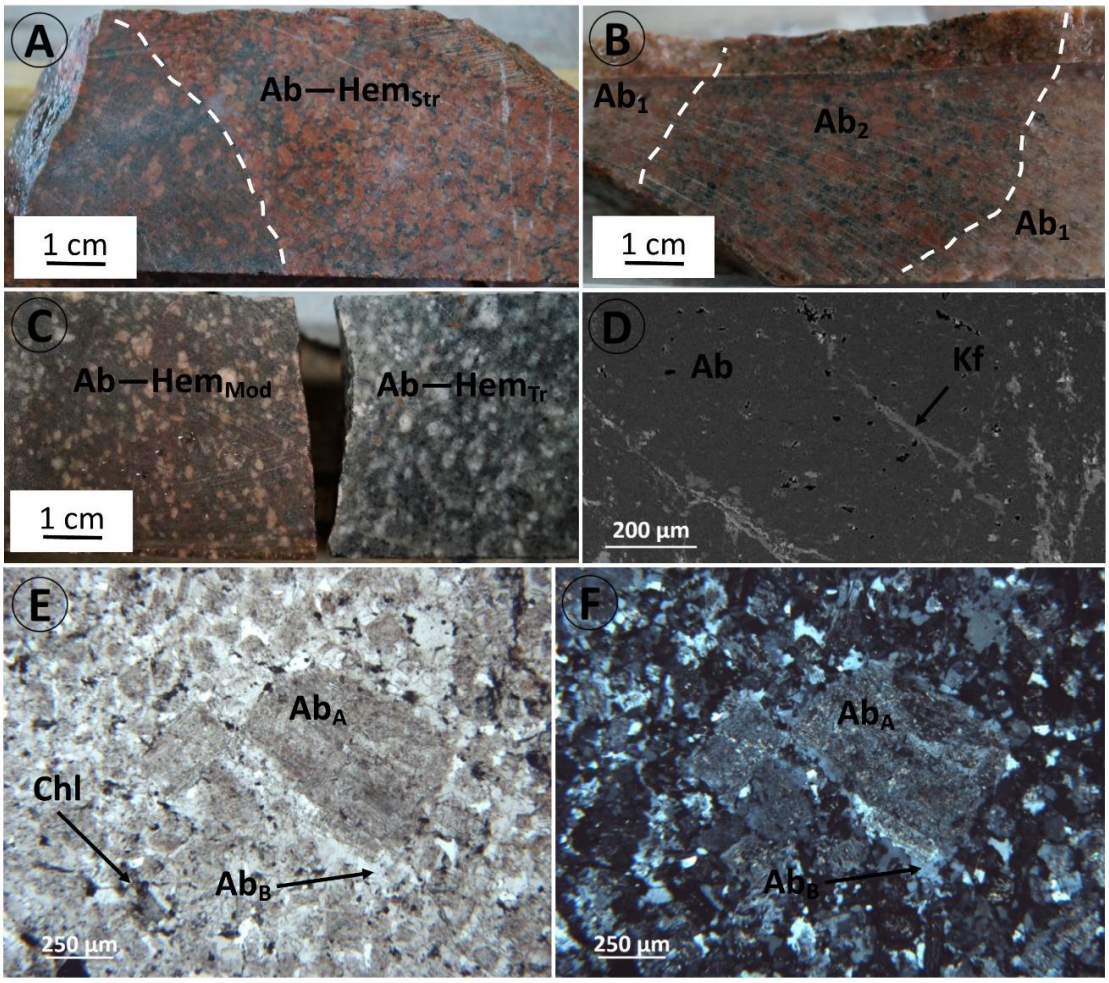

Figure 10. Examples of albite alteration type 2. A) shows a dark red equigranular dyke with strong presence of albite replacing primary feldspars; this dyke is being intruded by a darker porphyritic dyke. B) The zones labelled Ab_1 represent two proximal albite alteration haloes around quartz veins (not observed in the photo) and the white dashed line marks the limit with the distal Ab_2 zone where albite is replacing feldspar phenocrysts and it is generally accompanied by chlorite and calcite. C) Comparison of two porphyritic dykes with different degrees of hematite alteration associated with the albite alteration; in both cases the feldspars are dominantly Ab_{100}. The sample on the left shows a very light red colour in phenocrysts and groundmass whereas the one on the right shows white feldspars and dark grey groundmass with hematite only associated to fractures. D) Back scattered electron image showing abundant micro-porosity in secondary sodic plagioclase (Ab_{100}) with cross-cutting fractures controlling K-feldspar alteration. E) and F) show the same sample in PPL and CPL respectively; a porphyritic

dyke is shown where the primary feldspar phenocrysts have been replaced by Ab_{100} with cloudy-rusty appearance (Ab_A), when the larger crystals are observed under CPL abundant bright sericite inclusions are observed. Every rusty albite grain is rimmed by a lighter colored generation of albite Ab_{100}, labelled as Ab_B (Sample MI-AL-PET-28 2.5X PPL and CPL). Ab=Albite, Hem=Hematite, Chl=Chlorite, Str=Strong, Mod=Moderate, Tr=Trace.

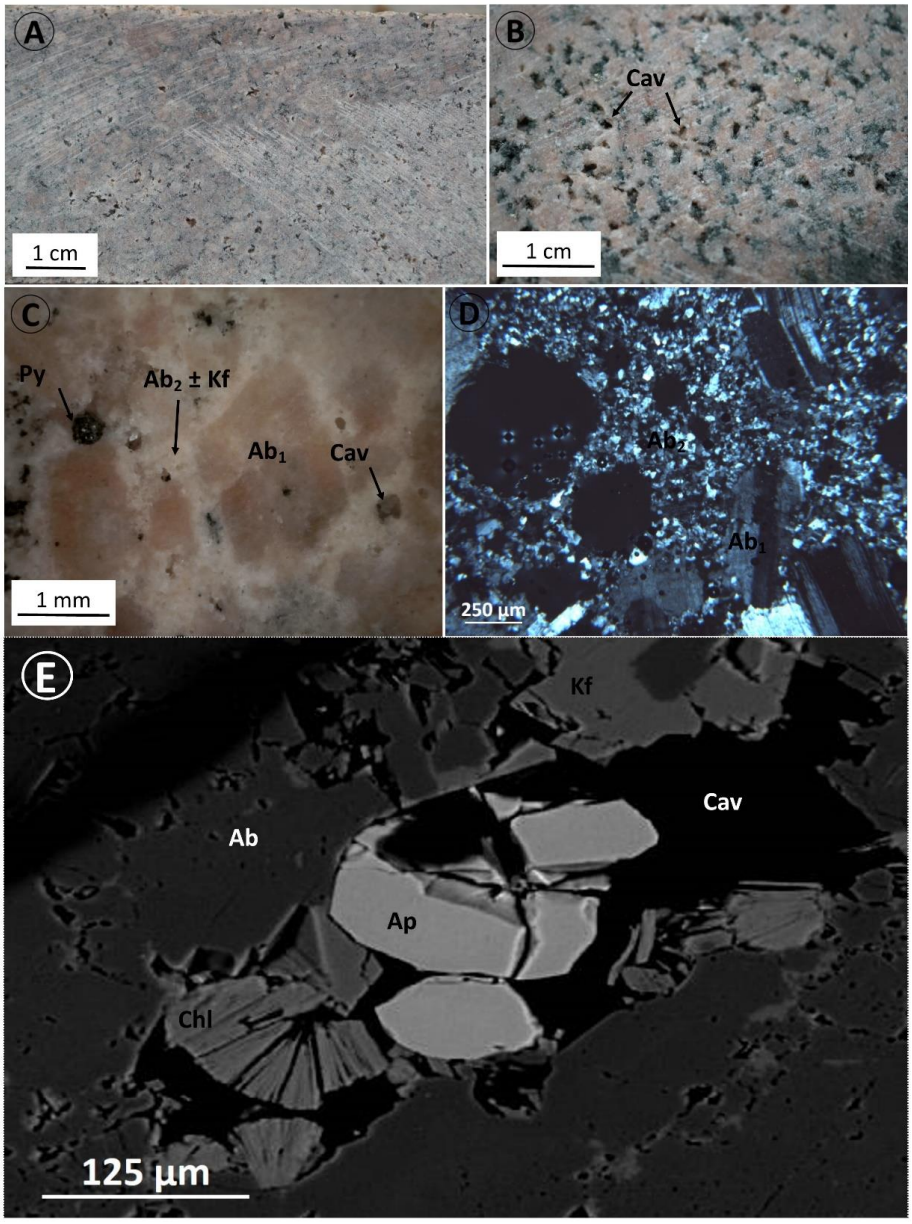

Figure 11. Details of sodic altered dykes showing the development of episyenite texture. A) and B) show the general appearance of dyke hand samples with high irregularly distributed porosity. Note the shape of the pores or cavities varies from sub-rounded to elongated. In B) can be noticed how most of the cavities show a green colour caused by the presence of chlorite C) shows a close-up of the texture with two variations of habit in albite; Ab_1 represents a primary subhedral feldspar crystal replaced by reddish albite whereas Ab_2 is very fine-grained

albite precipitated around crystals as well as lining some of the cavities. Ab_2 is occasionally accompanied by K-feldspar. Pyrite crystals are observed in some of the cavities. D) Thin section of a strongly altered dyke where subhedral feldspar crystals were replaced by albite Ab_1 where polysynthetic twinning can be appreciated; cavities or pores with semicircular shape are partially lined by a second generation of albite Ab_2 which is fine grained and forms irregular aggregates. Occasionally K-feldspar might be part of the fine-grained feldspar aggregate. Both Ab_1 and Ab_2 are sodic end member feldspar Ab_{100} (2.5x – CPL). Cav=Cavity, Ab=Albite, Py=Pyrite, Kf=K-Feldspar. E) SEM image of chlorite and apatite crystals filling a cavity with both albite and K-feldspar forming the walls.

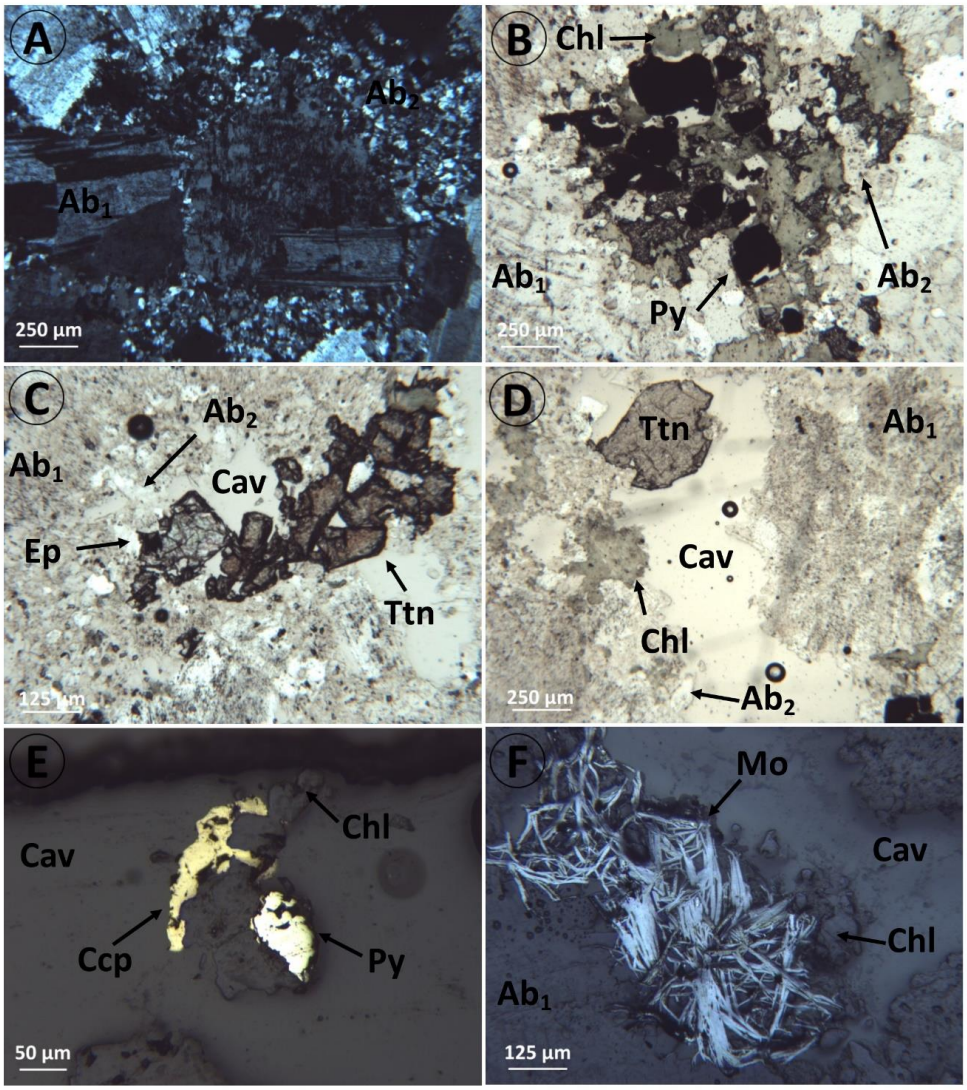

Figure 12. Minerals observed in cavities. In most cases, two generations of albite are observed; Ab_1 is primary feldspar replaced by Ab_{100} whereas Ab_2 is an agglomerate of fine-grained second albite grains formed in open spaces or cavities. A) A cavity around the margin of feldspar crystals almost filled by Ab_2 (CPL-2.5x). B) Chlorite and pyrite lining cavity with Ab_2 on the walls. (PPL-2.5x). C) Subhedral titanite and epidote in a cavity (PPL-5x). D) Relatively large cavity with elongate shape hosting a large titanite and smaller chlorite agglomerates (PPL-2.5x). E) Pyrite, chalcopyrite, and chlorite lining a cavity (Reflected light – 10x). F) Flakes of molybdenite and chlorite precipitated within a cavity (Reflected light – 5x). Ab=Albite, Chl=Chlorite, Py=Pyrite, Ep=Epidote, Ttn=Titanite, Ccp=Chalcopyrite, Mo=Molybdenite, Cav=Cavity.

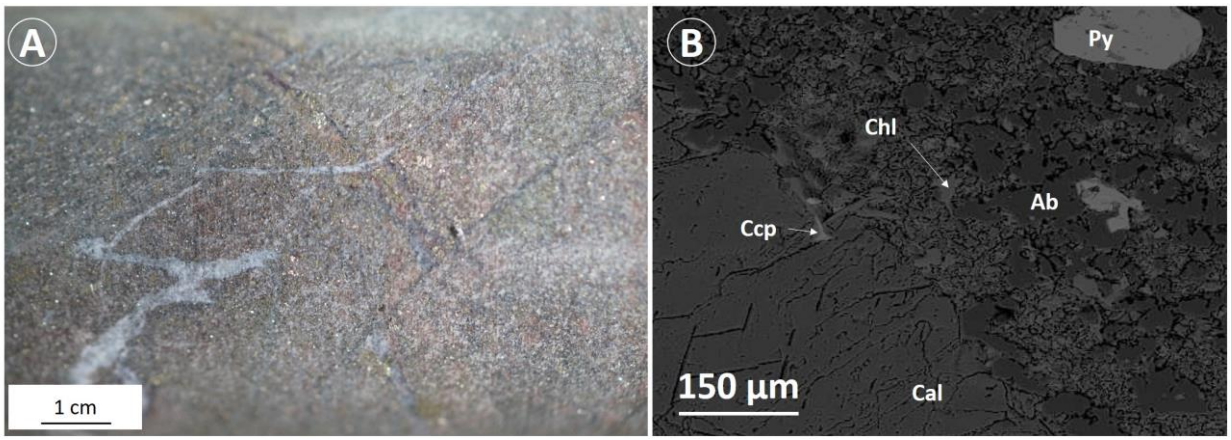

Figure 13. A) Drill core sample of intensely altered (Fine Ab, Chl, Cal, Ser, Py) mafic volcanic rock close to the contact with a felsic dyke rock. B) Back scattered electron (BSE) image showing some of the fine-grained intergrown mineralogy of the mentioned alteration zone. Albite = Ab, Chlorite = Chl, Calcite = Cal, Pyrite= Py, Chalcopyrite = Ccp.

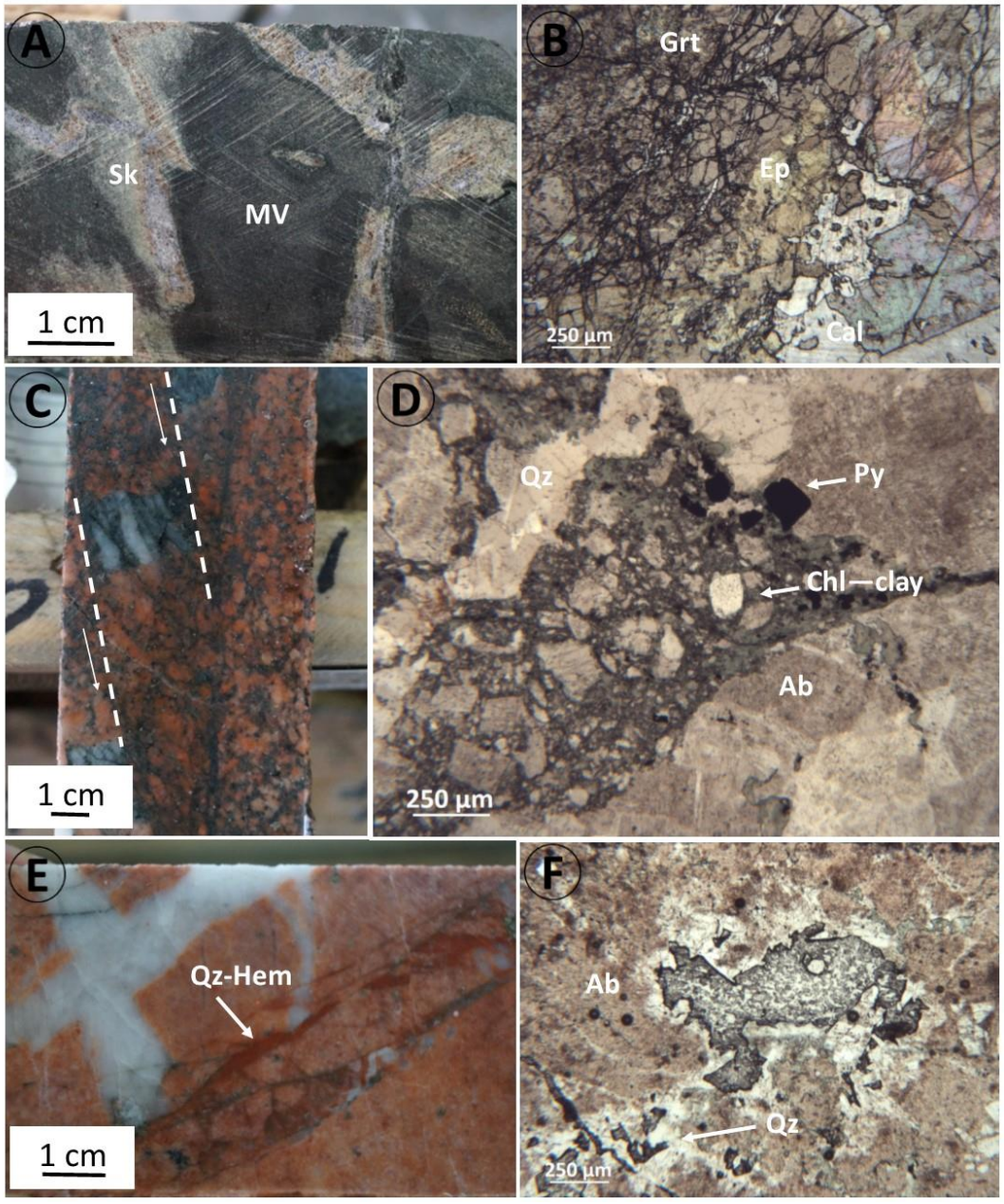

Figure 14. A) Irregular patches of skarn alteration in metavolcanic rock. B) Mineralogy of one of these alteration zones. (Grt=garnet; Ep=epidote; Ca=calcite). B) Core sample showing a quartz vein which has been broken and displaced by small fault zone lined by chlorite-clay. C). Photomicrographic image of a breccia zone showing a matrix of chlorite, clay and pyrite cementing clasts of quartz veins and plagioclase. E) Quartz vein truncated by a mm-scale zone of reddish quartz breccia. F). Quartz crystals lining fracture zones in strongly red altered plagioclase.

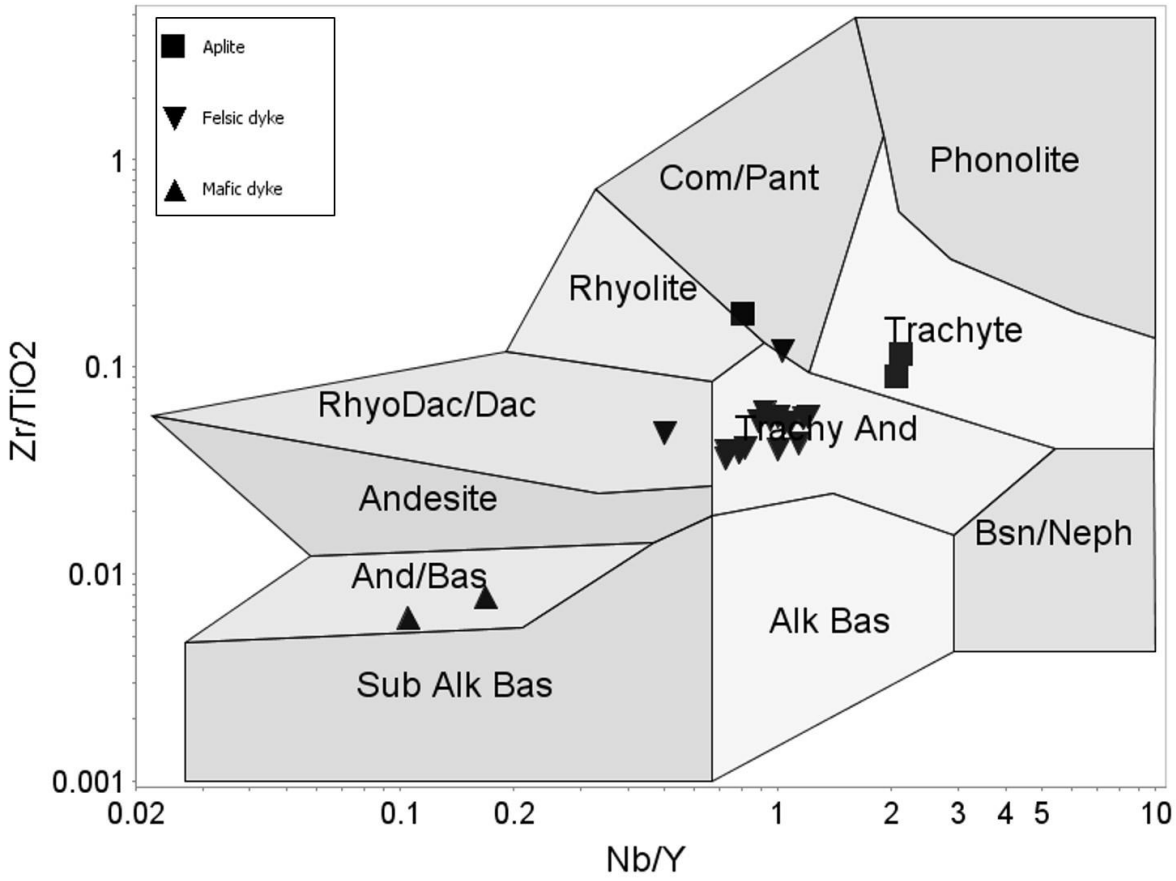

Figure 15. Plot of Zr/TiO_2 versus Nb/Y (Winchester and Floyd, 1977) with samples from the MDC.

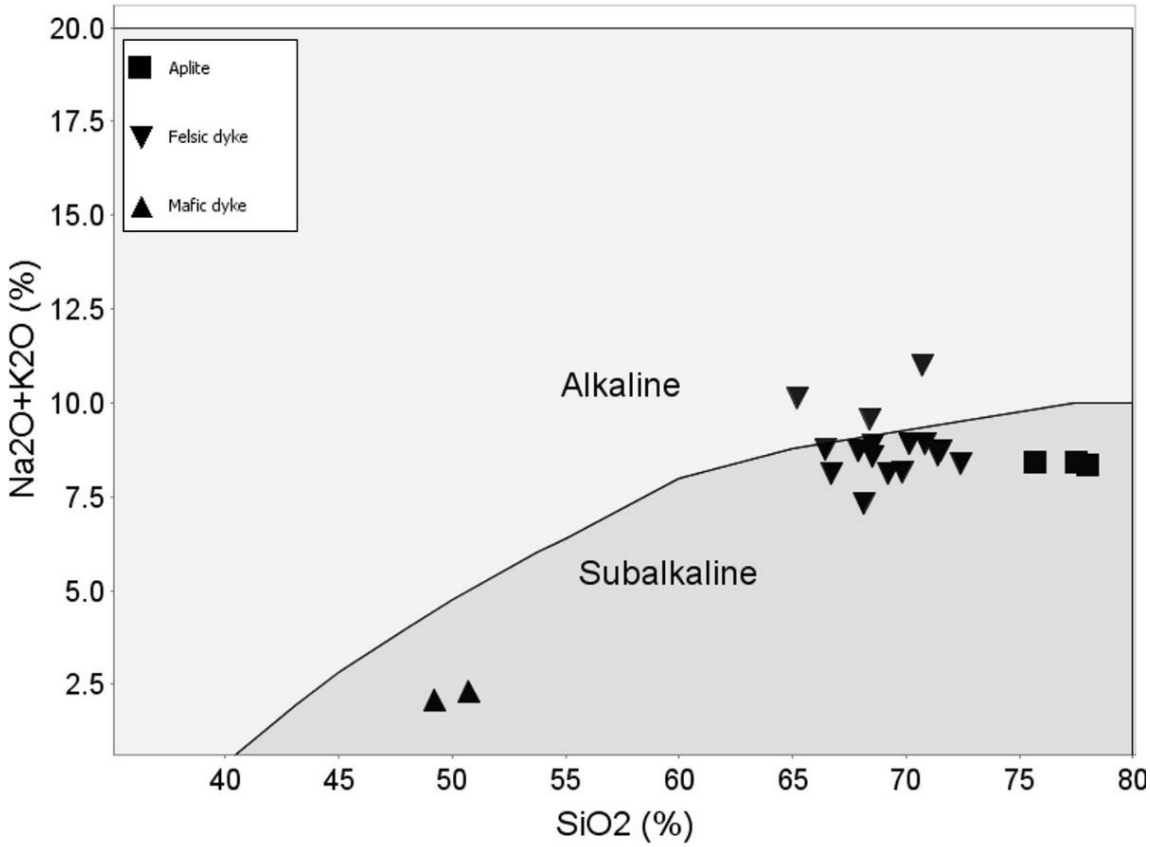

Figure 16. Alkaline/subalkaline diagram based on plot of total alkali versus. silica (curve after Irvine and Baragar, 1971) for intrusive rocks from the MDC (n=21). The diagram is presented to illustrate and stress the particular situation of alkalinity of the MDC dykes due to Na enrichment of probably different original compositions.

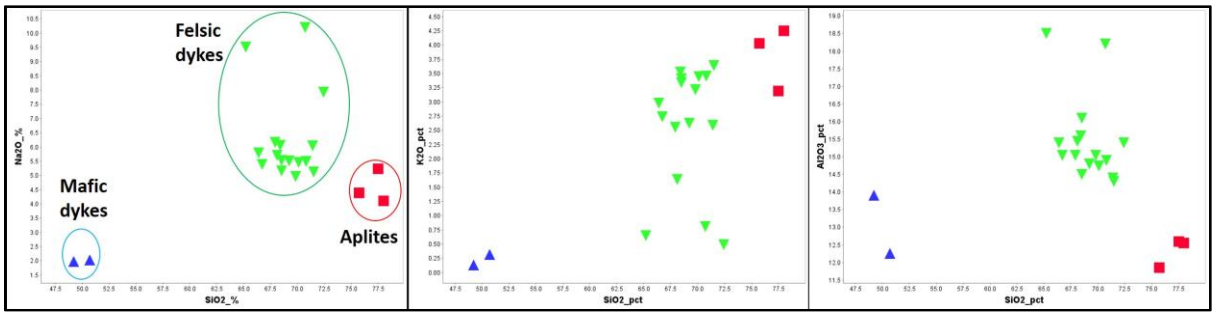

Figure 17. Harker-like diagrams for Na_2O, K_2O, Al_2O_3. Despite the mobility of major elements, the diagram is presented to illustrate the three groups of dykes.

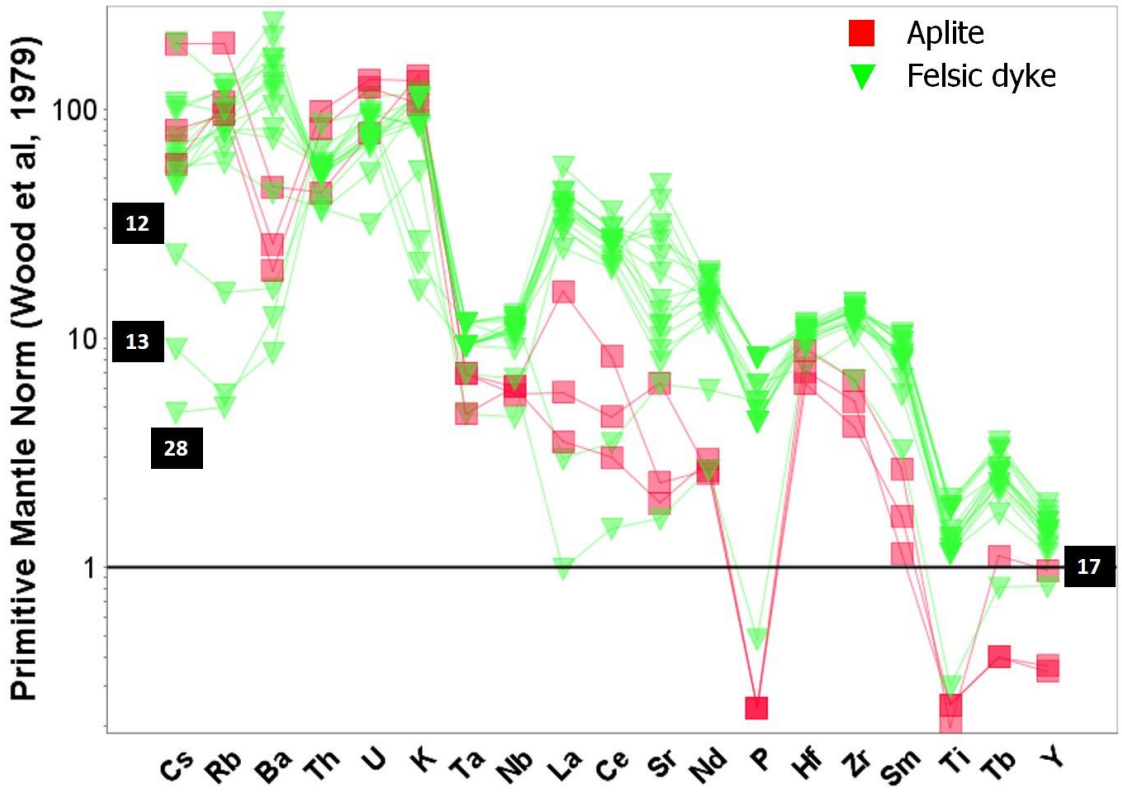

Figure 18. Primitive mantle normalised extended spider diagram for intrusive rocks of the Miller project (normalising values from Wood et al., 1979). Mafic dykes are not included to simplify the diagram. Samples 12, 13, 17 and 28 are labelled to be tracked in following diagrams

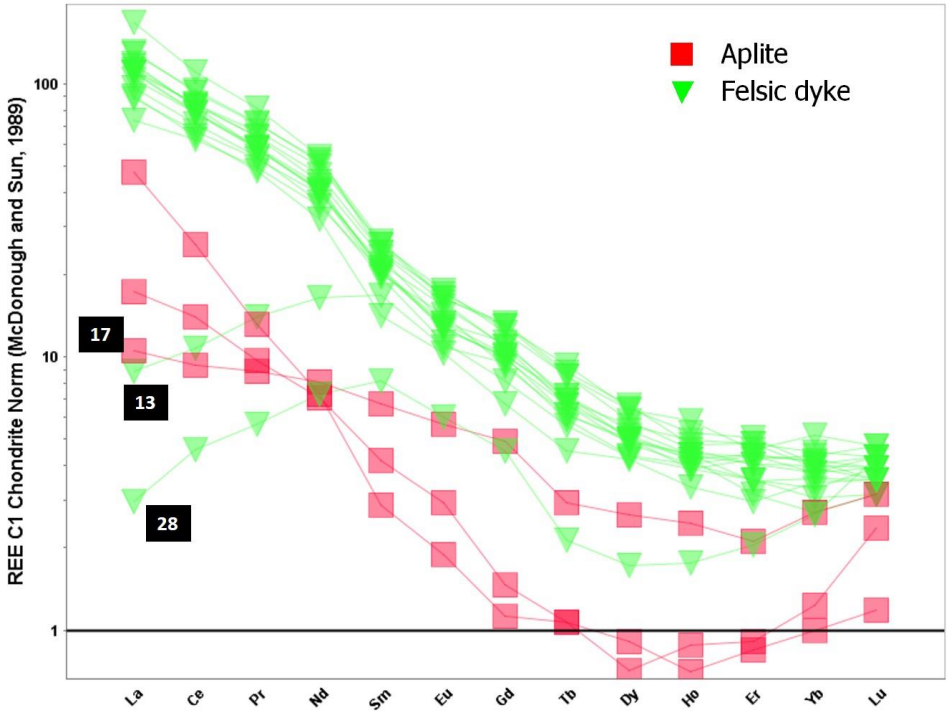

Figure 19. Chondrite normalised REE diagram for intrusive rocks of the MDC (values from McDonough and Sun, 1989). Samples 17, 13 and 28 are labelled to be tracked in following diagrams

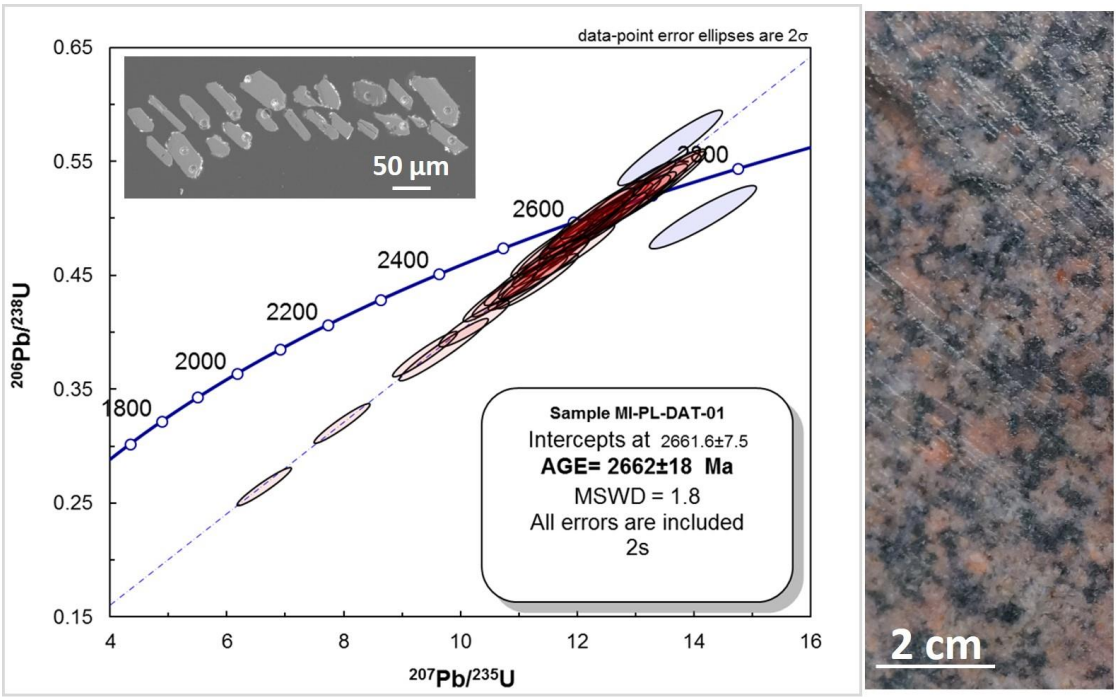

Figure 20. Concordia plot for U-Pb zircon geochronology of the felsic dykes. The analysed sample (MI-PL-DAT-01) is shown to the right side; a reddish equigranular dyke, medium-grained with abundant feldspar, minor quartz, biotite and hornblende which represents the least altered sample of the project. The inset shows an SEM image of the separated zircon grains for analysis.

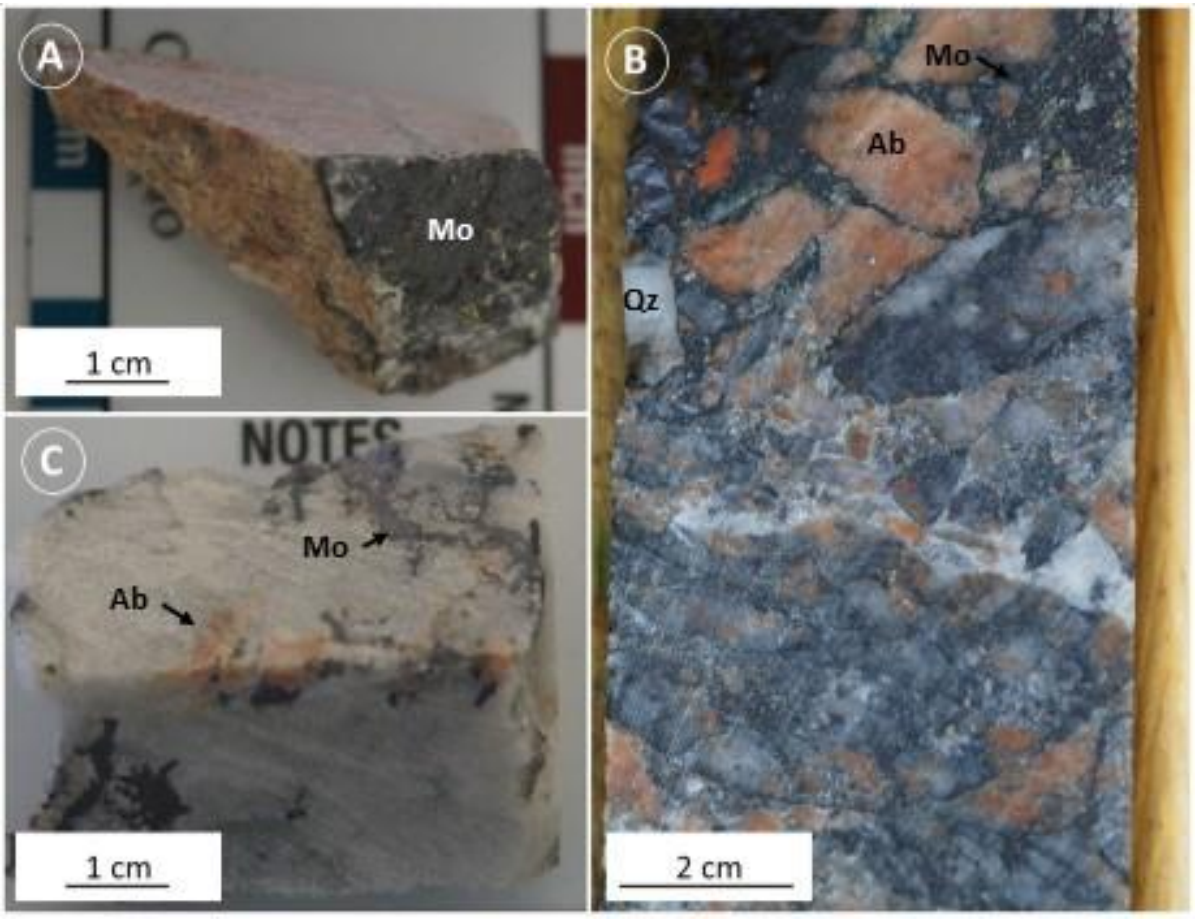

Figure 21. Molybdenite samples selected for Re-Os geochronology. A) Sample MI-PL-DAT-12 from the Planet zone; felsic dyke with carbonate, molybdenite and chalcopyrite in fractures. B) Sample MI-AL-DAT-18, from the Allied zone; hydrothermal breccia with fragments of albite altered dyke and quartz veins, cemented by calcite and molybdenite. C) Sample MI-ME-DAT-17, from the Meilleur zone; quartz vein with ribbons of albite altered intrusive and molybdenite resembling crack and seal texture. Mo = molybdenite, Ab= albite, Qz= quartz

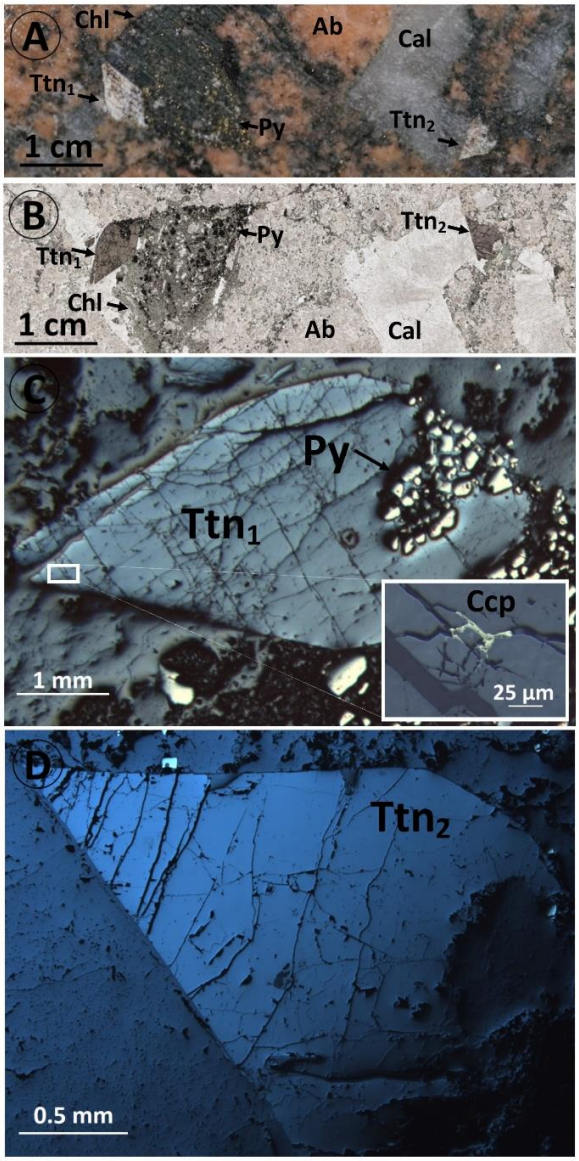

Figure 22. Details of sample MI-AL-PET-70, selected for in situ U-Pb geochronology of hydrothermal titanite. A) Hand sample before cutting the polished-thin section where two large titanite grains Ttn1 and Ttn2 are observed associated to cavities filled with pyrite – chlorite and calcite, respectively. The dyke hosting the cavities and titanites is strongly albitized. B) Scanned image of the thin section showing the same two crystals. C) Detail of Ttn1 in reflected light (2.5x) showing pyrite inclusions and chalcopyrite trace hosted in fractures (inset). D) Detail of the grain 2 Ttn2 in reflected light (2.5x). Ttn=Titanite, Py=Pyrite, Ccp=Chalcopyrite, Ab=Albite, Chl=Chlorite, Cal=Calcite

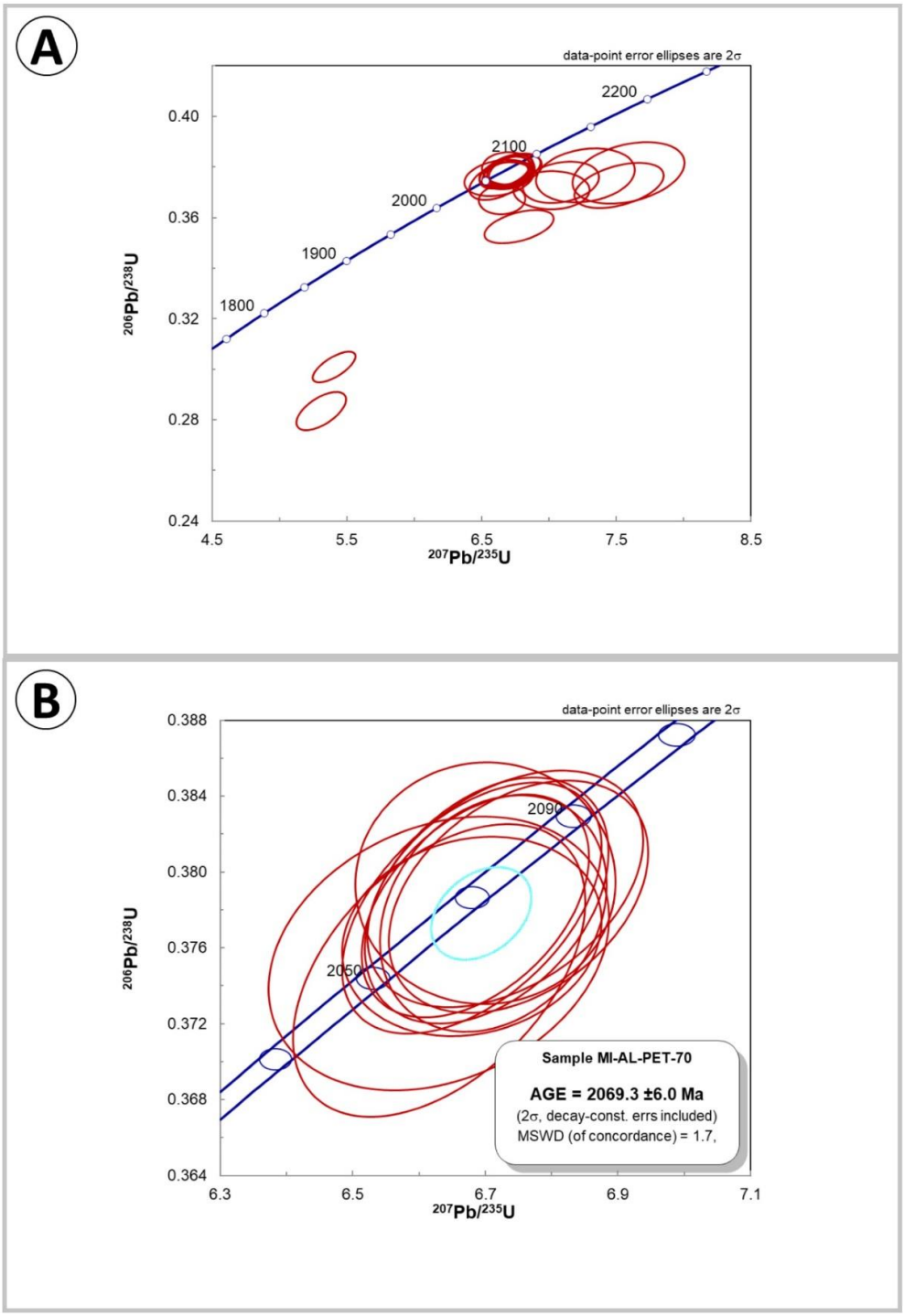

Figure 23. A) Concordia diagram for 20 analyses on Ttn1. Note that 9 of the measurements are not concordant presumably due to Pb loss. B) Cluster of the concordant data (n=11; shown in A) that yields an age of 2069.3 ± 6.0 Ma.

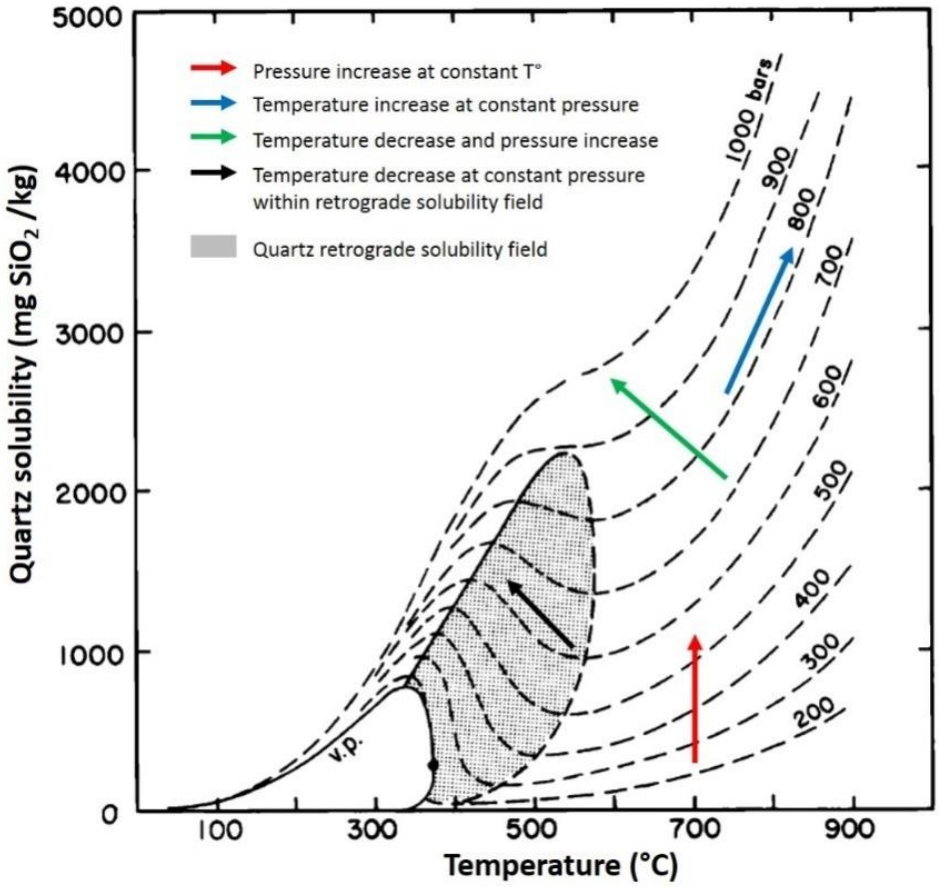

Figure 24. Plot of quartz solubility versus water temperature from 0° to 900°C contoured with isobars from 200 to 1000 bars. The coloured arrows show four different mechanisms that increase quartz solubility and might trigger quartz dissolution. Diagram is modified from Fournier (1999).

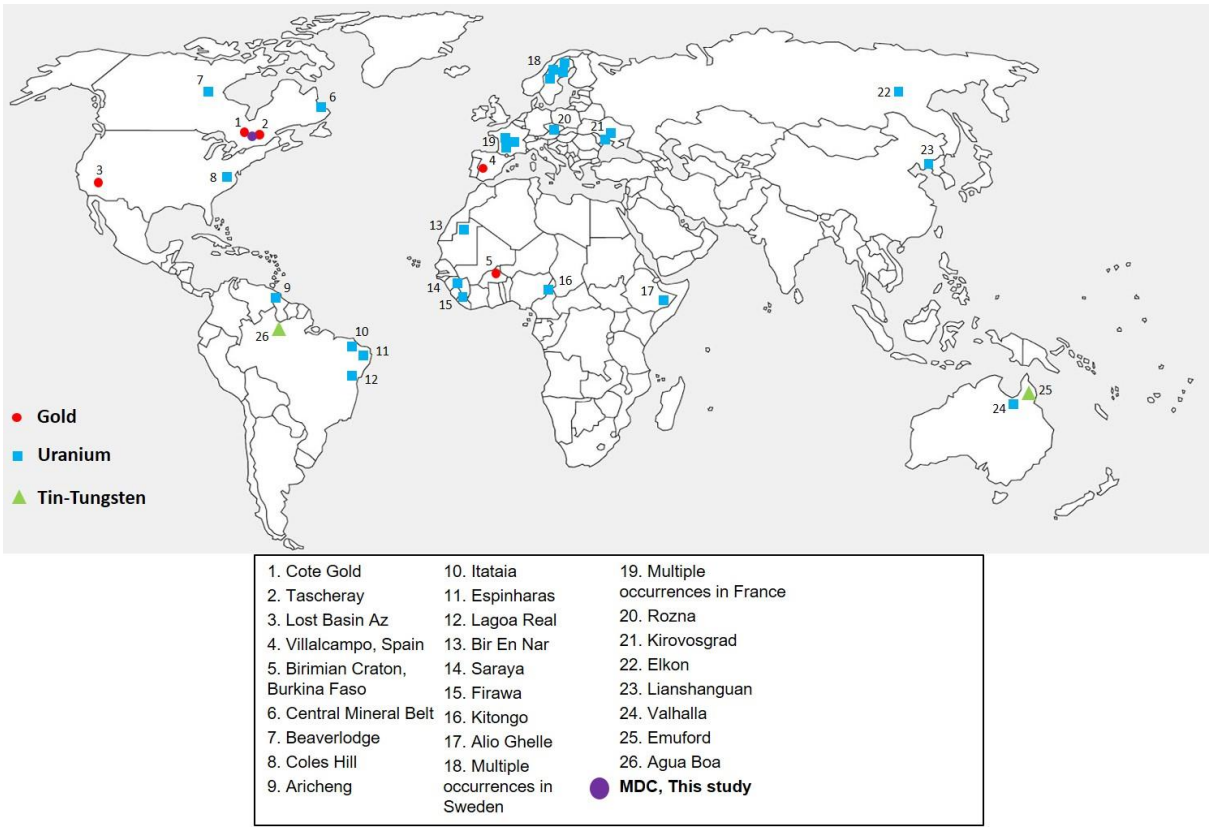

Figure 25. Global distribution of some of the best-known ore bearing episyenites reported in the literature. Only three places, including this work, have reported Au-bearing episyenites in Canada, all of them associated with Archean intrusions in the Abitibi greenstone belt. Deposits included in the map taken from Ashton (2010); Boulvais (2007); Borges et al. (2009); Charoy & Pollard (1989); Jebrak & Doucet (2002); Lopez Moro (2013); Theodore et al.(1987); Wilde (2013).

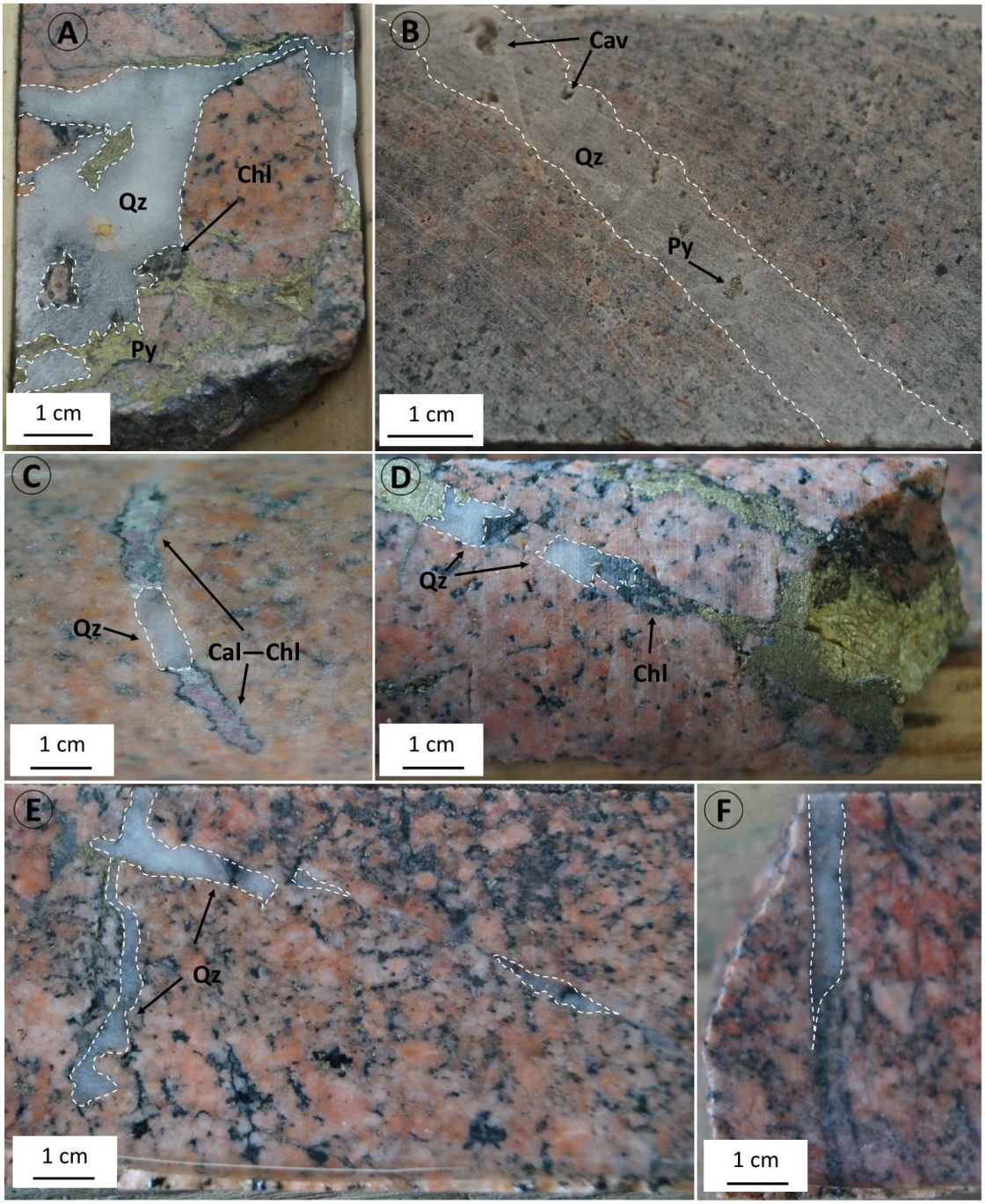

Figure 26. Close spatial relationship between irregular shaped veins, episyenitic texture and Cu sulfides. A) Irregularly shaped quartz vein showing intense dissolution along its margins and albitization in the wall rock. Note internal formation of chlorite, albite, and pyrite. Chlorite is also forming an outer rim around the vein. B) Quartz vein, its alteration halo, and its wall-rock all showing evidence of dissolution cavities suggesting that episyenitisation is post quartz

veining. C) An early quartz vein is laterally truncated suggesting that quartz has been leached and the space filled by chlorite and calcite. D) A quartz vein that has been partially dissolved and re-filled by chlorite and chalcopyrite. E) Dissolved quartz veins where the original fracture has been sealed by secondary albite. The wallrock is intensely albitised with presence of episyenitic texture, where the cavities are lined by chlorite and albite. F) A laterally truncated quartz vein with chlorite filling the original fracture. Qz=Quartz, Chl=Chlorite, Py=Pyrite, Cal=Calcite, Cav=Cavity.

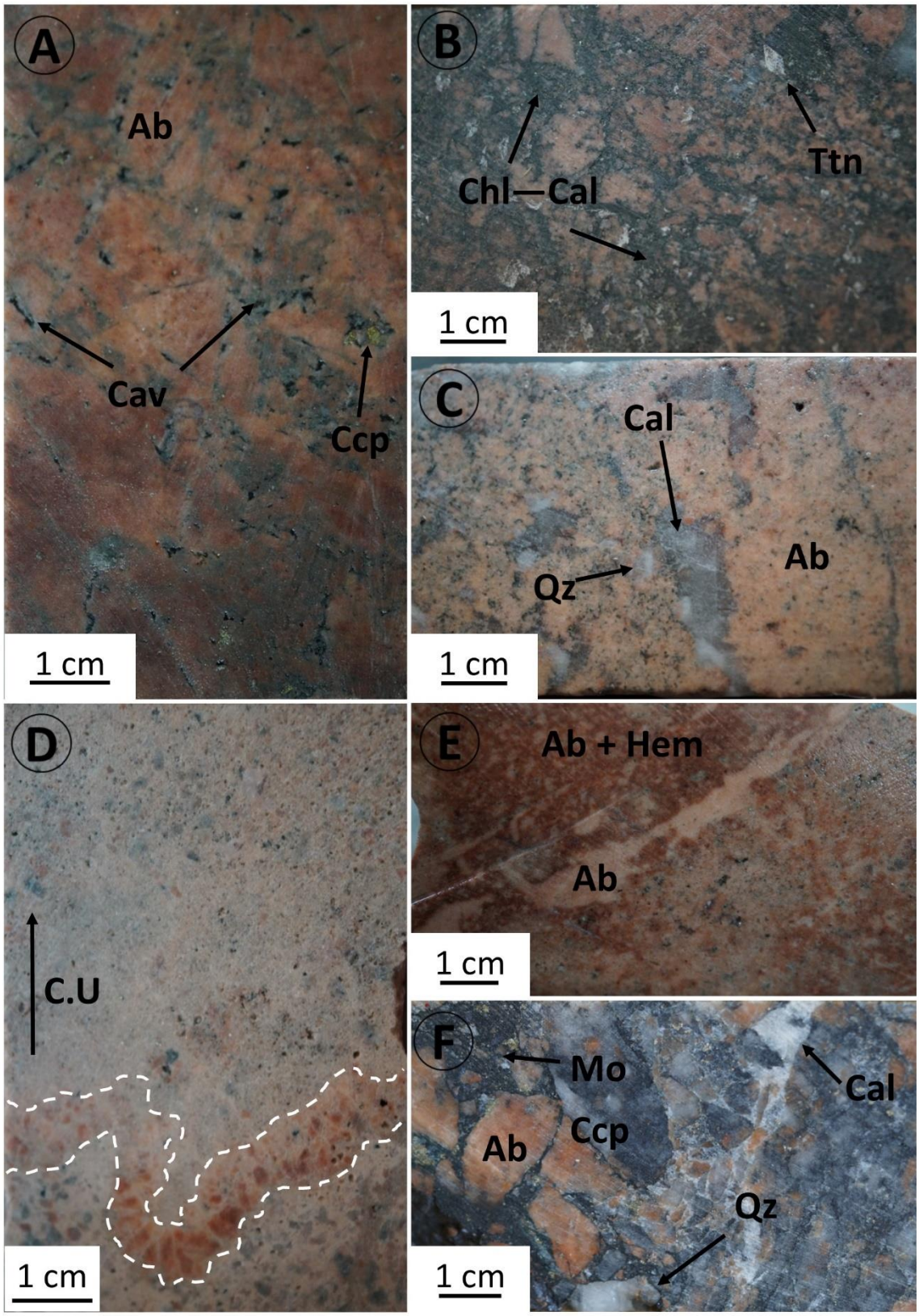
A
Ab
Cav
Ccp
1 cm
B
Chl—Cal
Ttn
1 cm
C
Cal
Ab
Qz
1 cm
D
C.U
1 cm
E
Ab + Hem
Ab
1 cm
F
Mo
Cal
Ccp
Ab
Qz
1 cm

Figure 27. Different types of breccias and episyenite textural variations due to multiple episodes of fluid flow through sodic alteration zones. A) Crackle or mosaic breccia with intensely albitised clasts and a secondary feldspar matrix with abundant dissolution cavities. Note the presence of chalcopyrite (Ccp) in the porous area. B) Example of a hydrothermal matrix supported breccia with fragments of angular albitised material in a matrix of chlorite (Chl) – calcite (Cal) with locally abundant titanite (Ttn). C) Brecciated albitic (Ab) episyenite with quartz (Qz) and calcite filling centimetric dissolution cavities. D) Strongly albitised rock with fragmental and episyenitic texture and apparent grain size gradation. A curvilinear coarse-grain horizon (outlined by dashed white line) might represent the separation between two grain size domains. The texture is alike to those observed associated with dissolution and collapse in some karstic systems E) Intensely albitized dyke with irregular episyenitic texture and patchy red colouring. The sodic alteration and episyenitisation forms multiple zones with this bizarre texture. F) Hydrothermal breccia with quartz vein and albite-rich fragments in a matrix of molybdenite (Mo), trace chalcopyrite and calcite indicating that molybdenite is coeval with the brecciation process and post-dates the quartz veins. Ab=Albite, Ccp=Chalcopyrite, Chl=Chlorite, Cal=Calcite, Ttn=Titanite, Qz=Quartz, Hem=Hem, Mo=Molybdenite, Cav=Cavity, C. U= Coarsening Upwards.

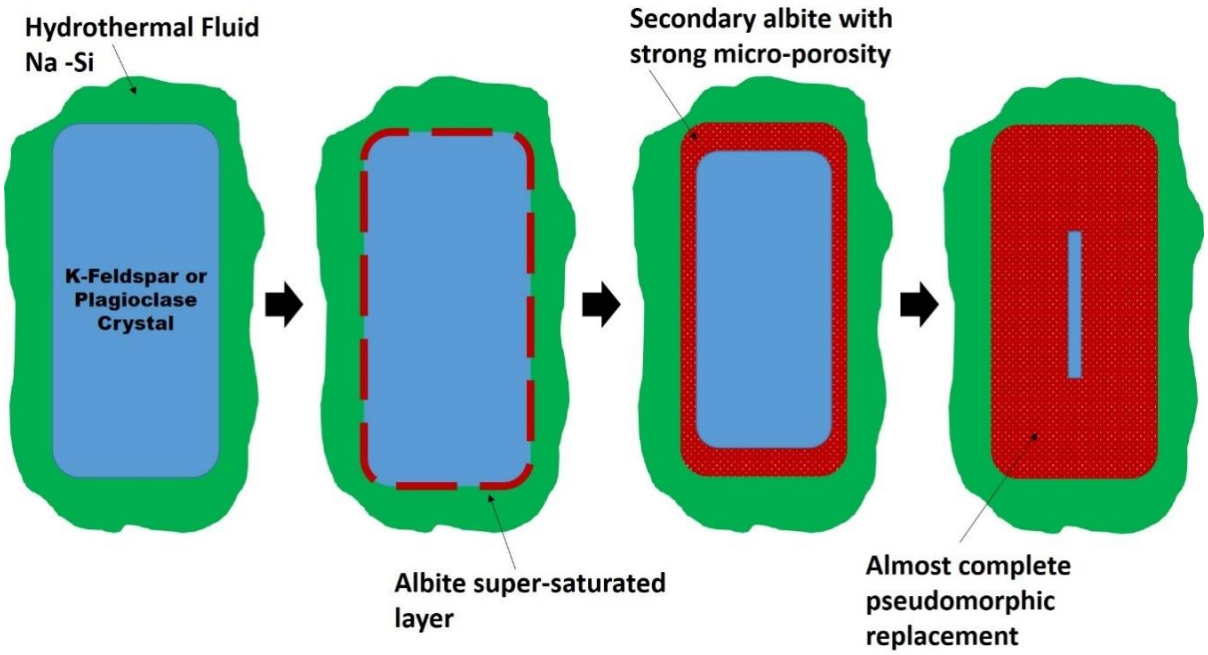

Figure 28. A schematic illustration of the albitization of an earlier feldspar crystal via coupled dissolution-precipitation (CDP). The cartoon represents the ideal situation where perfect pseudomorphic replacement takes place. Figure modified after that of Ruiz-Agudo et al. (2014).

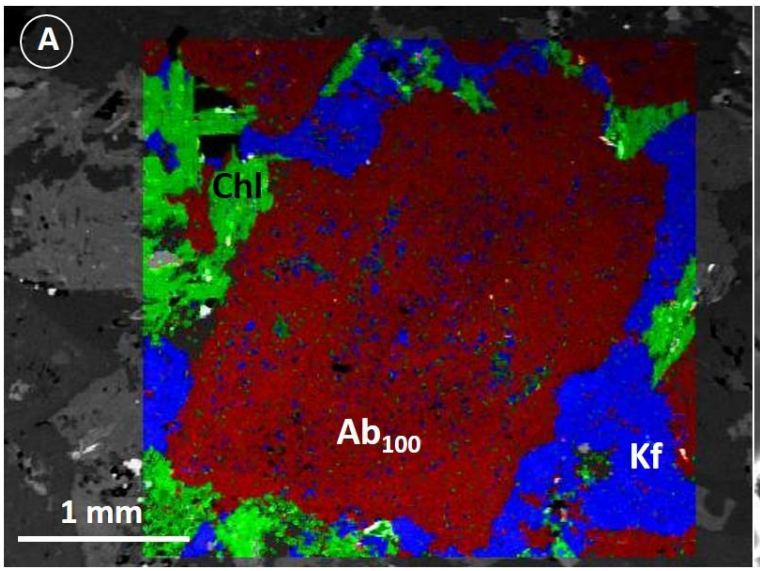

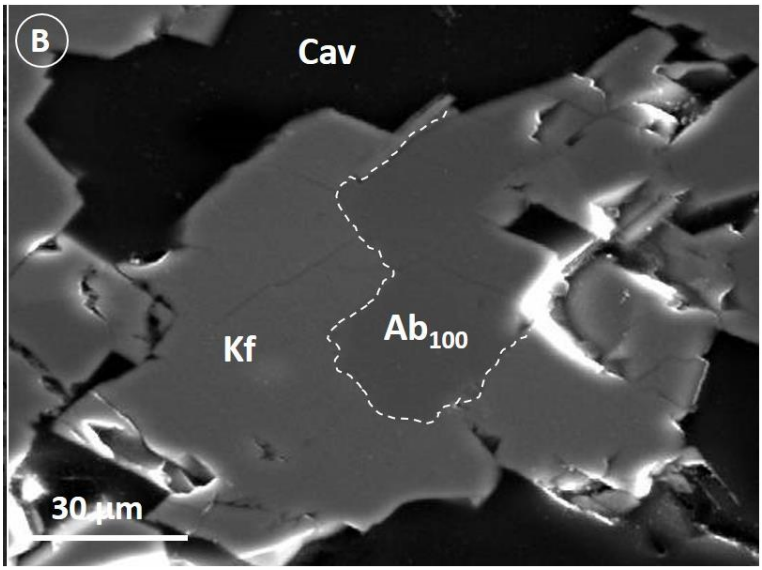

Figure 29. Two examples showing evidence of repeated replacement of feldspar by the CDP process at the MDC. A) Euhedral crystal of hydrothermal albite (Ab_{100}) with strong micro-porosity with an overgrowth of K-Feldspar (Kf). Note that chlorite (Chl) is filling fractures or dissolution zones in and around the K-feldspar. B) Fine-grained hydrothermal albite (Ab_{100}) being replaced by later K-Feldspar.

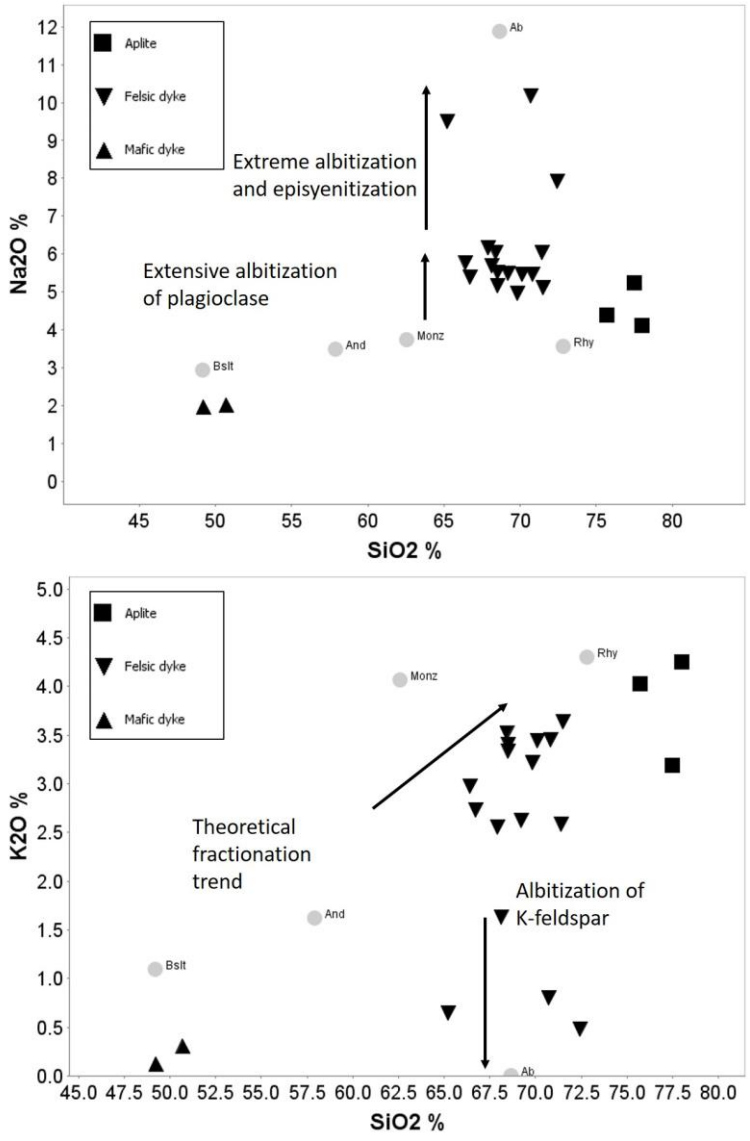

Figure 30. Diagrams showing the behaviour of Na_2O and K_2O (in wt. %) in samples from the MDC. Inverted triangles represent felsic dyke rocks, which is the group most affected by sodic alteration. For comparative purposes, the grey dots shown represent the compositions of typical igneous rocks (Cox et al. 1979) and the composition of albite (Ab) is also shown to highlight the intensity of the alteration process. Bslt=Basalt, And=Andesite, Monz=Monzonite, Rhy=Rhyolite.

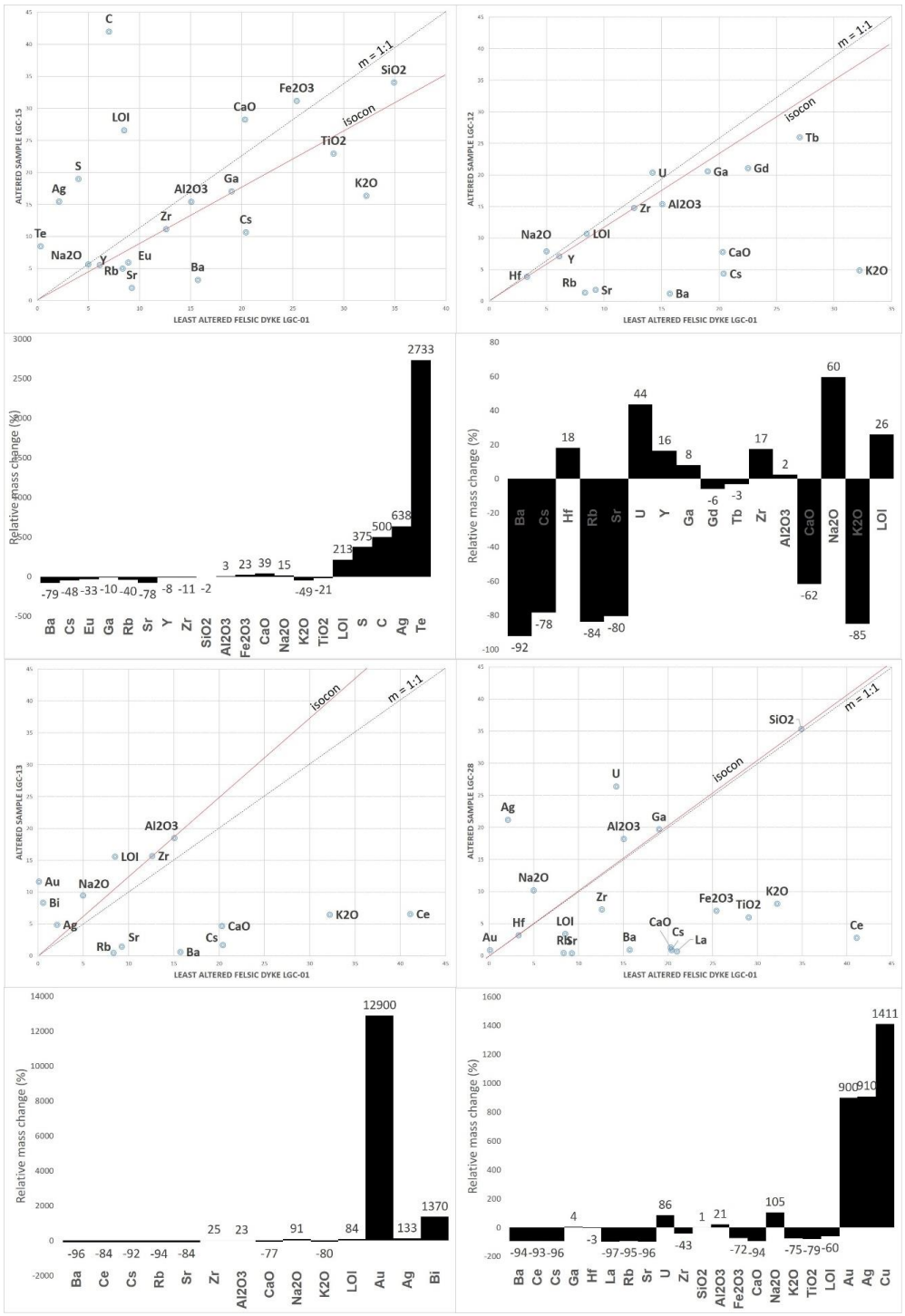

Figure 31. Isocon diagrams (after Grant, 1986) for four felsic dykes samples with different degrees of alteration (Table 6) showing the relative gains and losses and the relative mass

changes. Major elements are plotted as % of the oxides whereas trace elements are plotted as part per million (ppm). According to Grant (1986), elements are scaled to have a clearer view and to highlight the changes in some trace elements that otherwise would not be visible. For every case, the least altered sample is the same (MI-LGC-01), an equigranular dyke from the Planet area. Samples are organised according to the sodium content. A) Sample LGC-15, B) Sample LGC-12, C) Sample LGC-13, and D) Extremely altered sample LGC-28.

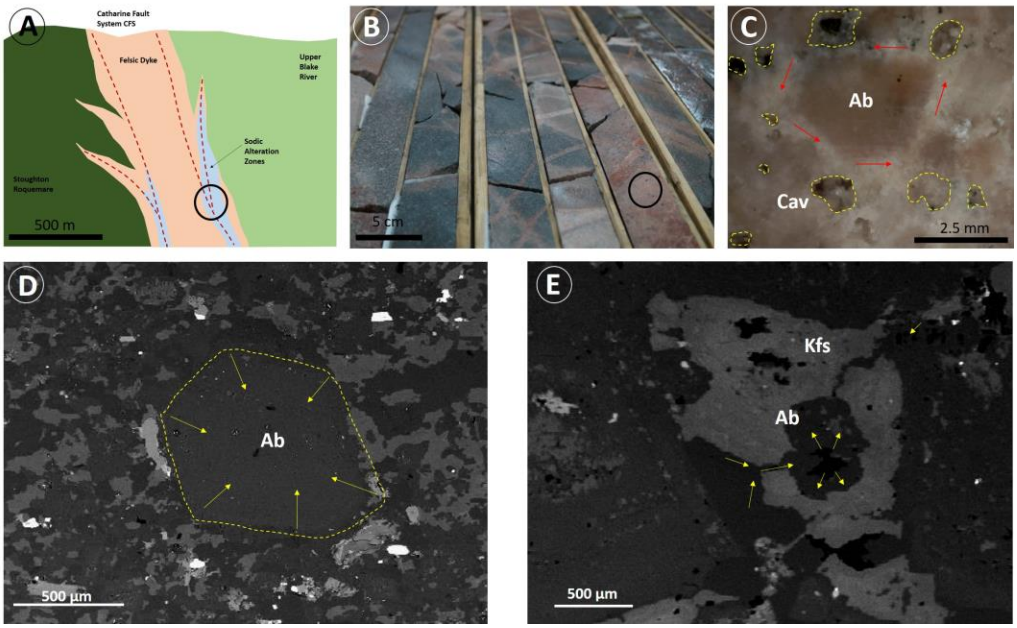

Figure 32. A summarized illustrative diagram showing the different scales at which the sodic alteration occurs at the MDC. A) simplified ideal cross section of the MDC, felsic dykes not wider than 500m have been emplaced along the strike of the CFS close to the contact between mafic and felsic volcanic rocks; sodic alteration zones are controlled by fault or fracturing zones. B) example of an structurally controlled alteration zone like the one circled in black color in A. The felsic dykes show albite – hematite alteration for several meters in core where the movement of fluids and precipitation of albite is controlled by fracturing. C) detail of an episyenitic texture like the one circled in B; the red arrows illustrate how alkaline fluids circulated through the cavities (yellow) generated by the dissolution of quartz and mafic minerals from the original felsic dyke, facilitating the CDP processes in single crystals. D) and E) two different ways how the crystal replacement can take place. In D, a single subhedral feldspar crystal was replaced inwards keeping the shape of the crystal (pseudomorphic replacement) with high porosity observed in the newly formed mineral, whereas in E, an anhedral K-Feldspar crystal is being replaced from its core outwards, the hydrothermal fluids entered to the centre of the grain using micro-porosity, in this case the replacement is partial and not pseudomorphic, the shape of the grain is modified and two different compositions are observed in the final product.

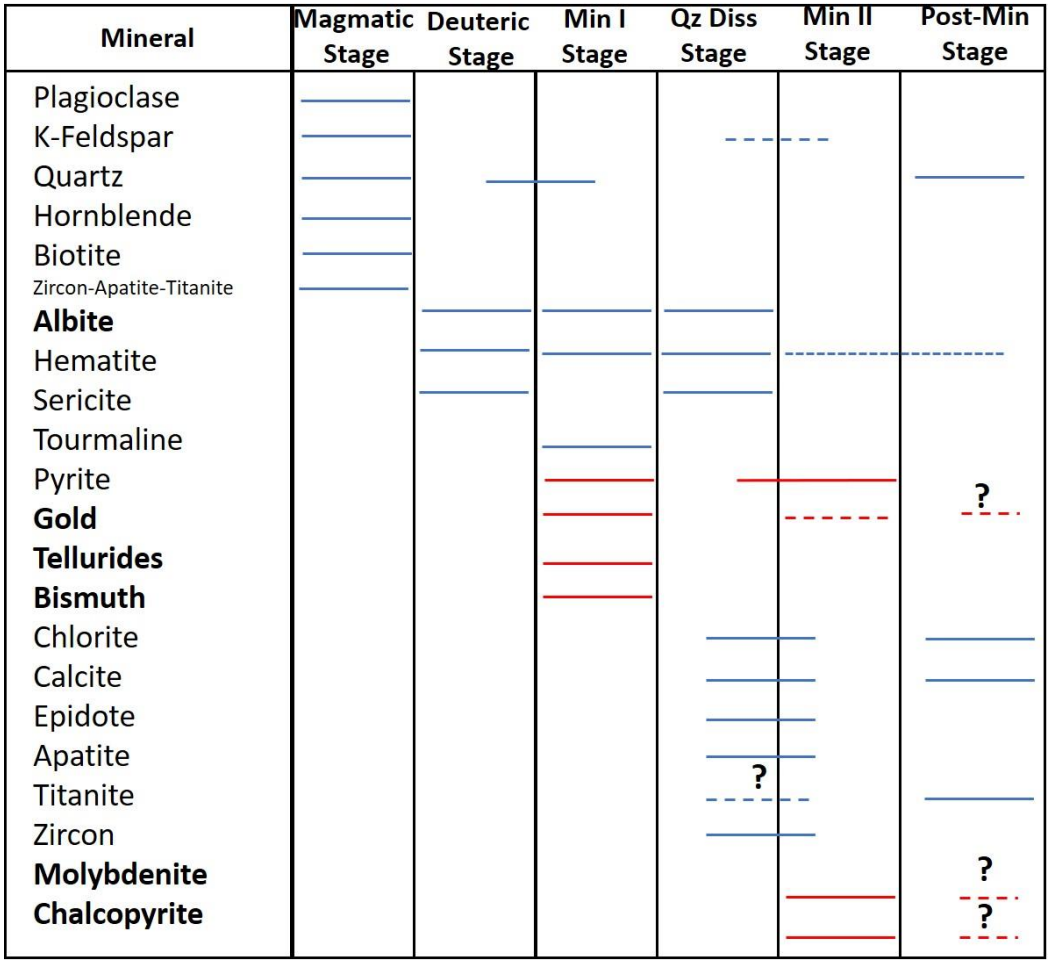

Figure 33. A generalized paragenetic sequence for the evolution of the MDC. Six stages have been observed: magmatic, deuteric, mineralisation I, episyenitisation, mineralisation 2, and late mineral stage. Note that dashed bars denote uncertainties about the timing. Red bars are used to highlight ore minerals.

Appendices

Appendix 1. Summary of petrographic examination of thin sections

Sample	Location	Drill hole	Depth	Macro Description	Texture	Plag	KF	Qz	Bio	Hnb
MI-PL-PET-01	Planet - outcrop			Equigranular intrusive with aplitic dykes	Granular Hypidiomorphic	63.9	13.5	13.2	6.6	2.2
MI-PL-PET-02	Planet - outcrop			Porphyritic intrusive	Porphyritic	50	8.8	30.8	2.9	7.5
MI-PL-PET-03	Planet - outcrop			Fine grained aplite	Granular Allotriomorphic - Sacharoidal	28.6	33.2	28.6	4.8	4.8
MI-AL-PET-04	Allied	MG-14-01	90.2	QF porphyry	Porphyritic	63.2		36.8		
MI-AL-PET-05	Allied	MG-14-09	86.5	Episyenite	Granular Hypidiomorphic with dissolution cavities	68.75	7.5		2.5	
MI-AL-PET-06	Allied	MG-14-10	126	Episyenite	Granular Hypidiomorphic with dissolution cavities	59.2	2.7			
MI-AL-PET-07	Allied	MG-14-10	99.3	Chl-Ca Hydrothermal breccia	Granular Hypidiomorphic locally brecciated	73.6	8	18.4		
MI-AL-PET-08	Allied	MG-14-10	134.1	Equigranular intrusive with aplitic dyke	Granular Hypidiomorphic	68.2	11.4	13.6		2.5
MI-AL-PET-09	Allied	MG-14-11	133	Episyenite with weak dissolution process	Granular Hypidiomorphic with dissolution cavities	63.6	14.8	15.9	5.7	
MI-AL-PET-11	Allied	MG-14-11	127	Qz vein with tourmaline	Granular Hypidiomorphic with quartz vein	85.2		14.8		
MI-AL-PET-12	Allied	MG-14-11	14.4	Equigranular intrusive with clast	Granular Hypidiomorphic	50	10.4			
MI-AL-PET-13	Allied	MG-15-16	147	Skarn alteration in volcanic host rock	Granoblastic					
MI-AL-PET-14	Allied	MG-14-07	120	Equigranular unaltered intrusive	Granular Hypidiomorphic	67.9	13.1	11.9	7.1	
MI-AL-PET-15	Allied	MG-14-12	52	Equigranular intrusive with strong sericitic alteration - Episyenite	Granular Hypidiomorphic with dissolution cavities	48.7	21.1		1.3	
MI-AL-PET-16	Allied	MG-14-12	138	Ca-Ser alteration in volcanics	Granular hypidiomorphic intrusive in contact with massive fine grained volcanics	60.8	4.5	34.7		
MI-AL-PET-18	Allied	MG-15-16	28	Altered volcanics	Massive fine grained					
MI-AL-PET-19	Allied	MG-15-16	180.6	Altered volcanics with quartz vein	Porphyritic					

MI-AL-PET-20	Allied	MG-15-16	210.6	Hydrothermal breccia with calcite, moly and silica	Brecciated					
Sample	**Location**	**Drill hole**	**Depth**	**Macro Description**	**Texture**	**Plag**	**KF**	**Qz**	**Bio**	**Hnb**
MI-AL-PET-21	Allied	MG-15-16	25.5	Mafic dyke	Porphyritic					Remnants
MI-AL-PET-24	Allied	MG-14-03	41	Chlorite breccia with possible illite	Brecciated	33.5	6.5	10		
MI-AL-PET-25	Allied	MG-14-03	47.5	Breccia with jasper silica in intrusive rock	Brecciated	80		20		
MI-AL-PET-26	Allied	MG-14-03	83.1	Quartz vein with alteration haloes	Aplitic - mirmekitic	53		47		
MI-AL-PET-27	Allied	MG-14-07	99	Feldspar porphyry with volcanic fragment and quartz vein	Porphyritic					
MI-AL-PET-28	Allied	MG-14-07	65	Porphyritic intrusive rock hosting two fine grained aplitic dykes	Porphyritic - Aplitic	70	15	15		
MI-AL-PET-29	Allied	MG-14-07	116.4	Feldspar porphyry	Porphyritic	60		34	4	
MI-AL-PET-30	Allied	MG-14-09	111.4	Chlorite disturbed intrusive	Brecciated	76		21		3
MI-AL-PET-31	Allied	MG-14-07	10.1	Porphyritic aplite	Porphyritic with aplitic matrix	44	4	52		
MI-AL-PET-32	Allied	MG-14-07	4.9	Equigranular intrusive with aplitic dyke	Granular hypidiomorphic	55.5	25	16.6	2.9	
MI-AL-PET-33	Allied	MG-14-09	131.5	Hydrothermal breccia with chlorite, intrusive and vein clasts	Brecciated					
MI-AL-PET-34	Allied	MG-14-03	35.1	Fine grained aplite	Aplitic - Granular hypidiomorphic	43	7	50		
MI-AL-PET-35	Allied	MG-14-03	80.4	Feldspar porphyry	Porphyritic	50	15	35		
MI-AL-PET-36	Allied	MG-14-07	61.5	Feldspar porphyry	Porphyritic	59	36	5	Tr	
MI-AL-PET-37	Allied	MG-14-09	44	Equigranular intrusive with quartz veins	Granular Hypidiomorphic with dissolution cavities	74.2	9.4	16.4		
MI-AL-PET-38	Allied	MG-14-09	125.8	Mafic volcanics	Porphyritic					
MI-AL-PET-39	Allied	MG-14-01	122.8	QF porphyry	Porphyritic	64.8	35.2			
MI-PL-PET-40	Planet core	MG-15-25	243	Equigranular intrusive in proximal zone of high grade Au vein	Granular hypidiomorphic	48.1	37	14.9		

MI-PL-PET-41	Planet core	MG-15-25	274.8	Pegmatite with Qz and KF in equigranular intrusive	Aplitic - Pegmatitic	39.4	3.1	57.5		
Sample	**Location**	**Drill hole**	**Depth**	**Macro Description**	**Texture**	**Plag**	**KF**	**Qz**	**Bio**	**Hnb**
MI-PL-PET-42	Planet core	MG-15-25	206	Quartz vein with pyrite, tellurides and moly	Crystalline					
MI-PL-PET-43	Planet core	MG-15-25	197.8	Equigranular intrusive with strong KF or albite alteration and high grade of Au	Granular hypidiomorphic	86		7		
MI-PL-PET-44	Planet core	MG-15-25	95.6	Calcite - actinolite vein hosted by equigranular intrusive	Granular hypidiomorphic	68	8	24		
MI-PL-PET-45	Planet core	MG-15-25	68.3	Intrusive with radial texture of plagioclase and hornblende	Granular Radial?	48.5	8.9	37	2.8	2.8
MI-PL-PET-46	Planet core	MG-15-25	58	Intrusive with possible ust textures	Equigranular with pegmatitic? Ust					
MI-PL-PET-47	Planet core	MG-15-25	32.4	Zoned skarn alteration in mafic volcanics	Granoblastic					
MI-PL-PET-48	Planet core	MG-15-24	42.6	Basalt with strong ser-carb-py alteration	Aphanitic - weakly foliated					
MI-PL-PET-49	Planet core	MG-15-24	261.2	Py, Ccp, Mo around quartz vein with anomalous Ag and Bi	Aphanitic (host) and crystalline (vein)					
MI-PL-PET-50	Planet core	MG-15-24	197	Ca-Qz vein with Ccp hosted by pegmatitic intrusive	Pegmatitic-Graphic-Mirmekitic					
MI-PL-PET-51	Planet core	MG-15-24	197.5	Pegmatitic dykes with graphic texture	Pegmatitic - graphic	23	50	27		
MI-PL-PET-52	Planet core	MG-15-24	114.8	Porphyritic intrusive with fine-grained alteration groundmass	Porphyritic	88	12			
MI-PL-PET-53	Planet core	MG-15-24	101	Unaltered equigranular intrusive	Granular hypidiomorphic	59.4	10.8	16.2	5.4	8.2
MI-PL-PET-54	Planet core	MG-15-24	74.8	Qz vein with ChPy-Te-Mo-Bi	Granular hypidiomorphic	69.5	8.8	21.7		
MI-PL-PET-55	Planet core	MG-15-24	51	Intrusive with sericitic alteration and anomalous Au	Granular hypidiomorphic	70	3	27		
MI-ME-PET-56	Meilleur core	MG-15-26	248.4	Qz vein with moly and tellurides	Crystalline - Granular hypidiomorphic					
MI-ME-PET-57	Meilleur core	MG-15-26	238	Porphyritic intrusive with strong dissolution process	Porphyritic	70	7.5	10	2.5	
MI-ME-PET-58	Meilleur core	MG-15-26	182	Mafic dyke	Porphyritic	71				

MI-ME-PET-59	Meilleur core	MG-15-26	17.5	Unaltered intermediate volcanics	Porphyritic	78			14	8
MI-ME-PET-60	Meilleur core	MG-15-26	23.4	Strongly altered volcanics	Aphanitic					
Sample	**Location**	**Drill hole**	**Depth**	**Macro Description**	**Texture**	**Plag**	**KF**	**Qz**	**Bio**	**Hnb**
MI-ME-PET-61	Meilleur core	MG-15-27	209.7	Hydrothermal breccia with quartz, Cpy and Moly	Brecciated - Granular hypidiomorphic					
MI-ME-PET-62	Meilleur core	MG-15-27	198.6	Quartz vein with molybdenite	Crystalline - porphyritic	83		17		
MI-ME-PET-63	Meilleur core	MG-15-27	158.4	Episyenite with strong dissolution and moly dissemination	Granular Hypidiomorphic with dissolution cavities	59.5				
MI-ME-PET-64	Meilleur core	MG-15-27	83.4	Possible pyroxene crystals in porphyritic volcanics	Porphyritic					
MI-AL-PET-65	Allied core	MG-15-18	375.5	Qz vein with tellurides and moly	Crystalline - Granular hypidiomorphic	82		18		
MI-AL-PET-66	Allied core	MG-15-18	276.7	Qz vein with anomalous Au,Ag,Bi,Pb	Crystalline					
MI-AL-PET-67	Allied core	MG-15-18	102.5	Mafic volcanics with strong ser-ca-py alteration	Aphanitic					
MI-AL-PET-68	Allied core	MG-15-19	37	Feldspar porphyry	porphyritic	59.5		27	5.4	8.1
MI-AL-PET-69	Allied core	MG-15-19	164.2	Brecciated episyenite	Brecciated with dissolution cavities					
MI-AL-PET-70	Allied core	MG-15-19	159.6	Episyenite with masses of quartz and large titanite crystals	Episyenitic - brecciated					
MI-AL-PET-71	Allied core	MG-15-19	152.95	Aplite dykes in feldspar porphyry	Porphyritic					
MI-AL-PET-72	Allied core	MG-15-19	146.3	Episyenite with strong dissolution and quartz patches	Granular Hypidiomorphic with dissolution cavities	81		9		
MI-AL-PET-73	Allied core	MG-15-20	341.6	Quartz vein with chlorite halo and hosted by episyenite with strong dissolution	Crystalline - Granular hypidiomorphic - Dissolution cavities					
MI-AL-PET-74	Allied core	MG-15-17	115	Feldspar porphyry with strong green sericite alteration	porphyritic					
MI-AL-PET-75	Allied core	MG-15-21	434	Unaltered feldspar porphyry	porphyritic	73		27		

Sample	Dissolution Cavities	Chl	Ser	Hem	Alb	KF	Sil	Ca	Ep	Alt2	Alt3	Py	CPy	Mo
MI-PL-PET-01		Mod	Mod	Mod				Wk	Wk			Wk	Tr	
MI-PL-PET-02		Wk	Mod	Wk					Mod			Wk		
MI-PL-PET-03		Wk	Wk	Wk					Wk			Wk		
MI-AL-PET-04		Mod	Mod				Wk - Veins		Wk	Clay				
MI-AL-PET-05	21.25	Mod	Wk	Mod	Mod					Titanite		Wk	Tr	
MI-AL-PET-06	38.1	Mod		Mod	Str				Mod	Titanite		Mod		
MI-AL-PET-07		Strong	Wk	Wk	Mod			Wk	Wk			Wk	Wk	
MI-AL-PET-08	4.3	Mod	Mod	Mod				Wk		Titanite		Wk		
MI-AL-PET-09	Wk	Mod	Mod	Mod				Wk				Wk		
MI-AL-PET-11	Wk	Mod	Mod	Mod	Mod		Mod	Wk	Wk	Tourmaline		Wk	Wk	
MI-AL-PET-12	39.6	Strong		Mod	Str					Titanite		Mod		
MI-AL-PET-13		Mod					Mod	Str	Str	Garnet		Mod	Wk	
MI-AL-PET-14	Wk	Mod	Mod	Mod				Wk	Wk			Wk		
MI-AL-PET-15	28.9	Strong	Str	Mod						Titanite		Wk	Wk	
MI-AL-PET-16		Wk	Str		Str		Str	Mod				Str		
MI-AL-PET-18		Strong	Str		Str		Str	Str				Str		
MI-AL-PET-19		Strong	Str					Str				Str		
MI-AL-PET-20							Str	Str				Str		Str
Sample	**Dissolution Cavities**	**Chl**	**Ser**	**Hem**	**Alb**	**KF**	**Sil**	**Ca**	**Ep**	**Alt2**	**Alt3**	**Py**	**CPy**	**Mo**
MI-AL-PET-21		Strong	Mod				Wk		Str			Wk	Wk	
MI-AL-PET-24	3.5	VStr		Mod	Wk		Wk					Wk		
MI-AL-PET-25		Mod	Wk	Str	Mod		Str		Wk	Tourmaline		Wk		
MI-AL-PET-26				Mod	Mod		Mod					Wk		
MI-AL-PET-27		Mod	Mod						Mod			Wk		
MI-AL-PET-28		Mod	Mod	Str					Wk			Wk		
MI-AL-PET-29	2	Mod	Mod	Mod			Wk		Wk	Apatite		Wk		
MI-AL-PET-30		Strong		Mod			Wk					Wk		

MI-AL-PET-31		Mod	Mod	Str				Wk				Wk		
MI-AL-PET-32		Mod	Mod	Mod				Wk	Wk			Wk	Tr	
MI-AL-PET-33		Strong			Mod		Mod			Tourmaline		Mod	Mod	
MI-AL-PET-34			Wk	Mod								Wk		
MI-AL-PET-35		Wk	Wk	Mod								Wk		
MI-AL-PET-36		Mod	Mod	Mod				Str						
MI-AL-PET-37	Weak	Mod	Wk	Mod	Wk		Mod			Titanite		Wk	Wk	Wk
MI-AL-PET-38		Strong								Leucoxene?		Mod		
MI-AL-PET-39		Mod	Mod						Mod			Wk	Wk	
MI-PL-PET-40			Wk	Mod	Wk	Str		Mod		Tourmaline		Mod	Wk	
Sample	**Dissolution Cavities**	**Chl**	**Ser**	**Hem**	**Alb**	**KF**	**Sil**	**Ca**	**Ep**	**Alt2**	**Alt3**	**Py**	**CPy**	**Mo**
MI-PL-PET-41		Wk	Mod	Mod	Str									
MI-PL-PET-42				Wk			VStr	Mod		Tourmaline		Mod		Wk
MI-PL-PET-43	7	Mod		Wk	Str							Wk		
MI-PL-PET-44		Mod	Str	Str			Str	Str				Mod		
MI-PL-PET-45		Mod	Mod	Mod					wk			Wk		
MI-PL-PET-46			Mod	Mod										
MI-PL-PET-47		Strong						Str	Str	Amph?	Px?	Mod	wk	
MI-PL-PET-48					Str			Str				Str	Wk	
MI-PL-PET-49		Str		Mod			Str	Str	Str			Str	Wk	
MI-PL-PET-50		Mod	Wk	Mod			Str	Str					Mod	
MI-PL-PET-51		Wk	Wk	Mod			mod					wk		
MI-PL-PET-52			str	Str	Mod	wk	Mod		mod			Wk		
MI-PL-PET-53		Wk	Wk	Mod								Py		
MI-PL-PET-54			Mod	Str	Mod		mod	mod				Mod		Mod
MI-PL-PET-55		Wk	Str	Mod				wk				Py		
MI-ME-PET-56			Mod	Mod	Str	mod	str	Mod				Wk		Str
MI-ME-	10	Wk	Wk	Mo	Mo							Mo	Wk	

PET-57				d	d							d		
MI-ME-PET-58								Wk		Serpentine ?				
Sample	**Dissolution Cavities**	**Chl**	**Ser**	**Hem**	**Alb**	**KF**	**Sil**	**Ca**	**Ep**	**Alt2**	**Alt3**	**Py**	**CPy**	**Mo**
MI-ME-PET-59		mod	wk	wk								wk		
MI-ME-PET-60			mod				str	wk	str	zoisite-str		wk		
MI-ME-PET-61			wk	wk	mod		str					wk	wk	wk
MI-ME-PET-62			wk	wk	w		str					mod	wk	mod
MI-ME-PET-63	40.5	mod			str					titanite		mod		wk
MI-ME-PET-64		str	wk				mod		str	Actinolite		wk	wk	
MI-AL-PET-65			wk	mod	str		str					wk		wk
MI-AL-PET-66							str					mod		
MI-AL-PET-67			??		??		??	Str				str		
MI-AL-PET-68		mod	mod	mod					wk			Wk		
MI-AL-PET-69		mod	wk	mod	str		wk			titanite		wk		
MI-AL-PET-70		Str	wk	mod	str		str			titanite		Mod	Wk	
MI-AL-PET-71		Mod		mod	mod			mod	wk	titanite		str		
MI-AL-PET-72	10		wk	mod	str		str			titanite		Wk		
MI-AL-PET-73	str	mod	wk	mod	str					titanite		Wk	Wk	
MI-AL-PET-74		mod	vstr				mod	str	str			Wk		
MI-AL-PET-75		wk	mod	wk								Wk		

Sample	General Description	Classification
MI-PL-PET-01	Equigran QzMzDio with Chl, Ser, Ca, Py and 2 aplitic dykes. No Dissolution	Hnb Bio QzMzDio
MI-PL-PET-02	Porphyritic intrusive with large phenocrysts of plagioclase and KFeldspar as well as smaller phenocrysts of biotite and hornblende within a finer grained matrix of plagioclase, quartz and minor KFeldspar. Chlorite, sericite and epidote alteration are common as well as pyrite dissemination.	Porphyritic Granodiorite
MI-PL-PET-03	medium grained granular allotriomorphic monzogranite with a finer grained aplitic dyke of the same composition affected by sericite, chlorite and epidote alteration and showing quartz intergrowth within feldspar crystals along the contact of the dyke.	Monzogranite
MI-AL-PET-04	Porphyritic intrusive with phenocrysts of quartz and plagioclase in a very fine grained matrix made up by quartz and feldspars that cannot be assessed. The sample has some veins of Qz+Chl+Ep and moderate sericitic alteration.	Porphyritic Tonalite
MI-AL-PET-05	Granular hypidiomorphic textured anorthosite with a secondary process of quartz and mafic minerals dissolution (episyenitization?) that has totally leached the quartz from the rock forming cavities subsequently filled with hydrothermal albite?, chlorite, titanite, pyrite and traces of chalcopyrite. The original composition of the rock before the dissolution process could be quartz-dioritic or quartz-monzodioritic.	Albitite, Episyenite
MI-AL-PET-06	Granular hypidiomorphic textured anorthosite produced by a secondary process of quartz and mafic minerals dissolution (episyenitization?) that has totally leached the quartz from the rock, forming cavities subsequently filled with hydrothermal albite?, chlorite, epidote, titanite and pyrite. The original composition of the rock before the dissolution process could be quartz-dioritic? or quartz-monzodioritic?	Albitite, Episyenite
MI-AL-PET-07	Granular hypidiomorphic intrusive composed by plagioclase large crystals, sometimes surrounded by a not well developed matrix of fine grained K-Feldspar and quartz. The sample is locally brecciated by the introduction of coarse grained chlorite and minor amounts of calcite, epidote and chalcopyrite.	Brecciated Quartz-Diorite
MI-AL-PET-08	The sample is a granular hypidiomorphic textured quartz-monzodiorite with a clast of aplitic rock of finer grain with approximately the same composition. The rock is mainly composed by plagioclase, quartz and K-feldspar with traces of hornblende as mafic mineral. The rock has been weakly affected by dissolution processes evident by the presence of cavities partially filled with chlorite, hydrothermal plagioclase, pyrite and titanite.	Quartz-MonzoDiorite
MI-AL-PET-09	Granular hypidiomorphic textured quartz-monzodiorite dominated by plagioclase and K-Feldspar with interstitial fine grained feldspar and quartz forming a not well developed matrix or groundmass. Dissolution process is weak in this sample but some cavities filled with chlorite and pyrite were observed. Plagioclase and K-Feldspar intergrowns are common	Bio Quartz Monzo-diorite
Sample	**General Description**	**Classification**
MI-AL-PET-11	Intrusive rock with granular hypidiomorphic texture, hosting a milimetric quartz vein with pyrite and tourmaline associated, showing moderate albite alteration on its selvages. Some parts of the rock show development of a fine grained matrix of quartz and feldspar. The sample is weakly affected by quartz dissolution.	Quartzdiorite
MI-AL-PET-12	The sample is a granular hypidiomorphic monzodiorite with a clast of a different rock richer in plagioclase. The classification given here indicates the current composition since both rocks have undergone an intensive dissolution process that has leached all the quartz and mafic minerals from them.	Monzodiorite

MI-AL-PET-13	Volcanic rock with obliterated texture and mineralogy, the sample is pervasively affected by skarn alteration. The observed assemblage is Garnet – Epidote – Chlorite – Quartz – Calcite – Pyrite – Chalcopyrite	Mafic metavolcanic with skarn alteration
MI-AL-PET-14	Medium grained quartz-monzodiorite with granular hypidiomorphic texture and magmatic crystallization of plagioclase, quartz, K-Feldspar and biotite with later hydrothermal alteration to chlorite, sericite, and epidote. The rock has been affected by a post-magmatic process of dissolution that is weak in this sample but that has leached part of the quartz and biotite forming cavities that were subsequently cemented by chlorite, pyrite, epidote and fine-grained albite? Most of the feldspar crystals are affected by hematite staining which gives them a reddish – pink color on hand sample.	Bio Quartz Monzo-diorite
MI-AL-PET-15	Granular hypidiomorphic textured monzodiorite with a secondary dissolution texture (episyenitization).	Monzodiorite
MI-AL-PET-16	The sample is a strongly altered volcanic rock in contact with a fine grained aplitic dyke. No volcanic textures or primary minerals are preserved due to the alteration.	Tonalite
MI-AL-PET-18	The sample is a strongly altered fine grained volcanic rock hosting a quartz vein with an alteration halo of albite-calcite and calcite.	Mafic metavolcanic
MI-AL-PET-19	The sample is a strongly altered fine grained volcanic with porphyritic texture which is hosting 3 milimetric quartz veins.	Mafic metavolcanic
MI-AL-PET-20	The sample is a hydrothermal breccia with clasts of intrusive rock and quartz veinlets cemented by calcite, pyrite and molybdenite.	Hydrothermal breccia
MI-AL-PET-21	The sample is a fine grained intensely altered porphyritic intrusive of mafic composition.	Altered mafic dyke
MI-AL-PET-24	the rock is basically a brecciated monzodiorite or a breccia with tectonic and hydrothermal processes involved in its formation.	Brecciated monzodiorite
MI-AL-PET-25	The sample is a breccia with tectonic and hydrothermal component. Poorly calibrated fragments of a plagioclase rich intrusive and quartz veinlets are strongly disturbed by hematite, chlorite – pyrite and silica.	Brecciated quartzdiorite
Sample	**General Description**	**Classification**
MI-AL-PET-26	Fine grained tonalitic intrusive with saccharoidal or aplitic texture mainly composed by quartz and plagioclase hosting a quartz vein that develops a proximal albite halo and a more distal halo of quartz – plagioclase intergrowth characterized by mirmekitic textures of probable metasomatic origin?	Aplitic Tonalite with quartz vein
MI-AL-PET-27	Porphyritic intrusive rock with a fragment of volcanic rock intensely altered. A quartz vein is cutting both lithologies.	Feldspar porphyry
MI-AL-PET-28	Porphyritic intrusive rock hosting two fine grained aplitic dykes	Porphyritic quartz-monzodiorite
MI-AL-PET-29	Porphyritic intrusive with large phenocrysts of plagioclase and minor remnants of biotite and hornblende phenocrysts replaced by chlorite and surrounded by a quartz - plagioclase matrix	Porphyritic tonalite
MI-AL-PET-30	Granular hypidiomorphic textured plagioclase rich intrusive cut by a tectonic breccia zone with abundant infill of chlorite.	Brecciated tonalite
MI-AL-PET-31	Fine grained aplitic intrusive mostly composed by quartz and plagioclase and minor KF that shows the presence of some isolated plagioclase phenocrysts	Porphyritic tonalite
MI-AL-PET-32	Granular hypidiomorphic quartz-monzodioritic intrusive of medium grain intruded by a very fine grained aplitic dyke.	Quartz-MonzoDiorite
MI-AL-PET-33	Breccia with fragments of plagioclase rich intrusive and quartz veins. The matrix and/or cement consists on chlorite-pyrite and chalcopyrite	Hydrothermal breccia
MI-AL-PET-34	Fine - medium grained intrusive, equigranular made up of quartz, plagioclase and Kfeldspar with common mirmekitic textures. Hematite and sericite alteration with weak pyrite alteration	Fine grained tonalite
MI-AL-PET-35	Porphyritic intrusive with phenocrysts of plagioclase and Kfeldspar within a	Porphyritic granodiorite

	fine grained matrix of Qz-Plag-KF. Some remnants of biotite are totally chloritized	
MI-AL-PET-36	Porphyritic textured intrusive with plagioclase phenocrysts and minor biotite phenocrysts within a matrix of fine grained Qz-Plag-KF	Porphyritic tonalite
MI-AL-PET-37	medium to coarse grained granular intrusive partially affected by quartz? dissolution and hosting two milimetric quartz veins with associated sulfide mineralization.	Quartz-MonzoDiorite
MI-AL-PET-38	Mafic volcanic rock with large plagiocalse aggregates in semiradial textures surrounded by a chloritized matrix and showing abundant dissolution pits caused by alteration. Plag is moderately altered to sericite and abundant leucoxene?	Mafic metavolcanic
MI-AL-PET-39	Medium grained porphyritic intrusive with phenocrysts of euhedral quartz and plagioclase and minor hornblende altered to chlorite and epidote within a fine-grained matrix of quartz and plagioclase	Porphyritic tonalite
MI-PL-PET-40	Medium grain equigranular intrusive in proximal zone of high grade vein. Kfeldspar replacing Plag is a common feature. Ca and Py are associated and filling fractures and possible open spaces by dissolution since no mafic minerals are observed. Py growing after magnetite and Cp as inclusions within pyrite.	QzMonzonite
Sample	**General Description**	**Classification**
MI-PL-PET-41	Coarse grained aplitic or pegmatitic dyke cutting the equigranular intrusive rock causing no alteration. The dyke is being strongly albitized and also shows chlorite and sericite alteration of the feldspars.	Tonalite
MI-PL-PET-42	The sample is a Qz vein where different quartz events are interacting with the wallrock and causing silicification and local brecciation in the same direction of the vein. Only Py and Moly were observed forming a narrow ribbon parallel to the margin of the vein	Qz Vein
MI-PL-PET-43	The sample is a plagioclase rich intrusive with granular hypidiomorphic texture and dissolution cavities. It seems that quartz and mafic minerals have been leached from the rock and probably most of the current plagioclase is secondary albite	QzDiorite
MI-PL-PET-44	The sample is a granular hypidiomorphic intrusive rich in plagioclase with strong sericitic alteration hosting a calcite-chlorite vein which is postdating and breaking an earlier quartz vein. Sample was collected for checking possible act-ca vein representing Na-Ca assemblage but is only chl-ca	Tonalite
MI-PL-PET-45	The sample is a medium grained intrusive made up of plag, qz, hnb and bio showing a very particular radial texture where long-narrow plag crystals and honrb-bio are symmetrically surrounded by qz.	Tonalite
MI-PL-PET-46	The sample is part of an equigranular intrusive showing UST textured zone consisting on irregular parallel intergrowns of aplitic dykes and quartz-KF crystals.Ust is not perfectly symmetric but is consistent with fine aplite zones surrounding the margins of perfect pointing quartz crystals	No% calculated. UST is not representative of all the intrusive rock
MI-PL-PET-47	The sample is a mafic volcanic rock strongly affected by skarn alteration. All the primary minerals have been replaced by alteration minerals remaining only some plag relicts in parts of the rock	Skarn with mafic volcanic protolith
MI-PL-PET-48	The sample is a fine grained mafic volcanic strongly altered with calcite and strong diss of pyrite. All the carbonate and sulfide is floating within a matrix of plagioclase of possible hydrothermal origin.	Altered mafic volcanics
MI-PL-PET-49	The sample is showing the halo zone of a quartz vein with a proximal zone of Chl, Ca, Ep. The vein is hosted by mafic volcanics rich in plag affected by chlorite alteration. All the mafic minerals were replaced by chl. Py dissemination is strong in all the sample with zones of massive py in the proximal zone	Altered mafic volcanics in selvage of quartz vein
MI-PL-PET-50	The sample is a qz-ca vein hosted by a felsic intrusive with graphic and mirmekitic textures	Felsic intrusive with qz-ca vein and volcanic rock fragments
MI-PL-PET-51	The sample is an intrusive with pegmatitic exsolution textures of Qz, Kfeldspar	Pegmatitic granite

	and plagioclase hosting a quartz vein that is branched towards the host rock	
MI-PL-PET-52	The sample is a medium to fine grained intrusive with plag, KF and remnants of biotite and hornblende with a fine grained green alteration assemblage which is made up of epidote, chlorite, sericite, KF, apatite?	Monzodiorite
Sample	**General Description**	**Classification**
MI-PL-PET-53	The rock is a medium to coarse grained granular hypidiomorphic intrusive with plagioclase, Kfeldspar, Qz, Bio and Hnb and no evidences of dissolution. The alteration is restricted to sericite-hem in plagioclase and weak chlorite over biotite and hornblende	QzMonzodiorite
MI-PL-PET-54	The sample shows a qz vein with an alteration halo of fine plagioclase and sulfides passing to a less altered zone of calcite and sericite. The sample also shows a milimetric aplitic dyke cutting the least altered zone	Tonalite
MI-PL-PET-55	The sample is an intrusive rock with a central Qz vein which has a strong halo of albite alteration. The distal halo or the rest of the sample is strongly affected by sericitic alteration. Several parts of the sample are rich in fine quartz which is surrounding all the plag crystals and which is likely an alteration product forming a phyllic assemblage	Tonalite
MI-ME-PET-56	The sample is a quartz-calcite vein with a strong sulfide margin hosted by an equigranular intrusive with strong silicification and albitization.	Qz Vein
MI-ME-PET-57	The sample is a porphyritic intrusive with phenocrysts of Qz, plag and biotite surrounded by a matrix of quartz and plagioclase. The feldspars are partially altered to albite, sericite and hematite and the rock is affected by dissolution (episyenitization). The cavities are partially filled with by pyrite - Cpy with minor amounts of chlorite	QzDiorite
MI-ME-PET-58	The sample is a porphyritic dyke with phenocrysts of plagioclase and pyroxene, probably augite? Floating in a fine matrix partially trachitic with the same composition	Gabbro
MI-ME-PET-59	The sample is a volcanic rock of porphyritic texture with plagioclase>Bio>Hnb in a fine grained matrix of apparently pure plagioclase	Andesite or basalt
MI-ME-PET-60	The sample is a volcanic rock strongly altered where the protolith is not clear since the rock is currently is a mass of epidote-zoisite-quartz and sericite. All the primary minerals have been replaced	Altered volcanics
MI-ME-PET-61	The sample is a hydrothermal breccia where quartz is breaking and cementing fragments of plagioclase rich intrusive. Monomictic, matrix supported and badly sorted. The cementing hyd fluid is causing albite alteration and sulfide dissemination on the intrusive clasts	Hydrothermal breccia
MI-ME-PET-62	The sample is mostly a quartz vein hosted by a porphyritic QF intrusive. The intrusive shows weak albite alteration and the vein contains several zones of sulfides from which Moly is always deposited in dissolution zones along the margins of the Qz crystals	Qz Vein
MI-ME-PET-63	The sample is a medium to coarse grained equigranular intrusive with strong dissolution process that created dissolution cavities partially filled with chlorite, Qz, Moly, etc. Most of the plagioclase is secondary albite with chessboard twinning	Albitite, Episyenite
MI-ME-PET-64	The sample is a porphyritic volcanic rock strongly altered to propylitic assemblage. The phenocrysts are Hnb, Bio and remnants of Plag floating in a very fine matrix. All the phenocrysts are being replaced by chl, ep and actinolite. Some patches and veins of quartz-ser associated to epidote-zoisite were observed	Altered volcanics
Sample	**General Description**	**Classification**
MI-AL-PET-65	The sample is a Qz vein hosted by a plagioclase rich intrusive where most of the plag is secondary albite. The vein has tourmaline and py-Moly associated. Au was observed as native Au filling fractures in plag within the proximal halo of the vein	QzDiorite - Qz Vein

MI-AL-PET-66	The sample is 100% quartz vein with several narrow parallel bands of the original host rock (Plag rich intrusive) that were ripped off by the quartz. The qz is well fractured and there is a central zone of sulfide concentration within a fracture zone parallel to those bands	Qz Vein
MI-AL-PET-67	The sample is a totally metasomatized mafic volcanics where the texture and original mineralogy has been totally obliterated and it is now a fine mass of calcite, plagioclase, quartz and abundant diss pyrite. Possible Au was observed disseminated within the fine alteration groundmass	Altered mafic volcanics
MI-AL-PET-68	The sample is a porphyritic intrusive with phenocrysts of plagioclase, hnb and biotite. No Qz eyes. The matrix is made up of quartz and plagioclase and is fine grained, but the mineralogy may be identified	Porphyritic Tonalite
MI-AL-PET-69	The sample is an episyenite with a very strong process of dissolution that has leached all the quartz/Kfeldspar and mafic minerals of the rock. Broad zones of the sample are covered by fine grained secondary plagioclase and broken, rotated plagioclase crystals	Na episyenite
MI-AL-PET-70	The sample is an intrusive strongly affected by dissolution that created large cavities probably with fracturing control where secondary plagioclase has been formed. Chl and Py are also filling those cavities but the rock is dominated by large quartz masses and large titanite crystals	Episyenite
MI-AL-PET-71	The sample is a porphyritic intrusive with a single dyke of aplite. The porphyritc intrusive is partially affected by dissolution having variable sized cavities with titanite and chlorite. The aplite dyke is pyrite rich with chlorite rims	Feldspar porphyry
MI-AL-PET-72	The sample is a medium grained equigranular intrusive with dissolution process that created variable sized cavities partially filled with chl, titanite, and some of them quartz including a central one of centimetric size.	Albitite, Episyenite
MI-AL-PET-73	The sample shows a qz vein with a narrow chlorite - py ribbon that is hosted by an intensely dissolved intrusive whose plagioclase has been totally replaced by secondary albite evident by chessboard twinning and very irregular margins.	Albitite, Episyenite
MI-AL-PET-74	The sample is a porphyritic intrusive whose matrix and partially the phenocrysts have been totally altered to ser>ca>ep>chl (saussurite?)	Altered feldspar porphyry
MI-AL-PET-75	The sample is a porphyritic intrusive with phenocrysts of plagioclase, biotite and quartz and fine grained matrix of quartz and plagioclase	Porphyritic Tonalite

SAMPLE	Location	Simplified composition	Texture	Simplified classification	Petrographic Classification
MI-PL-LGC-01	Planet	Felsic dyke	Equigranular	Equigranular intrusive	QzMonzoDiorite
MI-PL-LGC-02	Planet	Aplite	Aplitic	Aplite	Aplitic Monzogranite
MI-AL-LGC-03	Allied	Felsic dyke	Equigranular	Porphyritic intrusive	Tonalite
MI-AL-LGC-04	Allied	Felsic dyke	Equigranular	Equigranular intrusive	QzMonzoDiorite
MI-AL-LGC-05	Allied	Felsic dyke	Equigranular	Equigranular intrusive	Monzodiorite
MI-AL-LGC-06	Allied	Felsic dyke	Porphyritic	Porphyritic intrusive	QzMonzoDiorite
MI-AL-LGC-08	Allied	Felsic dyke	Porphyritic	Porphyritic intrusive	Feldspar porphyry
MI-AL-LGC-09	Allied	Felsic dyke	Porphyritic	Porphyritic intrusive	Porphyritic tonalite
MI-AL-LGC-11	Allied	Felsic dyke	Porphyritic	Porphyritic intrusive	QzMonzoDiorite?
MI-AL-LGC-12	Allied	Felsic dyke	Porphyritic	Porphyritic intrusive	QzDiorite
MI-AL-LGC-13	Allied	Felsic dyke	Modified	Texturally modified	QzMonzoDiorite
MI-AL-LGC-15	Allied	Felsic dyke	Porphyritic	Porphyritic intrusive	Tonalite
MI-AL-LGC-16	Allied	Aplite	Aplitic	Aplite	Aplitic Tonalite
MI-AL-LGC-17	Allied	Aplite	Aplitic	Aplite	Tonalite
MI-AL-LGC-21	Allied	Mafic dyke	Porphyritic	Gabbro	Gabbroic Dyke?
MI-AL-LGC-23	Allied	Felsic dyke	Equigranular	Equigranular intrusive	QzMonzoDiorite
MI-ME-LGC-24	Mellieur	Mafic dyke	Porphyritic	Gabbro	Gabbroic Dyke
MI-ME-LGC-25	Mellieur	Felsic dyke	Porphyritic	Porphyritic intrusive	QzMonzoDiorite
MI-ME-LGC-26	Mellieur	Felsic dyke	Porphyritic	Porphyritic intrusive	QzMonzoDiorite
MI-AL-LGC-27	Allied	Felsic dyke	Porphyritic	Porphyritic intrusive	Monzodiorite?
MI-AL-LGC-28	Allied	Felsic dyke	Modified	Texturally modified	Albitite?

Appendix 2. Geochemical results

SAMPLE	Ba ppm	Ce ppm	Cr ppm	Cs ppm	Dy ppm	Er ppm	Eu ppm	Ga ppm	Gd ppm	Hf ppm	Ho ppm	La ppm	Lu ppm	Nb ppm	Nd ppm	Pr ppm	Rb ppm	Sm ppm
MI-PL-LGC-01	1570	41.1	30	2.04	1.27	0.52	0.89	19	2.25	3.3	0.24	21	0.08	6.9	18.5	5.08	83.4	3.35
MI-PL-LGC-02	344	8.6	10	3.66	0.23	0.14	0.17	18.2	0.3	2.2	0.04	4.1	0.03	3.5	3.3	0.92	167	0.64
MI-AL-LGC-03	1180	50.6	20	1.96	1.25	0.67	0.74	19.2	2.06	3.6	0.25	28.2	0.1	7.4	19.2	5.57	103	3.27
MI-AL-LGC-04	994	47.8	20	1.23	1.37	0.72	0.73	19.3	2.09	3.8	0.25	24.7	0.1	7.3	19	5.48	87.6	3.22
MI-AL-LGC-05	562	43.8	20	0.92	1.09	0.59	0.66	20	1.68	3.5	0.22	23.1	0.1	6.9	17.3	5.16	68.6	3.02
MI-AL-LGC-06	627	68.1	30	1.33	1.31	0.73	0.92	21.2	2.24	3.7	0.24	39.9	0.09	7.7	25.3	7.77	68.7	3.7
MI-AL-LGC-08	1070	57.2	30	1.16	1.64	0.84	0.96	20.1	2.66	3.7	0.3	31.1	0.11	6.8	24.7	6.78	73.7	4.06
MI-AL-LGC-09	783	51	40	1.11	1.62	0.76	0.99	20.6	2.69	3.8	0.33	27.7	0.12	6.7	21.8	6.15	74.3	3.72
MI-AL-LGC-11	960	51.9	20	1.44	1.42	0.8	0.77	18.6	2.33	3.8	0.28	26.2	0.11	7.7	20.6	6.1	83.9	3.56
MI-AL-LGC-12	124	38.5	20	0.44	1.27	0.7	0.77	20.6	2.11	3.9	0.22	17.5	0.12	6.5	16.7	4.71	13.6	3.15
MI-AL-LGC-13	65.3	6.6	20	0.17	1.11	0.59	0.63	23.9	1.95	4.1	0.23	2.1	0.08	7.9	7.7	1.34	4.9	2.57
MI-AL-LGC-15	326	39.7	40	1.07	1.07	0.49	0.6	17.1	1.39	2.6	0.19	21.5	0.09	2.8	15	4.57	50.3	2.18
MI-AL-LGC-16	149	15.8	10	1.54	0.18	0.15	0.11	19.1	0.23	2.5	0.05	11.3	0.06	3.8	3.4	1.25	81.2	0.44
MI-AL-LGC-17	193.5	5.7	20	1.09	0.67	0.35	0.33	16.5	1.01	3.1	0.14	2.5	0.08	3.8	3.8	0.84	92.5	1.03
MI-AL-LGC-21	104.5	13.2	10	0.85	6.18	3.98	1.39	22.6	5.23	3	1.33	4.8	0.5	3.6	11.3	2.2	9.2	3.99
SAMPLE	**Ba ppm**	**Ce ppm**	**Cr ppm**	**Cs ppm**	**Dy ppm**	**Er ppm**	**Eu ppm**	**Ga ppm**	**Gd ppm**	**Hf ppm**	**Ho ppm**	**La ppm**	**Lu ppm**	**Nb ppm**	**Nd ppm**	**Pr ppm**	**Rb ppm**	**Sm ppm**
MI-AL-LGC-23	1815	51.4	20	3.75	1.48	0.67	1.02	21.1	2.53	3.8	0.26	26.9	0.1	5.6	23.4	6.38	111.5	3.97
MI-ME-LGC-24	96.7	18.7	140	6.33	4.36	2.68	1.14	19.2	3.94	2.5	0.98	8.6	0.42	4.2	12.2	2.64	5.7	3.57
MI-ME-LGC-25	1260	48	20	1.86	1.27	0.58	0.83	19.6	1.9	3.6	0.25	26	0.09	6.5	18.8	5.55	105	3.07
MI-ME-LGC-26	1250	48.7	20	0.9	1.22	0.72	0.75	19.3	2.01	3.4	0.23	26.2	0.11	6.2	19.9	5.62	85.9	3.12
MI-AL-LGC-27	908	58.1	40	1.01	1.69	0.8	0.95	19.7	2.74	4	0.27	30.7	0.09	6.6	24.2	6.86	58.6	3.95
MI-AL-LGC-28	93.8	2.8	10	0.09	0.44	0.34	0.35	19.7	0.93	3.2	0.1	0.7	0.11	4.1	3.4	0.54	4.3	1.25

SAMPLE	Sn ppm	Sr ppm	Ta ppm	Tb ppm	Th ppm	Tm ppm	U ppm	V ppm	W ppm	Y ppm	Yb ppm	Zr ppm
MI-PL-LGC-01	1	925	0.4	0.27	3.44	0.08	1.42	30	1	6.1	0.46	126
MI-PL-LGC-02	<1	146.5	0.3	0.04	4.13	0.03	2.12	<5	1	1.7	0.17	45
MI-AL-LGC-03	1	446	0.4	0.23	4.96	0.09	1.95	33	1	6.9	0.68	136
MI-AL-LGC-04	1	302	0.5	0.27	5.35	0.08	2.44	35	2	7	0.71	141
MI-AL-LGC-05	1	232	0.4	0.21	5.43	0.09	2.54	40	4	5.9	0.56	131
MI-AL-LGC-06	1	263	0.5	0.25	5.62	0.1	2.57	39	3	7.7	0.7	146
MI-AL-LGC-08	1	618	0.4	0.35	5.21	0.12	2.05	45	3	8.6	0.69	144
MI-AL-LGC-09	1	340	0.4	0.32	4.95	0.12	2.08	61	9	9.2	0.88	146
MI-AL-LGC-11	1	262	0.5	0.26	5.03	0.12	3.08	31	1	7.7	0.76	156
MI-AL-LGC-12	1	181	0.4	0.26	5.23	0.11	2.04	38	1	7.1	0.74	148
MI-AL-LGC-13	1	145	0.5	0.22	6.48	0.07	2.47	51	1	6.6	0.52	157
MI-AL-LGC-15	<1	204	0.2	0.17	3.54	0.07	0.85	31	2	5.6	0.59	112
MI-AL-LGC-16	<1	53.8	0.2	0.04	7.87	0.02	3.35	<5	1	1.8	0.21	58
MI-AL-LGC-17	<1	43.7	0.3	0.11	9.43	0.06	3.62	<5	1	4.7	0.46	72
MI-AL-LGC-21	1	200	0.3	0.94	0.34	0.55	0.14	408	1	34.3	3.57	106
MI-AL-LGC-23	1	1090	0.4	0.32	3.91	0.08	1.86	41	<1	7.7	0.64	144
MI-ME-LGC-24	1	350	0.3	0.68	0.72	0.42	0.2	348	<1	25	2.74	92
SAMPLE	**Sn ppm**	**Sr ppm**	**Ta ppm**	**Tb ppm**	**Th ppm**	**Tm ppm**	**U ppm**	**V ppm**	**W ppm**	**Y ppm**	**Yb ppm**	**Zr ppm**
MI-ME-LGC-25	1	673	0.4	0.23	5.08	0.1	1.9	28	<1	6.8	0.61	130
MI-ME-LGC-26	1	723	0.5	0.25	5.43	0.15	2.14	29	<1	7	0.64	134
MI-AL-LGC-27	1	527	0.4	0.33	5.31	0.11	1.97	41	1	8.1	0.67	151
MI-AL-LGC-28	<1	37.1	0.3	0.08	8.23	0.06	2.64	<5	<1	4	0.45	72

SAMPLE	SiO2 %	Al2O3 %	Fe2O3 %	CaO %	MgO %	Na2O %	K2O %	Cr2O3 %	TiO2 %	MnO %	P2O5 %	SrO %	BaO %	LOI %	Total %
MI-PL-LGC-01	69.8	15.05	2.54	2.03	0.94	4.97	3.22	<0.01	0.29	0.04	0.13	0.11	0.17	0.85	100.14
MI-PL-LGC-02	78	12.55	0.86	0.51	0.13	4.1	4.25	<0.01	0.05	0.01	<0.01	0.02	0.04	0.28	100.8
MI-AL-LGC-03	71.5	14.3	2.38	1.43	0.8	5.12	3.64	<0.01	0.25	0.03	0.1	0.05	0.13	1.3	101.03
MI-AL-LGC-04	68.5	14.5	2.29	1.7	0.78	5.54	3.34	<0.01	0.26	0.02	0.09	0.04	0.11	1.79	98.96
MI-AL-LGC-05	71.4	14.4	1.97	1.33	0.74	6.05	2.59	<0.01	0.23	0.02	0.09	0.03	0.06	1.76	100.67
MI-AL-LGC-06	67.9	15.05	2.98	1.89	1.19	6.17	2.56	<0.01	0.36	0.03	0.17	0.03	0.07	2.23	100.63

MI-AL-LGC-08	66.7	15.05	3.18	2.55	1.28	5.4	2.74	0.01	0.37	0.05	0.17	0.07	0.12	1.9	99.59
MI-AL-LGC-09	66.4	15.4	3.06	2.81	1.06	5.79	2.98	0.01	0.4	0.03	0.17	0.04	0.09	3.03	101.27
MI-AL-LGC-11	68.4	15.6	2.25	1.55	0.94	6.06	3.53	<0.01	0.27	0.03	0.11	0.03	0.11	1.68	100.56
MI-AL-LGC-12	72.4	15.4	2.3	0.78	1.1	7.93	0.49	<0.01	0.24	0.02	0.1	0.02	0.01	1.07	101.86
MI-AL-LGC-13	65.2	18.5	3.41	0.47	1.74	9.51	0.65	<0.01	0.27	0.02	0.11	0.02	0.01	1.56	101.47
MI-AL-LGC-15	68.1	15.45	3.12	2.83	1.53	5.71	1.64	0.01	0.23	0.05	0.13	0.02	0.04	2.66	101.52
MI-AL-LGC-16	77.5	12.6	0.81	0.36	0.06	5.24	3.19	<0.01	0.05	0.01	<0.01	<0.01	0.02	0.46	100.3
SAMPLE	**SiO2 %**	**Al2O3 %**	**Fe2O3 %**	**CaO %**	**MgO %**	**Na2O %**	**K2O %**	**Cr2O3 %**	**TiO2 %**	**MnO %**	**P2O5 %**	**SrO %**	**BaO %**	**LOI %**	**Total %**
MI-AL-LGC-17	75.7	11.85	0.82	2.02	0.06	4.38	4.03	<0.01	0.04	0.01	<0.01	<0.01	0.02	1.74	100.67
MI-AL-LGC-21	50.7	12.25	18.6	8.09	4.39	2.03	0.31	<0.01	1.71	0.25	0.13	0.02	0.01	1.76	100.25
MI-AL-LGC-23	68.5	16.1	3.25	2.47	1.2	5.17	3.41	<0.01	0.36	0.05	0.17	0.12	0.2	0.85	101.85
MI-ME-LGC-24	49.2	13.9	12.8	11.35	7.33	1.97	0.13	0.02	1.18	0.22	0.13	0.04	0.01	2.58	100.86
MI-ME-LGC-25	70.1	14.75	2.17	1.57	0.77	5.47	3.45	<0.01	0.23	0.04	0.09	0.08	0.14	1	99.86
MI-ME-LGC-26	70.8	14.9	2.14	1.61	0.75	5.49	3.46	<0.01	0.24	0.04	0.09	0.08	0.14	0.71	100.45
MI-AL-LGC-27	69.2	14.8	3.01	2.16	1.32	5.51	2.63	0.01	0.37	0.05	0.17	0.06	0.1	1.63	101.02
MI-AL-LGC-28	70.7	18.2	0.7	0.13	0.14	10.2	0.81	<0.01	0.06	<0.01	0.01	<0.01	0.01	0.34	101.3

SAMPLE	Au ppm	S %	C %	Ag ppm	Al %	As ppm	Be ppm	Bi ppm	Ca %	Cd ppm	Co ppm	Cu ppm	Fe %	Ge ppm	In ppm	K %
MI-PL-LGC-01	<0.001	0.04	0.07	0.021	7.11	0.18	2.03	0.057	1.33	0.032	4.72	11.35	1.66	0.12	0.016	2.7
MI-PL-LGC-02	<0.001	0.02	0.02	0.041	5.9	0.19	2.48	0.201	0.35	0.013	0.663	10.6	0.55	0.08	0.008	3.56
MI-AL-LGC-03	<0.001	0.03	0.19	0.007	7.23	0.2	2.69	0.107	1.02	0.014	4.18	27	1.63	0.12	0.014	3.12
MI-AL-LGC-04	0.046	0.17	0.29	0.013	6.87	0.11	2.38	0.179	1.15	<0.005	3.87	8.66	1.48	0.12	0.006	2.76
MI-AL-LGC-05	0.034	0.53	0.23	0.043	6.73	0.31	2.78	0.708	0.88	0.005	4	25.1	1.29	0.12	0.013	2.13
MI-AL-LGC-06	2.15	0.73	0.29	0.187	7.58	0.19	2.36	0.822	1.35	0.005	6.64	7.17	2.05	0.17	0.017	2.21
MI-AL-LGC-08	0.144	0.16	0.31	0.04	7.53	0.13	2.44	0.323	1.79	0.011	7.22	15.65	2.17	0.15	0.014	2.33
MI-AL-LGC-09	0.101	0.91	0.47	0.129	6.9	0.27	1.98	0.719	1.83	0.008	6.75	14.75	1.92	0.15	0.015	2.34
MI-AL-LGC-11	0.003	0.12	0.26	0.008	7.11	0.22	2.31	0.123	1.02	<0.005	3.84	7.41	1.45	0.13	0.017	2.81
MI-AL-LGC-12	<0.001	0.06	0.09	0.014	7.13	0.08	2.27	0.052	0.52	<0.005	4.68	2.99	1.48	0.14	0.009	0.39
MI-AL-LGC-13	0.117	0.89	0.01	0.049	8.14	0.09	1.77	0.838	0.31	0.01	10.1	2.06	2.2	0.11	0.011	0.55
SAMPLE	**Au ppm**	**S %**	**C %**	**Ag ppm**	**Al %**	**As ppm**	**Be ppm**	**Bi ppm**	**Ca %**	**Cd ppm**	**Co ppm**	**Cu ppm**	**Fe %**	**Ge ppm**	**In ppm**	**K %**
MI-AL-LGC-15	0.011	0.19	0.42	0.155	7.59	0.16	1.04	0.05	1.96	0.059	7.96	8.1	2.1	0.12	<0.005	1.38
MI-AL-LGC-16	0.552	0.21	0.05	0.084	5.4	0.16	1.86	1.425	0.24	0.016	0.497	11.65	0.5	0.07	0.007	2.68
MI-AL-LGC-17	0.12	0.19	0.42	0.052	5.5	0.18	1.58	0.237	1.41	<0.005	0.717	16.25	0.53	0.08	<0.005	3.28
MI-AL-LGC-21	0.003	0.28	0.04	0.037	6.49	0.71	0.61	0.124	5.62	0.14	47.4	130	12.7	0.22	0.106	0.27
MI-AL-LGC-23	<0.001	0.04	0.07	0.032	7.67	0.54	2.2	0.059	1.69	0.03	6.64	15.05	2.19	0.13	0.018	2.82
MI-ME-LGC-24	0.003	0.02	0.03	0.044	7.28	0.13	0.61	0.014	7.66	0.125	51.2	154	8.51	0.16	0.062	0.11
MI-ME-LGC-25	<0.001	0.01	0.13	0.02	7.62	0.42	2.58	0.054	1.15	0.024	4.18	26	1.53	0.15	0.015	3.08
MI-ME-LGC-26	<0.001	0.01	0.08	0.013	7.34	0.2	2.04	0.026	1.1	0.026	3.94	15.55	1.45	0.12	0.009	3
MI-AL-LGC-27	0.004	0.16	0.21	0.041	7.2	0.1	2.21	0.12	1.45	0.015	6.77	6.95	2.02	0.13	0.019	2.23
MI-AL-LGC-28	0.009	0.2	<0.01	0.212	6.13	0.08	1.42	0.213	0.08	<0.005	2.46	171.5	0.37	0.05	0.008	0.69

SAMPLE	Li ppm	Mg %	Mn ppm	Mo ppm	Na %	Nb ppm	Ni ppm	P %	Pb ppm	Re ppm	Sb ppm	Sc ppm	Se ppm	Te ppm	Ti %	Tl ppm	Zn ppm
MI-PL-LGC-01	13.2	0.51	293	0.79	3.58	4.84	7.85	0.057	18.75	<0.002	0.09	2.74	<0.2	<0.04	0.169	0.521	50.3

MI-PL-LGC-02	2.8	0.07	102.5	4.15	2.95	3.59	3.63	0.003	30.4	<0.002	0.09	0.52	<0.2	0.08	0.031	1.195	14.4
MI-AL-LGC-03	10.7	0.44	258	0.62	3.73	6.88	7.02	0.045	12.45	<0.002	0.07	2.67	<0.2	<0.04	0.134	0.655	44.7
MI-AL-LGC-04	8.6	0.41	174	0.43	3.9	6.85	6.76	0.043	8.69	<0.002	0.07	2.56	<0.2	0.04	0.137	0.514	28.5
MI-AL-LGC-05	11.1	0.4	117.5	0.58	4.16	6.5	6.04	0.039	7.71	<0.002	0.08	2.16	<0.2	0.34	0.114	0.414	20
MI-AL-LGC-06	15.7	0.66	222	4.9	4.52	7.37	11.45	0.076	7.95	0.002	0.09	4.3	0.3	0.45	0.193	0.42	33.5
MI-AL-LGC-08	13	0.7	376	33.2	3.96	7.29	11.7	0.075	13.6	0.005	0.09	4.32	<0.2	0.17	0.217	0.378	53.7
MI-AL-LGC-09	12.6	0.53	228	0.6	3.91	7.08	11.95	0.071	6.93	<0.002	0.11	4.56	<0.2	0.51	0.215	0.415	26.4
MI-AL-LGC-11	12.8	0.51	206	0.38	4.14	7.47	6.46	0.047	6.67	<0.002	0.07	2.69	<0.2	0.04	0.15	0.494	27.4
MI-AL-LGC-12	11.4	0.57	134.5	0.35	5.48	6.55	6.27	0.04	3.48	<0.002	0.06	2.57	0.2	<0.04	0.128	0.067	25.6
MI-AL-LGC-13	17.1	0.94	158.5	0.19	7.02	8.99	13.9	0.051	4.46	<0.002	0.06	2.82	0.3	0.34	0.164	0.025	30.2
MI-AL-LGC-15	20	0.83	337	0.84	4.2	3.03	17.7	0.055	3.64	<0.002	0.09	4.37	0.2	0.85	0.129	0.235	52.5
MI-AL-LGC-16	1	0.03	40.4	0.77	3.81	3.78	1.1	0.002	11.3	<0.002	0.07	0.33	0.2	0.78	0.025	0.514	4.7
MI-AL-LGC-17	0.9	0.03	78.7	0.76	3.11	4.24	1.03	0.001	6.6	<0.002	0.07	0.56	<0.2	0.13	0.022	0.553	2.7

SAMPLE	**Li ppm**	**Mg %**	**Mn ppm**	**Mo ppm**	**Na %**	**Nb ppm**	**Ni ppm**	**P %**	**Pb ppm**	**Re ppm**	**Sb ppm**	**Sc ppm**	**Se ppm**	**Te ppm**	**Ti %**	**Tl ppm**	**Zn ppm**
MI-AL-LGC-21	29	2.53	1770	1.21	1.5	3.9	22.3	0.06	1.75	0.002	0.12	42.1	0.5	<0.04	1.015	0.064	156
MI-AL-LGC-23	12.8	0.65	399	0.63	3.74	6.07	7.32	0.075	22.9	<0.002	0.07	3.51	<0.2	<0.04	0.219	0.742	65.5
MI-ME-LGC-24	18	4.25	1590	0.95	1.44	4.47	92.8	0.058	8.76	<0.002	0.06	42.3	<0.2	<0.04	0.697	0.33	100.5
MI-ME-LGC-25	9.8	0.44	309	0.44	4.17	7.83	6	0.043	16	<0.002	0.07	2.6	<0.2	<0.04	0.145	0.721	42.1
MI-ME-LGC-26	7.5	0.42	300	0.4	4.03	6.69	5.63	0.042	18.1	<0.002	0.07	2.54	<0.2	<0.04	0.144	0.571	39.7
MI-AL-LGC-27	10.5	0.71	355	0.53	4	7.02	11.65	0.074	13.05	<0.002	0.06	3.87	<0.2	<0.04	0.212	0.314	48.5

MI-AL-LGC-28	1.6	0.07	31.1	1.26	7.58	4.66	1.44	0.005	2.52	<0.002	0.05	0.75	0.2	0.12	0.037	0.025	3.8

Appendix 3. Geochronological results

U/Pb Zircon Geochronology. Sample MI-PL-DAT-01											
Sample Name	**U ppm**	**U/Th**	**$^{207}Pb/^{235}U$**	**2s Abs Error**	**$^{206}Pb/^{238}U$**	**2s Abs Error**	**Corr. Coef.**	**$^{238}U/^{206}Pb$**	**2s Abs Error**	**$^{207}Pb/^{206}Pb$**	**2s Abs Error**
PL1_1	1862	1.6	11.32609	0.56985	0.44459	0.01975	0.944	2.2493	0.0999	0.1850	0.0031
PL1_2	1315	1.7	13.31918	0.65189	0.53032	0.02317	0.954	1.8856	0.0824	0.1823	0.0027
PL1_3	953	0.9	11.16487	0.55265	0.44323	0.01956	0.952	2.2561	0.0996	0.1829	0.0028
PL1_4	1778	1.0	12.72447	0.59933	0.50873	0.02122	0.952	1.9657	0.0820	0.1816	0.0027
PL1_5	1072	1.0	6.64438	0.38075	0.26416	0.01374	0.954	3.7855	0.1968	0.1826	0.0032
PL1_6	1120	1.5	12.20172	0.58589	0.49202	0.02105	0.954	2.0325	0.0870	0.1800	0.0026
PL1_7	2772	1.6	10.69948	0.52925	0.43208	0.01874	0.941	2.3144	0.1004	0.1798	0.0031
PL1_8	1591	1.9	12.10034	0.58768	0.48947	0.02120	0.954	2.0430	0.0885	0.1795	0.0027
PL1_9	3134	1.5	9.40173	0.45644	0.38057	0.01639	0.951	2.6276	0.1132	0.1794	0.0028
PL1_10	2122	1.2	7.97702	0.39393	0.31975	0.01411	0.954	3.1274	0.1380	0.1811	0.0027
PL1_11	1114	2.7	13.42794	0.63655	0.53333	0.02230	0.949	1.8750	0.0784	0.1828	0.0028
PL1_12	760	0.8	12.83820	0.63308	0.51100	0.02193	0.936	1.9570	0.0840	0.1824	0.0032
PL1_13	1528	1.2	11.72635	0.59667	0.47763	0.02186	0.956	2.0937	0.0958	0.1782	0.0027
PL1_14	1678	2.0	12.94323	0.61222	0.52278	0.02192	0.952	1.9128	0.0802	0.1797	0.0027
PL1_15	2224	1.5	10.24159	0.49210	0.40724	0.01655	0.920	2.4556	0.0998	0.1826	0.0035
PL1_16	1463	2.3	11.47119	0.61628	0.45522	0.02215	0.957	2.1967	0.1069	0.1829	0.0029
PL1_17	1135	0.9	11.94506	0.57590	0.46963	0.02017	0.954	2.1293	0.0914	0.1847	0.0027
PL1_18	1029	1.1	12.47912	0.58929	0.49665	0.02073	0.951	2.0135	0.0841	0.1824	0.0027
PL1_19	2808	1.8	11.59134	0.58493	0.47350	0.02098	0.940	2.1119	0.0936	0.1777	0.0031
PL1_20	1744	1.2	12.91636	0.64795	0.51257	0.02283	0.948	1.9510	0.0869	0.1829	0.0030
PL1_21	860	1.1	12.08515	0.58343	0.48942	0.02079	0.946	2.0433	0.0868	0.1793	0.0029
PL1_22	2100	1.5	12.45299	0.59370	0.50738	0.02141	0.951	1.9709	0.0832	0.1782	0.0027
PL1_23	2087	1.6	12.25905	0.60687	0.49969	0.02163	0.939	2.0013	0.0866	0.1781	0.0031
PL1_24	1351	1.1	11.43619	0.63805	0.45584	0.02218	0.928	2.1938	0.1067	0.1821	0.0038
PL1_25	2076	1.5	13.61080	0.73537	0.56143	0.02703	0.945	1.7812	0.0857	0.1760	0.0031
Sample Name	**U ppm**	**U/Th**	**$^{207}Pb/^{235}U$**	**2s Abs Error**	**$^{206}Pb/^{238}U$**	**2s Abs Error**	**Corr. Coef.**	**$^{238}U/^{206}Pb$**	**2s Abs Error**	**$^{207}Pb/^{206}Pb$**	**2s Abs Error**
PL1_26	1062	1.1	13.06098	0.69666	0.51769	0.02441	0.941	1.9317	0.0911	0.1832	0.0034
PL1_27	2474	1.5	9.72485	0.62420	0.38437	0.02281	0.961	2.6017	0.1544	0.1837	0.0033

PL1_28	2149	1.3	11.18046	0.62759	0.45109	0.02292	0.954	2.2169	0.1126	0.1799	0.0031
PL1_29	1138	1.6	12.42828	0.72020	0.49847	0.02613	0.951	2.0061	0.1052	0.1810	0.0033
PL1_30	69	8.1	14.16552	0.75041	0.50048	0.02288	0.925	1.9981	0.0913	0.2055	0.0042
PL1_31	2310	1.7	12.51007	0.62624	0.50641	0.02263	0.952	1.9747	0.0882	0.1793	0.0028
PL1_32	1294	1.0	13.30157	0.74978	0.52507	0.02693	0.957	1.9045	0.0977	0.1839	0.0030
PL1_33	1826	3.0	12.08104	0.59716	0.48431	0.02124	0.949	2.0648	0.0906	0.1811	0.0029
PL1_34	1833	3.4	11.73943	0.58652	0.47264	0.02106	0.952	2.1158	0.0943	0.1803	0.0028
PL1_35	1813	2.6	10.91188	0.56670	0.43795	0.02045	0.954	2.2834	0.1066	0.1809	0.0029
PL1_36	1300	1.2	11.55727	0.54556	0.46353	0.01938	0.952	2.1573	0.0902	0.1810	0.0027

	AGES							
	$^{207}Pb/^{235}U$	2s Abs Error	$^{206}Pb/^{238}U$	2s Abs Error	$^{207}Pb/^{206}Pb$	2s Abs Error	Best Age	2s Abs Error
Sample Name	**Ma**	**Ma**	**Ma (207 Corr)**	**Ma**	**Ma**	**Ma**	**Ma**	**Ma**
PL1_1	2550.4	46.4	2371.1	87.8	2697.8	13.9	**2697.8**	**13.9**
PL1_2	2702.5	45.7	2742.8	97.3	2674.2	12.3	**2674.2**	**12.3**
PL1_3	2537.0	45.6	2365.1	87.1	2679.1	12.7	**2679.1**	**12.7**
PL1_4	2659.5	43.9	2651.2	90.3	2667.5	12.2	**2667.5**	**12.2**
PL1_5	2065.3	50.0	1511.1	69.9	2676.7	14.3	**2676.7**	**14.3**
PL1_6	2620.0	44.6	2579.4	90.6	2653.3	12.1	**2653.3**	**12.1**
PL1_7	2497.4	45.4	2315.1	84.1	2650.8	14.1	**2650.8**	**14.1**
PL1_8	2612.2	45.0	2568.4	91.4	2648.1	12.3	**2648.1**	**12.3**
PL1_9	2378.0	44.1	2078.9	76.3	2646.9	12.7	**2646.9**	**12.7**
PL1_10	2228.4	44.1	1788.5	68.7	2663.2	12.5	**2663.2**	**12.5**
PL1_11	2710.2	44.3	2755.5	93.4	2678.3	12.6	**2678.3**	**12.6**
PL1_12	2667.9	45.9	2660.9	93.2	2674.8	14.5	**2674.8**	**14.5**
PL1_13	2582.8	47.1	2516.9	95.0	2636.6	12.6	**2636.6**	**12.6**
PL1_14	2675.5	44.1	2711.0	92.4	2650.5	12.2	**2650.5**	**12.2**
PL1_15	2456.8	44.0	2202.3	75.6	2676.5	15.8	**2676.5**	**15.8**
PL1_16	2562.2	49.6	2418.4	97.7	2679.8	13.1	**2679.8**	**13.1**
PL1_17	2600.1	44.7	2481.9	88.2	2695.2	12.2	**2695.2**	**12.2**
PL1_18	2641.2	43.9	2599.4	89.0	2675.0	12.3	**2675.0**	**12.3**
PL1_19	2572.0	46.6	2498.9	91.4	2631.8	14.4	**2631.8**	**14.4**
PL1_20	2673.6	46.7	2667.6	96.9	2679.8	13.3	**2679.8**	**13.3**
PL1_21	2611.0	44.8	2568.1	89.7	2646.1	13.2	**2646.1**	**13.2**
PL1_22	2639.2	44.3	2645.4	91.2	2636.1	12.5	**2636.1**	**12.5**
PL1_23	2624.4	46.0	2612.4	92.6	2635.4	14.3	**2635.4**	**14.3**
PL1_24	2559.4	51.4	2421.2	97.8	2672.5	17.3	**2672.5**	**17.3**
Sample Name	**Ma**	**Ma**	**Ma (207 Corr)**	**Ma**	**Ma**	**Ma**	**Ma**	**Ma**
PL1_25	2723.0	50.5	2872.5	111.1	2615.6	14.8	**2615.6**	**14.8**
PL1_26	2684.1	49.7	2689.4	103.3	2681.7	15.1	**2681.7**	**15.1**
PL1_27	2409.1	58.3	2096.6	105.8	2686.4	14.6	**2686.4**	**14.6**
PL1_28	2538.3	51.7	2400.1	101.4	2652.3	14.1	**2652.3**	**14.1**
PL1_29	2637.3	53.7	2607.2	111.9	2662.2	14.9	**2662.2**	**14.9**
PL1_30	2760.9	49.6	2615.9	97.9	2870.3	16.5	**2870.3**	**16.5**
PL1_31	2643.5	46.5	2641.3	96.5	2646.9	12.9	**2646.9**	**12.9**
PL1_32	2701.3	52.5	2720.7	113.3	2688.5	13.6	**2688.5**	**13.6**

PL1_33	2610.7	45.8	2546.0	91.9	2663.0	13.1	**2663.0**	**13.1**
PL1_34	2583.8	46.2	2495.1	91.9	2655.9	12.9	**2655.9**	**12.9**
PL1_35	2515.6	47.7	2341.5	91.4	2661.0	13.0	**2661.0**	**13.0**
PL1_36	2569.2	43.6	2455.1	85.1	2662.2	12.2	**2662.2**	**12.2**

U concentration uncertainty is ~20%; individual errors are given as 2sigma standard deviation and only reflect the random error; error are 206Pb/238U = 1.2%, 207Pb/206Pb = 0.6% (2s)

U/Pb Titanite Geochronology. Sample MI-AL-PET-70								
Sample	**Ti49_CPS**	**U (ppm)**	**Th (ppm)**	**U/Th**	**204PbCps**	**2σ int**	**%**	**206Pbcps/**
MI-AL-PET-70_g1 - 1	24820000	21.01	0.685	30.672	47	18	38.298	681.702
MI-AL-PET-70_g1 - 2	24290000	5.521	0.125	44.168	39	12	30.769	213.333
MI-AL-PET-70_g1 - 3	26020000	16.77	0.269	62.342	21	16	76.190	1250.000
MI-AL-PET-70_g1 - 4	25310000	2.616	0.153	17.098	33	13	39.394	124.273
MI-AL-PET-70_g1 - 5	24310000	9.311	0.376	24.763	45	15	33.333	304.000
MI-AL-PET-70_g1 - 6	24100000	28.29	1.022	27.681	48	16	33.333	892.917
MI-AL-PET-70_g1 - 7	25280000	6.04	0.279	21.649	39	13	33.333	244.359
MI-AL-PET-70_g1 - 8	26980000	Below LOD	0.270	#VALEUR!	30	17	56.667	781.333
MI-AL-PET-70_g1 - 9	25520000	6.057	0.306	19.794	50	15	30.000	187.800
MI-AL-PET-70_g1 - 10	25450000	2.596	0.116	22.379	33	13	39.394	122.606
MI-AL-PET-70_g1 - 11	26090000	26.76	0.383	69.869	30	14	46.667	1389.333
MI-AL-PET-70_g1 - 12	24400000	44.55	4.117	10.821	45	15	33.333	1167.111
MI-AL-PET-70_g1 - 13	23500000	38.15	1.271	30.016	43	14	32.558	1295.349
MI-AL-PET-70_g1 - 14	26560000	38.96	0.588	66.259	43	19	44.186	1396.512
MI-AL-PET-70_g1 - 15	25240000	37.48	1.268	29.558	41	17	41.463	1361.463
Sample	**Ti49_CPS**	**U (ppm)**	**Th (ppm)**	**U/Th**	**204PbCps**	**2σ int**	**%**	**206Pbcps/**
MI-AL-PET-70_g1 - 16	24410000	34.88	0.996	35.020	40	23	57.500	1305.000
MI-AL-PET-70_g1 - 17	26550000	37.79	0.617	61.248	14	13	92.857	4148.571
MI-AL-PET-70_g1 - 18	24970000	38.3	0.790	48.481	44	15	34.091	1312.727
MI-AL-PET-70_g1 - 19	26260000	41.48	0.701	59.173	25	14	56.000	2562.000
MI-AL-PET-70_g1 - 20	24490000	47	5.440	8.640	78	18	23.077	693.718

Sample	%Pb*	cps	%2	207Pb/	2σ	206Pb/	2σ3	err.	207Pb/
MI-AL-PET-70_g1 - 1	99.38	1	FAUX	6.75	0.16	0.379	0.005	0.380	0.132
MI-AL-PET-70_g1 - 2	97.82	1	FAUX	7.02	0.23	0.371	0.006	0.012	0.139
MI-AL-PET-70_g1 - 3	98.74	1	FAUX	6.63	0.18	0.375	0.006	0.470	0.129
MI-AL-PET-70_g1 - 4	97.32	1	FAUX	7.27	0.3	0.377	0.009	0.202	0.142
MI-AL-PET-70_g1 - 5	97.83	1	FAUX	6.78	0.21	0.356	0.005	0.480	0.140
MI-AL-PET-70_g1 - 6	98.52	1	FAUX	6.653	0.14	0.367	0.005	0.057	0.133
MI-AL-PET-70_g1 - 7	98.33	1	FAUX	7.09	0.23	0.374	0.007	0.252	0.139
MI-AL-PET-70_g1 - 8	98.63	1	FAUX	6.63	0.21	0.376	0.006	0.259	0.130
MI-AL-PET-70_g1 - 9	97.29	1	FAUX	7.52	0.27	0.373	0.007	0.440	0.148
MI-AL-PET-70_g1 - 10	96.77	1	FAUX	7.59	0.34	0.378	0.010	0.326	0.150
MI-AL-PET-70_g1 - 11	98.37	1	FAUX	6.73	0.17	0.379	0.005	0.409	0.131
MI-AL-PET-70_g1 - 12	96.87	1	FAUX	5.407	0.13	0.301	0.005	0.699	0.133
MI-AL-PET-70_g1 - 13	99.6	1	FAUX	6.712	0.14	0.378	0.005	0.239	0.131
MI-AL-PET-70_g1 - 14	99.22	1	FAUX	6.68	0.16	0.378	0.005	0.494	0.130
MI-AL-PET-70_g1 - 15	99.45	1	FAUX	6.693	0.15	0.377	0.004	0.338	0.131
MI-AL-PET-70_g1 - 16	98.77	1	FAUX	6.68	0.16	0.377	0.004	0.154	0.130
Sample	**%Pb***	**cps**	**%2**	**207Pb/**	**2σ**	**206Pb/**	**2σ3**	**err.**	**207Pb/**
MI-AL-PET-70_g1 - 17	99.18	1	FAUX	6.7	0.16	0.379	0.005	0.012	0.130
MI-AL-PET-70_g1 - 18	99.06	1	FAUX	6.685	0.14	0.378	0.005	0.442	0.130
MI-AL-PET-70_g1 - 19	99.17	1	FAUX	6.702	0.15	0.379	0.005	0.392	0.130
MI-AL-PET-70_g1 - 20	95.71	1	FAUX	5.31	0.15	0.284	0.006	0.608	0.137

Sample	2σ	207Pb/	2σ	207Pb/	2σ	206Pb/	2σ	%conc	238U/	2σ	207Pb/	2σ	err.
MI-AL-PET-70_g1 - 12	0.003	2117	35	2078	21	2070	23	95.830	2.641	0.035	0.132	0.003	0.147
MI-AL-PET-70_g1 - 13	0.004	2197	55	2107	30	2032	29	91.129	2.697	0.045	0.139	0.004	0.015
MI-AL-PET-70_g1 - 14	0.003	2082	40	2061	24	2051	29	97.912	2.668	0.045	0.129	0.003	0.264
MI-AL-PET-70_g1 - 15	0.006	2240	68	2142	37	2058	41	89.978	2.655	0.061	0.142	0.006	0.339
MI-AL-PET-70_g1 - 16	0.004	2211	45	2078	28	1964	26	86.655	2.806	0.043	0.140	0.004	-0.177
MI-AL-PET-70_g1 - 17	0.002	2135	32	2065	19	2015	23	92.561	2.724	0.036	0.133	0.002	0.589
MI-AL-PET-70_g1 - 18	0.004	2203	49	2117	28	2047	32	91.426	2.675	0.048	0.139	0.004	0.212
MI-AL-PET-70_g1 - 19	0.003	2089	46	2061	27	2056	28	97.142	2.662	0.042	0.130	0.003	0.024
Sample	**2σ**	**207Pb/**	**2σ**	**207Pb/**	**2σ**	**206Pb/**	**2σ**	**%conc**	**238U/**	**2σ**	**207Pb/**	**2σ**	**err.**
MI-AL-PET-70_g1 - 20	0.005	2322	51	2170	32	2041	34	85.035	2.682	0.053	0.148	0.005	0.137

Re/Os Molybdenite Geochronology.								
Sample	**Re ppm**	**± 2s**	**187Re ppb**	**± 2s**	**187Os ppb**	**± 2s**	**Model Age (Ma)**	**± 2s with ƛ (Ma)**
MI-AL-DAT-18	46.74	0.14	29.38	0.09	1346	1	2690	12
MI- AL-DAT-18-RPT1	45.49	0.13	28.60	0.08	1308	1	2685	12
MI-PL-PET-12	29.86	0.09	18.77	0.05	855.5	0.6	2676	12
MI-ME-DAT-17	357.88	1.04	224.94	0.65	10257	8	2676	12